HYDROLOGIC CONNECTIVITY AND NUTRIENT TRANSPORT WITHIN THE GREAT BEND OF THE WABASH RIVER

by

Spencer Willem

A Thesis

Submitted to the Faculty of Purdue University

In Partial Fulfillment of the Requirements for the degree of

Master of Science

Department of Earth, Atmospheric and Planetary Sciences

West Lafayette, Indiana

August 2021

THE PURDUE UNIVERSITY GRADUATE SCHOOL
STATEMENT OF COMMITTEE APPROVAL

Dr. Lisa Welp, Chair

Department of Earth, Atmospheric, and Planetary Sciences

Dr. Greg Michalski

Department of Earth, Atmospheric, and Planetary Sciences

Dr. Marty Frisbee

Department of Earth, Atmospheric, and Planetary Sciences

Approved by:

Dr. Daniel J. Cziczo

To my parents, Steve and Judi, for their support of my endeavors throughout my life.

ACKNOWLEDGMENTS

I would like to first thank my advisor, Dr. Lisa Welp, for providing the opportunity to earn a graduate degree in an earth science discipline. My research and writing skills have greatly improved with her guidance and support. I would also like to thank Dr. Greg Michalski and Dr. Marty Frisbee for serving on my committee and offering advice in their areas of expertise. My conversations with Dr. Michalski enhanced my understanding of nitrogen biogeochemistry in agricultural landscapes, and my discussions with Dr. Frisbee provided valuable context about the hydrogeology of west-central Indiana.

I extend my sincere gratitude to Sarah Peel, Shannon Stanis, and Amy Krzton-Presson at the Wabash River Enhancement Corporation for the many hours they spend organizing the Wabash Blitz Sampling events. I am also deeply thankful for each and every volunteer citizen scientist who has taken part in any of the Wabash Blitz Sampling events; the field data and water samples they have collected over the last decade were crucial for this thesis work. Dr. Laura Bowling and Dr. Ron Turco performed much of the initial mapping and sampling design for the sampling events. Lindsey Crawley and Janine Sparks provided valuable assistance and support with laboratory measurements. I also extend my thanks to Bradley McGinley, Emma Beck, and Josh Allen for their help with preliminary data analysis. Additionally, I would like to thank Lafayette Renew for their assistance with the sampling events.

I also greatly appreciate the funding sources that made this research possible. I would like to thank the Indiana Water Resources Research Center for funding this research. Duke Energy and the Indiana Department of Environmental Management also provided funding for the sampling events.

TABLE OF CONTENTS

LIST OF TABLES

LIST OF FIGURES

LIST OF ABBREVIATIONS AND SYMBOLS

AA	Anhydrous Ammonia
AET	Actual Evapotranspiration
ANOVA	Analysis of Variance
BMP	Best Management Practice
δ^2H	$^2H/^1H$ ratio relative to a standard
$\delta^{18}O$	$^{18}O/^{16}O$ ratio relative to a standard
DEM	Digital Elevation Model
d_{excess}	Deuterium Excess
DOC	Dissolved Organic Carbon
EPA	United States Environmental Protection Agency
ESRI	Environmental Systems Research Institute
ET	Evapotranspiration
ET_0	Reference Evapotranspiration
GIS	Geographic Information System
gNATSGO	Gridded National Soil Survey Geographic Database
ha	Hectare
HAB	Harmful Algal Bloom
K	Hydraulic conductivity
K_{sat}	Saturated hydraulic conductivity
km	Kilometers
L	Flow path length
LMWL	Local Meteoric Water Line
m	Meters
masl	Meters above sea level
MRB	Mississippi River Basin
N	Nitrogen
NLCD	National Land Cover Database
NRCS	Natural Resources Conservation Service
‰	Permil (1/1000)

n	Total Porosity
n_e	Effective porosity
NHD	National Hydrography Dataset
NRCS	Natural Resources Conservation Service
PET	Potential Evapotranspiration
r^2	Coefficient of determination
s	Seconds
S_r	Specific retention
S_y	Specific yield
t	Travel time
TTD	Travel Time Distribution
UAN	Urea Ammonium Nitrate
USDA	United States Department of Agriculture
USGS	United States Geological Survey
VSMOW	Vienna Standard Mean Ocean Water
WREC	Wabash River Enhancement Corporation

ABSTRACT

In the midwestern United States, nitrogen (N) pollution of surface and groundwaters is a substantial threat to water quality because of its ecological and human health effects. Hypoxia in the Gulf of Mexico is primarily caused by N runoff within the Mississippi River basin, and nitrate in drinking water may negatively impact human health in both adults and children.
Agricultural tile drainage is a common practice that facilitates the transport of N from fields to streams. While the impacts of tile drainage have been studied extensively at the field scale, the impacts on hydrology, nutrient transport, and groundwater recharge are still uncertain at the watershed and landscape scales.

The overall goal of this thesis work is to assess how tile drainage affects landscape-scale connectivity, hydrologic travel times, and N transport across a large catchment in west-central Indiana using 10 years of bi-annual water chemistry and stable isotope data from a community science education event. Land use data and a previously developed travel time distribution (TTD) model were also incorporated to accomplish this goal. A secondary goal is to estimate seasonal differences in groundwater recharge in west-central Indiana using stable water isotope data from precipitation and groundwater samples.

Qualitative travel times derived from δ^2H and $\delta^{18}O$ variability support the idea that short travel times have greater nitrate concentrations than long travel times. Greater N concentrations are also observed during wetter conditions with increased connectivity. The results of the GIS TTD model support the hypothesis that increasing drainage intensity reduces travel times. Groundwater recharge appears negligible in Tippecanoe County using a traditional water balance approach, but an isotope mass balance approach suggests that about 55-65% of annual recharge occurs during the summer and may be linked to intense precipitation events.

This knowledge improves our understanding of N transport and hydrologic connectivity in tile drained landscapes. The results of this thesis also demonstrate the importance of drainage density for travel times and provide additional insight into the seasonality of groundwater recharge in west-central Indiana.

CHAPTER 1. INTRODUCTION

In the United States, nitrogen (N) pollution is a major threat to water quality with human health and ecological impacts (Conley et al., 2009). Drinking water with elevated nitrate-N can cause methemoglobinemia in infants, contribute to harmful algal blooms (HABs), and there is growing evidence linking nitrate exposure with health effects in adults, including some types of cancers (M. H. Ward et al., 2018). N pollution also causes eutrophication in surface waters which causes hypoxic zones to form in coastal regions such as the Gulf of Mexico near the mouth of the Mississippi River (Goolsby & Battaglin, 2000). Response plans have been in place to reduce hypoxia in the Gulf of Mexico for nearly 20 years, but the extent of hypoxia has not decreased (Rabalais et al., 2007). The current 5-year average extent is 15,520 km^2, which is over 3 times larger than the Mississippi River Nutrient/Hypoxia Task Force goal of 5,000 km^2 (May & NOAA Southeast Fisheries Science Center, 2019).

Excess N from the Mississippi River Basin (MRB) is the primary cause of hypoxia in the Gulf of Mexico (Anderson et al., 2002). Wastewater treatment plants, agriculture, and atmospheric deposition are the three main N sources in the MRB (David et al., 2010). About 60% of the total N load at the MRB outlet comes from agricultural activities, and this percentage is even higher in the Corn Belt states of Iowa, Illinois, and Indiana (Robertson et al., 2014). Despite containing less than 12% of the MRB's area, these three states contribute nearly 40% of the total N load entering the Gulf of Mexico (Robertson & Saad, 2019).

Biogeochemical processes in agricultural soils have a substantial influence on N loads in streams because they can regulate the availability and mobility of N in the soil (Schepers et al., 2008). The relevant processes often depend on what type of N fertilizer is applied, when it is applied, and how much is applied (Culman et al., 2020). In Indiana, most N fertilizer (~82%) is applied from January to June, and the remainder is applied during the latter half of the year (Office of Indiana State Chemist, 2017). About 63% of N fertilizer in Indiana is applied as urea ammonium nitrate (UAN), but smaller quantities of anhydrous ammonia (AA) and urea are also used (Table A.1). The urea in fertilizers is hydrolyzed into ammonia by urease enzymes present in the soil (Kissel et al., 2008). Most ammonia produced by urea hydrolysis or applied as AA reacts with soil water to form ammonium ions that adsorb to soil particles, but some ammonia volatilizes and escapes to the atmosphere (Bronson, 2008). In most agricultural soils, ammonium rapidly undergoes nitrification to produce nitrate (Norton, 2008). Plants can utilize the nitrate, or the nitrate can undergo denitrification to nitrogen gas or leach out of the soil into surface waterways (Coyne, 2015; Mulla & Strock, 2008).

Land management practices can have substantial impacts on the N loss from agricultural land (Gramlich et al., 2018). Tile drainage is a common drainage improvement in poorly-drained agricultural soils, and over 20% of Indiana's cropland has tile drainage with higher percentages in the northern two-thirds of the state (USDA National Agricultural Statistics Service, 2017; Valayamkunnath et al., 2020). It has been recognized that tile drainage increases N loss at the field and watershed scales, but observational studies of spatial variability in N loss are lacking (Ahiablame et al., 2011; Arenas Amado et al., 2017; Cambardella et al., 1999; Gramlich et al., 2018; Jiang et al., 2014; Kennedy et al., 2012; Kladivko et al., 1991, 1999, 2004; Liu et al., 2020; Saadat et al., 2018; Schilling et al., 2020; Skaggs et al., 2005; Sui & Frankenberger, 2008; Tiemeyer et al., 2006; Williams et al., 2018; Wilson et al., 2020; Zhao et al., 2016). Previous watershed-scale studies about tile drainage and N transport frequently sample a few watersheds, and they provide valuable insight into the temporal variability of N transport through tile drains (Arenas Amado et al., 2017; Gentry et al., 2009; Kennedy et al., 2012; Williams et al., 2018). However, they have a limited ability to capture spatial variability, but this thesis work leverages 10 years of water chemistry data from seasonal sampling of over 200 nested watersheds to capture the spatial variability of N transport in tile-drained landscapes.

Good water quality is a key objective to maintain the sustainability of our water resources, but adequate water quantity is an equally important objective. Therefore, an understanding of the processes that control water quantity and availability is crucial, and groundwater recharge is one of these processes. Groundwater is an essential water resource and critical for sustaining baseflow in streams during dry conditions when other water inputs may be unavailable (Fetter, 2018). Groundwater quality and quantity can be negatively impacted by pollution and overextraction, and recharge can replenish an aquifer but also carry pollutants from the surface into the aquifer (Charbeneau, 2006). An understanding of when and where recharge occurs is critically important for maintaining groundwater resources (A. D. Ward et al., 2016).

The Teays Bedrock Valley System is present beneath parts of 12 Indiana counties, and it is an important groundwater resource for north-central Indiana (Bruns & Steen, 2003). Previous studies have assumed recharge to be negligible during summer months because evapotranspiration

(ET) and streamflow (*Q*) losses are higher than precipitation during those months (Allison & Hughes, 1978; Reardon et al., 1980). This study estimates seasonal recharge of groundwater in Tippecanoe County, Indiana from stable water isotope data of precipitation and groundwater.

1.1 References

Ahiablame, L. M., Chaubey, I., Smith, D. R., & Engel, B. A. (2011). Effect of tile effluent on nutrient concentration and retention efficiency in agricultural drainage ditches. *Agricultural Water Management*, *98*(8), 1271–1279. https://doi.org/10.1016/j.agwat.2011.03.002

Allison, G. B., & Hughes, M. W. (1978). The use of environmental chloride and tritium to estimate total recharge to an unconfined aquifer. *Soil Research*, *16*(2), 181–195. https://doi.org/10.1071/sr9780181

Anderson, D. M., Glibert, P. M., & Burkholder, J. M. (2002). Harmful algal blooms and eutrophication: Nutrient sources, composition, and consequences. *Estuaries*, *25*(4), 704–726. https://doi.org/10.1007/BF02804901

Arenas Amado, A., Schilling, K. E., Jones, C. S., Thomas, N., & Weber, L. J. (2017). Estimation of tile drainage contribution to streamflow and nutrient loads at the watershed scale based on continuously monitored data. *Environmental Monitoring and Assessment*, *189*(9), 426. https://doi.org/10.1007/s10661-017-6139-4

Bronson, K. F. (2008). Forms of inorganic nitrogen in soil. In *Nitrogen in Agricultural Systems* (pp. 31–55). John Wiley & Sons, Ltd. https://doi.org/10.2134/agronmonogr49.c2

Bruns, T. M., & Steen, W. J. (2003). *Hydrogeology of the Lafayette (Teays) Bedrock Valley System, north-central Indiana* (Water Resource Assessment No. 2003–7) (p. 75). Indianapolis, Indiana, USA: Indiana Department of Natural Resources. Retrieved from https://www.in.gov/dnr/water/files/Teays.pdf

Cambardella, C. A., Moorman, T. B., Jaynes, D. B., Hatfield, J. L., Parkin, T. B., Simpkins, W. W., & Karlen, D. L. (1999). Water quality in Walnut Creek Watershed: Nitrate-nitrogen in soils, subsurface drainage water, and shallow groundwater. *Journal of Environmental Quality*, *28*(1), 25–34. https://doi.org/10.2134/jeq1999.00472425002800010003x

Charbeneau, R. J. (2006). *Groundwater hydraulics and pollutant transport*. Long Grove, IL: Waveland Press.

Conley, D. J., Paerl, H. W., Howarth, R. W., Boesch, D. F., Seitzinger, S. P., Havens, K. E., et al. (2009). Controlling Eutrophication: Nitrogen and Phosphorus. *Science*, *323*(5917), 1014–1015. https://doi.org/10.1126/science.1167755

Coyne, M. S. (2015). Biological Denitrification. In *Nitrogen in Agricultural Systems* (pp. 201–253). John Wiley & Sons, Ltd. https://doi.org/10.2134/agronmonogr49.c7

Culman, S., Fulford, A., Camberato, J., & Steinke, K. (2020). *Tri-state fertilizer recommendations for corn, soybean, wheat, and alfalfa* (No. Extension Bulletin 974) (p. 56). Columbus, OH: The Ohio State University. Retrieved from https://extensionpubs.osu.edu/tri-state-fertilizer-recommendations-for-corn-soybean-wheat-and-alfalfa-pdf/

David, M. B., Drinkwater, L. E., & McIsaac, G. F. (2010). Sources of nitrate yields in the Mississippi River Basin. *Journal of Environmental Quality*, *39*(5), 1657–1667. https://doi.org/10.2134/jeq2010.0115

Fetter, C. W. (2018). *Applied hydrogeology* (4th ed.). Long Grove, IL: Waveland Press.

Gentry, L. E., David, M. B., Below, F. E., Royer, T. V., & McIsaac, G. F. (2009). Nitrogen mass balance of a tile-drained agricultural watershed in east-central Illinois. *Journal of Environmental Quality*, *38*(5), 1841–1847. https://doi.org/10.2134/jeq2008.0406

Goolsby, D. A., & Battaglin, W. A. (2000). *Nitrogen in the Mississippi Basin--Estimating sources and predicting flux to the Gulf of Mexico* (USGS Numbered Series No. 135– 00). *Nitrogen in the Mississippi Basin--Estimating sources and predicting flux to the Gulf of Mexico* (Vol. 135–00). U.S. Geological Survey. https://doi.org/10.3133/fs13500

Gramlich, A., Stoll, S., Stamm, C., Walter, T., & Prasuhn, V. (2018). Effects of artificial land drainage on hydrology, nutrient and pesticide fluxes from agricultural fields – A review. *Agriculture, Ecosystems & Environment*, *266*, 84–99. https://doi.org/10.1016/j.agee.2018.04.005

Jiang, Y., Frankenberger, J. R., Sui, Y., & Bowling, L. C. (2014). Estimation of nonpoint source nitrate concentrations in Indiana rivers based on agricultural drainage in the watershed. *Journal of the American Water Resources Association*, *50*(6), 1501–1514. https://doi.org/10.1111/jawr.12216

Kennedy, C. D., Bataille, C., Liu, Z., Ale, S., VanDeVelde, J., Roswell, C. R., et al. (2012). Dynamics of nitrate and chloride during storm events in agricultural catchments with different subsurface drainage intensity (Indiana, USA). *Journal of Hydrology*, *466–467*, 1–10. https://doi.org/10.1016/j.jhydrol.2012.05.002

Kissel, D. E., Cabrera, M. L., & Paramasivam, S. (2008). Ammonium, ammonia, and urea reactions in soils. In *Nitrogen in Agricultural Systems* (pp. 101–155). John Wiley & Sons, Ltd. https://doi.org/10.2134/agronmonogr49.c4

Kladivko, E. J., Scoyoc, G. E. V., Monke, E. J., Oates, K. M., & Pask, W. (1991). Pesticide and Nutrient Movement into Subsurface Tile Drains on a Silt Loam Soil in Indiana. *Journal of Environmental Quality*, *20*(1), 264–270. https://doi.org/10.2134/jeq1991.00472425002000010043x

Kladivko, E. J., Grochulska, J., Turco, R. F., Scoyoc, G. E. V., & Eigel, J. D. (1999). Pesticide and nitrate transport into subsurface tile drains of different spacings. *Journal of Environmental Quality*, *28*(3), 997–1004. https://doi.org/10.2134/jeq1999.00472425002800030033x

Kladivko, E. J., Frankenberger, J. R., Jaynes, D. B., Meek, D. W., Jenkinson, B. J., & Fausey, N. R. (2004). Nitrate leaching to subsurface drains as affected by drain spacing and changes in crop production system. *Journal of Environmental Quality, 33*(5), 1803–1813. https://doi.org/10.2134/jeq2004.1803

Liu, W., Youssef, M. A., Birgand, F. P., Chescheir, G. M., Tian, S., & Maxwell, B. M. (2020). Processes and mechanisms controlling nitrate dynamics in an artificially drained field: Insights from high-frequency water quality measurements. *Agricultural Water Management*, *232*, 106032. https://doi.org/10.1016/j.agwat.2020.106032

May, N. & NOAA Southeast Fisheries Science Center. (2019). *Temperature, salinity, dissolved oxygen measurements collected using CTD, bottle from multiple platforms in the Gulf of Mexico from 2009 through 2015 as part of the Southeast Area Monitoring and Assessment Program (SEAMAP) (NCEI Accession 0131259)* (Dataset). NOAA National Centers for Environmental Information. Retrieved from https://www.ncei.noaa.gov/archive/accession/0131259

Mulla, D. J., & Strock, J. S. (2008). Nitrogen Transport Processes in Soil. In *Nitrogen in Agricultural Systems* (pp. 361–400). John Wiley & Sons, Ltd. https://doi.org/10.2134/agronmonogr49.c10

Norton, J. M. (2008). Nitrification in Agricultural Soils. In *Nitrogen in Agricultural Systems* (pp. 173–199). John Wiley & Sons, Ltd. https://doi.org/10.2134/agronmonogr49.c6

Office of Indiana State Chemist. (2017). Fertilizer section annual reports. Retrieved June 28, 2021, from https://www.oisc.purdue.edu/fertilizer/annual_reports.html

Rabalais, N. N., Turner, R. E., Sen Gupta, B. K., Boesch, D. F., Chapman, P., & Murrell, M. C. (2007). Hypoxia in the northern Gulf of Mexico: Does the science support the Plan to Reduce, Mitigate, and Control Hypoxia? *Estuaries and Coasts, 30*(5), 753–772. https://doi.org/10.1007/BF02841332

Reardon, E. J., Mozeto, A. A., & Fritz, P. (1980). Recharge in northern clime calcareous sandy soils: soil water chemical and carbon-14 evolution. *Geochimica et Cosmochimica Acta*, *44*(11), 1723–1735. https://doi.org/10.1016/0016-7037(80)90223-9

Robertson, D. M., & Saad, D. A. (2019). *Spatially Referenced Models of Streamflow and Nitrogen, Phosphorus, and Suspended-Sediment Loads in Streams of the Midwestern United States* (Scientific Investigations Report No. 2019–5114) (p. 74). U.S. Geological Survey. Retrieved from https://doi.org/10.3133/sir20195114

Robertson, D. M., Saad, D. A., & Schwarz, G. E. (2014). Spatial Variability in Nutrient Transport by HUC8, State, and Subbasin Based on Mississippi/Atchafalaya River Basin SPARROW Models. *JAWRA Journal of the American Water Resources Association*, *50*(4), 988–1009. https://doi.org/10.1111/jawr.12153

Saadat, S., Bowling, L., Frankenberger, J., & Kladivko, E. (2018). Nitrate and phosphorus transport through subsurface drains under free and controlled drainage. *Water Research*, *142*, 196–207. https://doi.org/10.1016/j.watres.2018.05.040

Schepers, J. S., Raun, W., & Agronomy, A. S. of. (2008). *Nitrogen in Agricultural Systems*. United States: American Society of Agronomy.

Schilling, K. E., Streeter, M. T., Vogelgesang, J., Jones, C. S., & Seeman, A. (2020). Subsurface nutrient export from a cropped field to an agricultural stream: Implications for targeting edge-of-field practices. *Agricultural Water Management*, *241*, 106339. https://doi.org/10.1016/j.agwat.2020.106339

Skaggs, R. W., Youssef, M. A., Chescheir, G. M., & Gilliam, J. W. (2005). Effect of Drainage Intensity on Nitrogen Losses from Drained Lands. *Transactions of the ASAE*, *48*(6), 2169–2177. https://doi.org/10.13031/2013.20103

Sui, Y., & Frankenberger, J. R. (2008). Nitrate Loss from Subsurface Drains in an Agricultural Watershed Using Swat2005. *Transactions of the ASABE*, *51*(4), 1263–1272.

Tiemeyer, B., Kahle, P., & Lennartz, B. (2006). Nutrient losses from artificially drained catchments in North-Eastern Germany at different scales. *Agricultural Water Management*, *85*(1), 47–57. https://doi.org/10.1016/j.agwat.2006.03.016

USDA National Agricultural Statistics Service. (2017). *2017 Census of Agriculture*. Washington, DC: U. S. Department of Agriculture. Retrieved from https://www.nass.usda.gov/AgCensus/

Valayamkunnath, P., Barlage, M., Chen, F., Gochis, D. J., & Franz, K. J. (2020). Mapping of 30-meter resolution tile-drained croplands using a geospatial modeling approach. *Scientific Data*, *7*(1), 257. https://doi.org/10.1038/s41597-020-00596-x

Ward, A. D., Trimble, S. W., Burckhard, S. R., & Lyon, J. G. (2016). *Environmental hydrology* (Third edition). Boca Raton, FL: CRC Press, Taylor & Francis Group.

Ward, M. H., Jones, R. R., Brender, J. D., de Kok, T. M., Weyer, P. J., Nolan, B. T., et al. (2018). Drinking Water Nitrate and Human Health: An Updated Review. *International Journal of Environmental Research and Public Health*, *15*(7), 1557. https://doi.org/10.3390/ijerph15071557

Williams, M. R., Livingston, S. J., Penn, C. J., Smith, D. R., King, K. W., & Huang, C. (2018). Controls of event-based nutrient transport within nested headwater agricultural watersheds of the western Lake Erie basin. *Journal of Hydrology*, *559*, 749–761. https://doi.org/10.1016/j.jhydrol.2018.02.079

Wilson, G. L., Mulla, D. J., Galzki, J., Laacouri, A., Vetsch, J., & Sands, G. (2020). Effects of fertilizer timing and variable rate N on nitrate–N losses from a tile drained corn-soybean rotation simulated using DRAINMOD-NII. *Precision Agriculture*, *21*(2), 311–323. https://doi.org/10.1007/s11119-019-09668-4

Zhao, X., Christianson, L. E., Harmel, D., & Pittelkow, C. M. (2016). Assessment of drainage nitrogen losses on a yield-scaled basis. *Field Crops Research*, *199*, 156–166. https://doi.org/10.1016/j.fcr.2016.07.015

CHAPTER 2. STREAMWATER NITRATE CONCENTRATIONS AND CATCHMENT TRAVEL TIMES INFERRED FROM STABLE WATER ISOTOPES VARY ACROSS A MIDWESTERN TILE-DRAINED LANDSCAPE

2.1 Abstract

High nitrogen (N) loads drive algal blooms that cause seasonal hypoxia in the Gulf of Mexico, and much of this N comes from tile drained agricultural land in the United States' Midwest. This chapter leverages 10 years of water quality and stable isotope data from 205 nested watersheds to answer questions about N transport and hydrologic connectivity in a tile drained landscape. The results of this study indicate that greater nitrate concentrations occur in watersheds with greater tile drainage intensity. Qualitative travel times derived from stable isotope variability suggest that shorter travel times lead to greater in-stream N concentrations. Antecedent moisture conditions and hydrologic connectivity are also key controls on stream N concentrations at the watershed scale. Consistently low nitrate concentrations during fall baseflow events suggest that groundwater nitrate concentrations in the study area are generally low (~1.5 mg L^{-1}).

2.2 Introduction

Human activities have profoundly altered the global nitrogen (N) cycle over the last century, and these changes have doubled the global production of biologically available N above pre-industrial levels (Vitousek et al., 1997). A substantial fraction of this additional N is applied to agricultural land as fertilizer. While N fertilizers are essential for modern agriculture, their use contributes to eutrophication in both marine and freshwater ecosystems (Carpenter et al., 1998; Wurtsbaugh et al., 2019).

High N loads in surface waters fuel algal blooms that can form hypoxic zones in aquatic ecosystems throughout the world (Diaz & Rosenberg, 2008). One such hypoxic zone occurs during the summer months in the Gulf of Mexico near the mouth of the Mississippi River (Goolsby & Battaglin, 2000). N export from agricultural land within the Mississippi River Basin (MRB) is a contributing factor to seasonal hypoxia in the Gulf of Mexico (Anderson et al., 2002). Nonpoint source N pollution from agricultural land including the Corn Belt across Iowa, Illinois, and Indiana, contributes around 40% of the total N load at the mouth of the Mississippi River

(Robertson & Saad, 2019). N export is unevenly distributed within the MRB, and the state of Indiana contributes 10.2% of the total N load at the mouth of the Mississippi River despite containing just 2.7% of the MRB's area (Robertson & Saad, 2019).

Within the MRB, many agricultural areas have a high density of subsurface tile drainage networks (Feick et al., 2005; Robertson & Saad, 2019). Tile drainage is a common agricultural practice that enhances drainage on otherwise poorly draining soils, and an estimated 50 to 75% of northern Indiana has tile drainage (Feick et al., 2005). Installing tile drainage substantially alters the hydrology of agricultural land by regulating the depth to the water table and changing the relative contributions of surface and subsurface flow paths to stream discharge (Gramlich et al., 2018). These hydrologic changes often cause increased N leaching to streams (Follett & Delgado, 2002; Kalita et al., 2007). A previous study of 25 large (113 to 2,150 km^2) Indiana watersheds found that 71% of the variation in flow-weighted mean concentration of nitrate-N could be explained by the percentage of the watershed drained by tiles (Jiang et al., 2014).

Many studies have examined the role of tile drainage in N transport at the field scale using edge-of-field water chemistry observations (Ahiablame et al., 2011; Cambardella et al., 1999; Gramlich et al., 2018; Kladivko et al., 1991, 1999, 2004; Liu et al., 2020; Saadat et al., 2018; Skaggs et al., 2005; Tiemeyer et al., 2006; Zhao et al., 2016). Other field-scale studies have estimated N losses from tile drained fields using modelling techniques and programs such as MODFLOW and DRAINMOD (Merriman et al., 2018; Nangia et al., 2008; Schilling et al., 2020; Wilson et al., 2020). Several factors tend to increase N loss through subsurface drainage at the field scale: (i) high annual precipitation (Cambardella et al., 1999; Tomer et al., 2003; Zhao et al., 2016), (ii) narrow drain spacing (Kladivko et al., 2004), and (iii) greater drain depth (Skaggs et al., 2005).

Some studies at the watershed scale and larger use modelling approaches to estimate N transport and predict the influence of tile drains (Boles et al., 2015; David et al., 2010; Feng et al., 2013; Green et al., 2006; Li et al., 2010; Robertson & Saad, 2019; Sui & Frankenberger, 2008). However, there are only a few observational studies about the role of tile drains in N transport at the watershed scale, and these studies have generally used observations from 5 or fewer watersheds (Arenas Amado et al., 2017; Jiang et al., 2014; Kennedy et al., 2012; Royer et al., 2004; Williams et al., 2018). While studies that frequently sample a few watersheds provide valuable information about temporal variability in N transport, their ability to answer questions about nested landscape-scale connectivity and spatial variability in N transport is limited. This watershed scale study differs from previous studies by dividing a large (~1,200 km^2) catchment into over 200 nested watersheds of varying sizes to investigate connectivity and N transport at the landscape scale.

In this study we leverage 10 years of water chemistry and stable isotope data from twice a year sampling of 205 nested watersheds to explore the relationships between landscape-scale connectivity, tile drainage, stream nitrate concentrations, antecedent moisture conditions, and travel times estimated from stable isotope data. We hypothesize that greater landscape-scale connectivity associated with wetter antecedent moisture conditions leads to greater N loss through tile drains and increases stream nitrate concentrations. Watersheds with more tile drainage are expected to have shorter travel times and greater N loss.

2.3 Methods

2.3.1 Study area

The Region of the Great Bend of the Wabash River catchment is located in west-central Indiana and covers 1,238 km^2 (Figure 2.1). It includes a 47-km reach of the Wabash River beginning immediately downstream of Wildcat Creek (near Battle Ground, Indiana) and ending immediately upstream of Big Pine Creek (near Attica, Indiana). The topography is generally flat in the upland areas, but steeper slopes are found near the Wabash River and its tributaries (Figure 2.2). Row crop agriculture and pasture are the dominant land use types and cover nearly 75% of the catchment (Figure 2.3). Urban development accounts for 12% of the catchment, including the cities of Lafayette and West Lafayette (combined population of about 110,000). The remaining 14% is covered by forests and wetlands. Tile drained areas cover approximately 40% of the watershed (Figure 2.4).

The catchment is divided into 205 nested watersheds with a sampling site at its outlet (Figure 2.1). The watersheds' areas range from 0.036 to 1,238 km^2 (average of 48.3 km^2). Each watershed is assigned to one of four classes based on land use within the watershed. If agricultural, developed, or forested land use covers more than 50% of a watershed's area, then it is classified as Agriculture, Urban, or Forest, respectively. Watersheds with no single land use type covering more than 50% of the area are classified as Mixed.

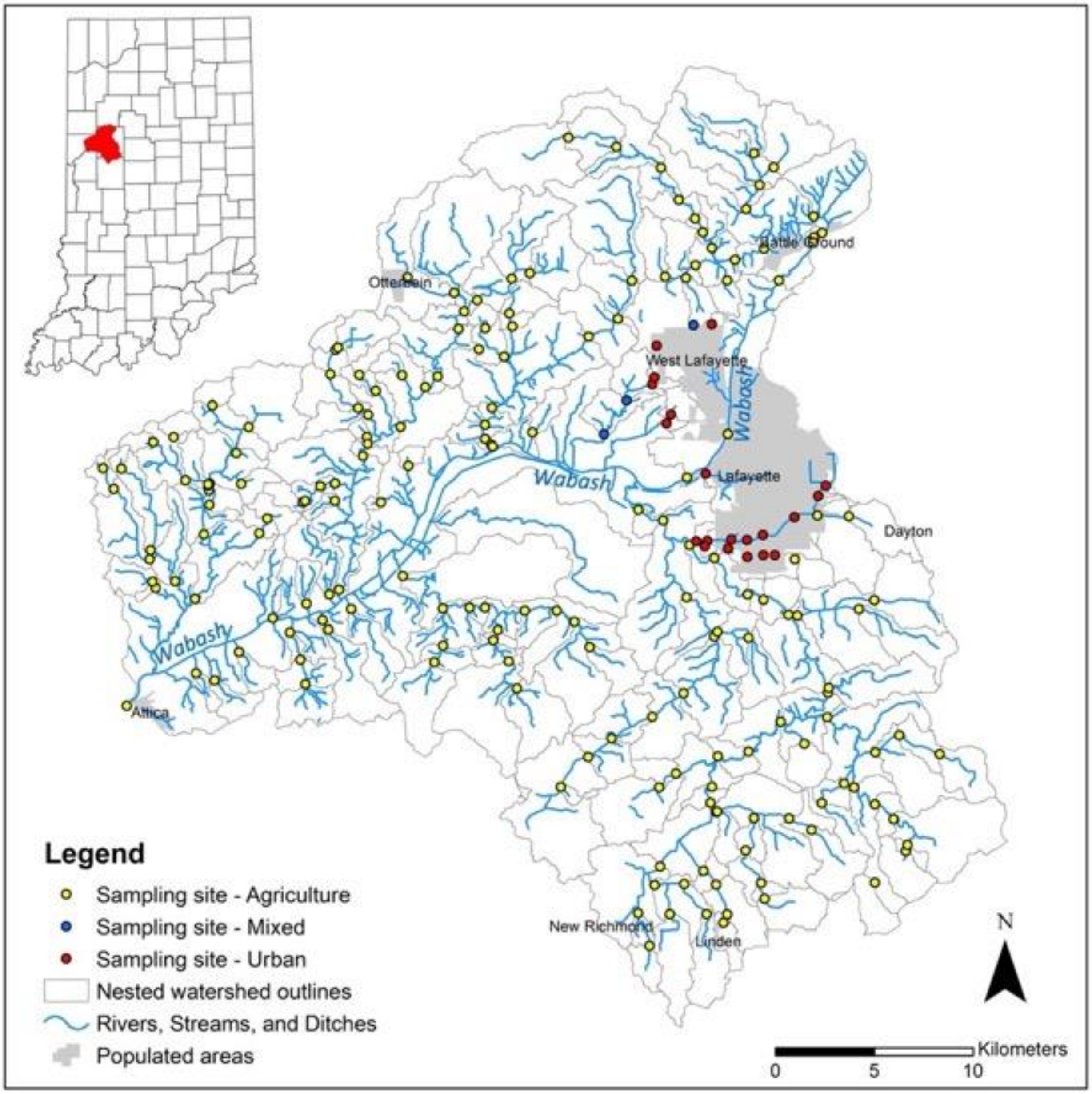

Figure 2.1. The Region of the Great Bend of the Wabash River catchment is divided into 205 nested watersheds (light gray lines). Gray shaded areas represent urban development, and blue lines represent rivers, streams, and ditches. The colored points indicate the location of sampling points, and the color represents the dominant land use within the corresponding watersheds. All sampling points are located along public roads (not shown).

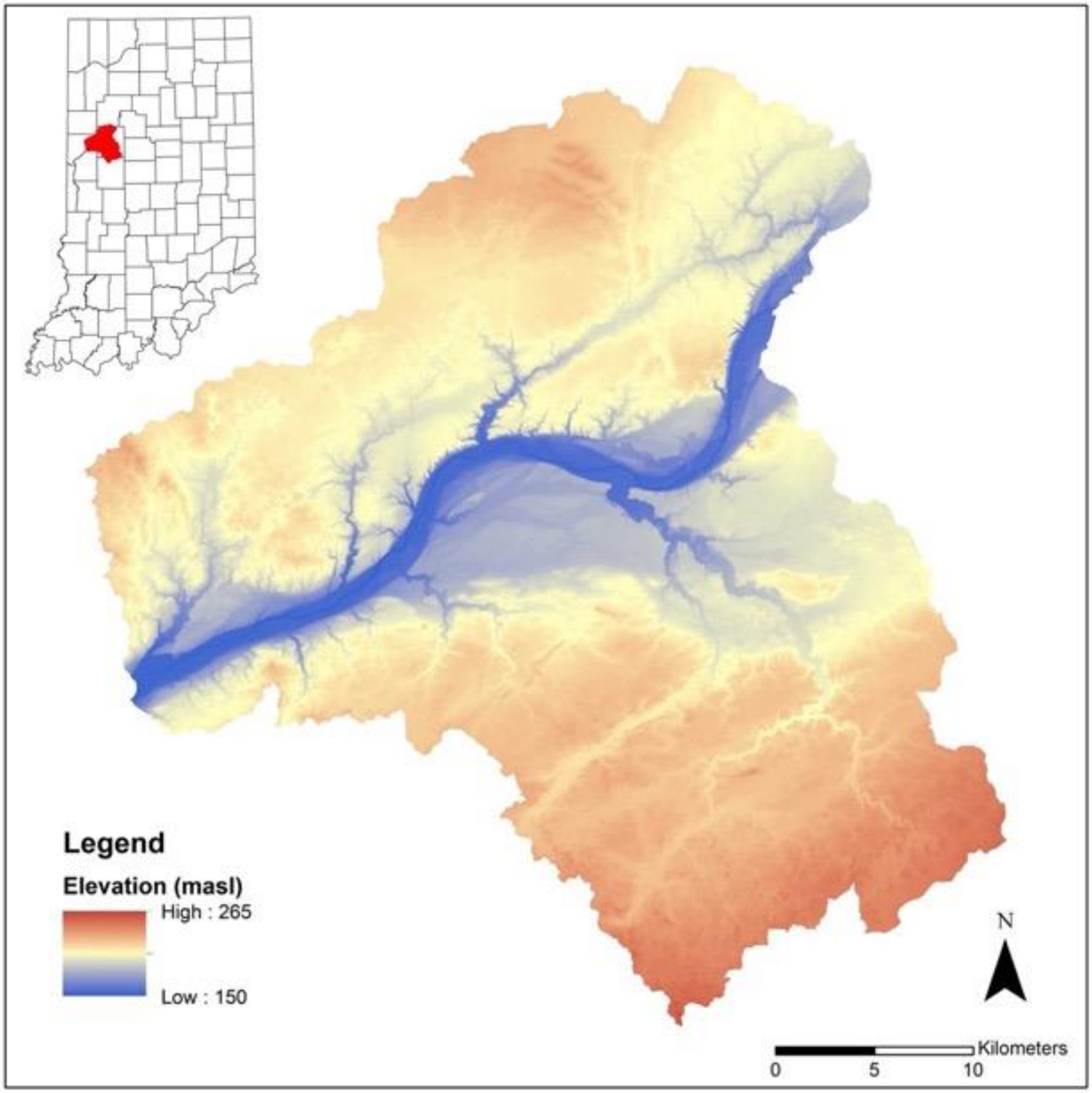

Figure 2.2. Topography of the catchment. Units are meters above sea level (masl).

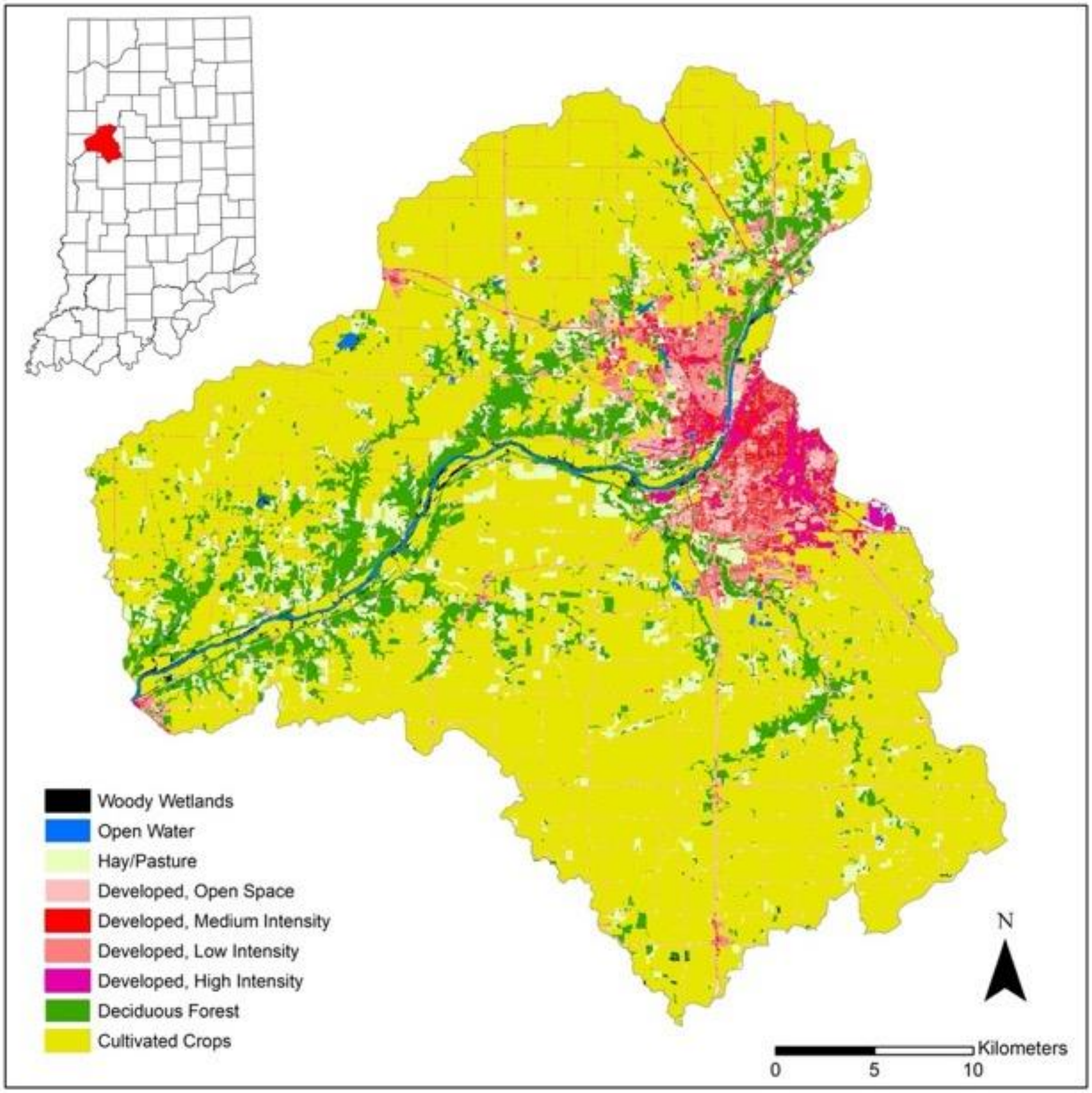

Figure 2.3. Land use within the catchment.

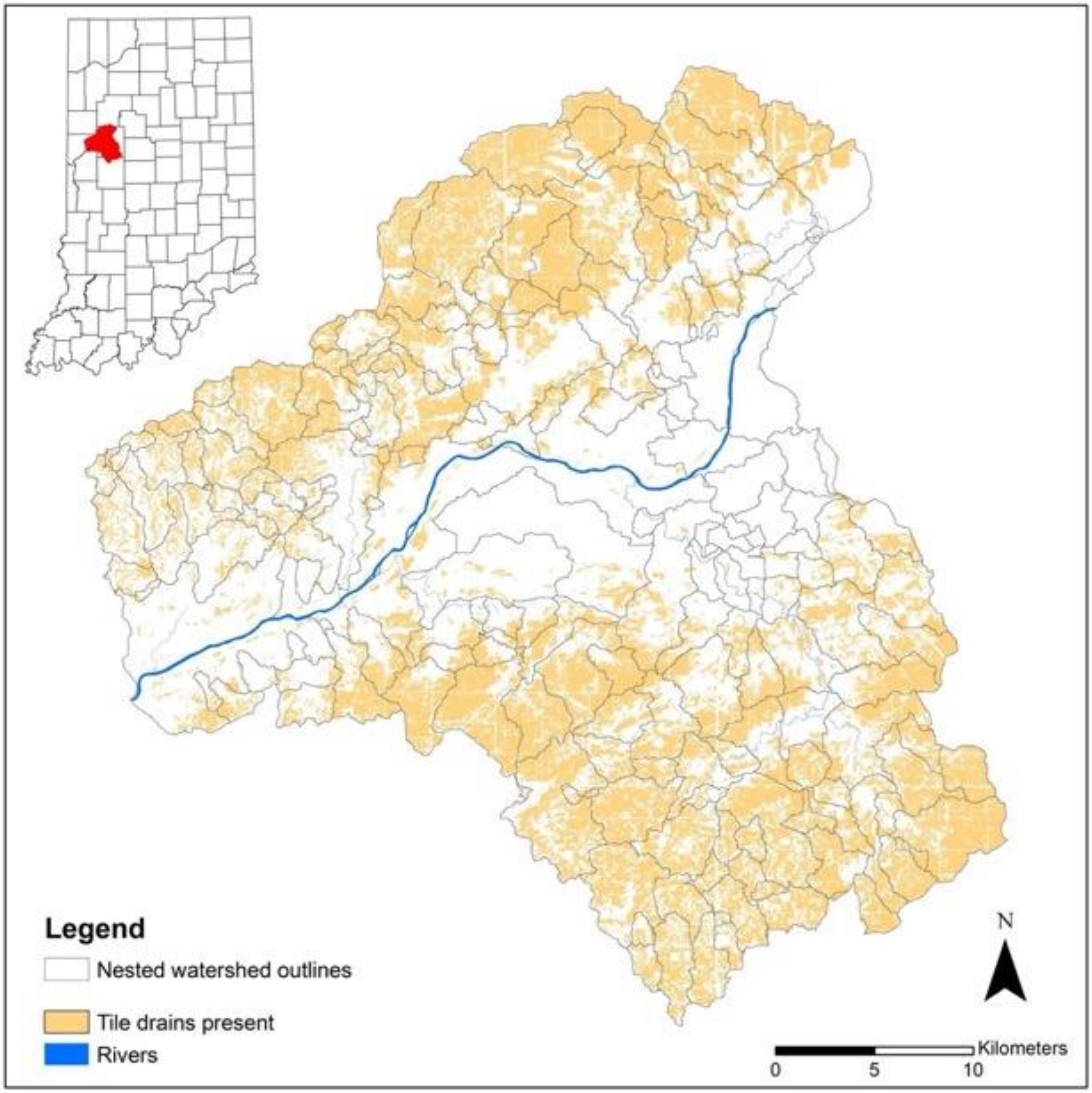

Figure 2.4. Tile drained areas within the catchment.

2.3.2 Citizen science water quality monitoring program

The Wabash River Enhancement Corporation (WREC) and researchers at Purdue University established a community science (also known as citizen science) water quality monitoring program in September 2009. As part of this program, community scientist volunteers collect stream samples from the sampling sites twice a year in April and September. All sampling sites are located where a public road and a stream intersect. At each site, they measure water transparency using a transparency tube with a secchi disc (cm), measure pH using field test strips, record water temperature (°C), and collect a water sample for further analyses. Samples were collected in approximately 250 mL wide-mouth bottles, and the sample bottles were rinsed with stream water three times prior to sample collection.

2.3.3 Nutrient measurements

The Purdue University Soil Science laboratory measured the concentration of ammonia-N (U.S. EPA, 1993a), nitrate plus nitrite-N (U.S. EPA, 1993b), and orthophosphate-P (U.S. EPA, 1993c) in each sample within 3 days following sample collection using an AQ2 Discrete Analyzer. Dissolved organic carbon (DOC) concentrations were measured during some sampling events using a Shimadzu TOC-V CSH with a detection limit of 4 μg/L. The detection limits for ammonia-N, nitrate plus nitrite-N, and orthophosphate-P are 0.004 mg/L, 0.03 mg/L, and 0.005 mg/L, respectively.

2.3.4 Stable water isotope measurements

The Purdue Stable Isotope (PSI) laboratory measured stable water isotope ratios (δ^2H and $\delta^{18}O$) for each water sample. Events after 2015 were analyzed using a laser absorption off-axis integrated cavity output spectrometer (Los Gatos Research (LGR) Triple Water Isotope Analyzer (TWIA)). Samples were injected ten times, discarding the first four to resolve memory effects and averaging the last six injections. Reproducible injection sizes minimized the water concentration dependence of the analyzer, but a small correction was made using the USGS LIMS post-processing software (Coplen & Wassenaar, 2015). Isotope ratios are expressed in δ notation in permil (‰) using Equation 2.1.

Equation 2.1

$$\delta = \left[\frac{R_{sample}}{R_{standard}} - 1\right] 1000$$

where R is the ratio of the heavy to light isotope ($^2H/^1H$ or $^{18}O/^{16}O$) in the sample or standard. All δ^2H and $\delta^{18}O$ values are reported relative to the Vienna Standard Mean Ocean Water (VSMOW) standard. Internal lab standards were used to define the VSMOW-SLAP scale. Analytical precision for repeated quality control samples was better than 0.2‰ for $\delta^{18}O$ and 1.0 ‰ for δ^2H. Deuterium excess (d_{excess}) is calculated for each sample using Equation 2.2.

Equation 2.2

$$d_{excess} = \delta^2\mathrm{H} - 8\,\delta^{18}\mathrm{O}$$

Each site was assigned a qualitative estimate of residence time based on that site's δ^2H and $\delta^{18}O$ standard deviations of repeat sampling over at least 4 events (Figure 2.5). Sites with δ^2H standard deviation $< 4.0‰$ and $\delta^{18}O$ standard deviation $< 0.75‰$ were classified as "Slow". Sites with δ^2H standard deviation $> 5.0‰$ and O standard deviation $> 1.0‰$ were classified as "Fast". All other sites were classified as "Medium". The δ^2H and $\delta^{18}O$ standard deviation criteria represents a simplification of the sine-wave approach for deriving travel time distributions (TTD) applied in previous publications (Jasechko et al., 2016; McGuire & McDonnell, 2006; Sprenger et al., 2019). Because all the sampling sites were in a relatively small geographic area, we assume the variability in the precipitation isotope values across the study area was similar. We propose that smaller standard deviations represent greater dampening of the seasonal cycle and intra-storm variability in precipitation stable isotope ratios by the watershed and indicate longer travel times than sites with larger standard deviations.

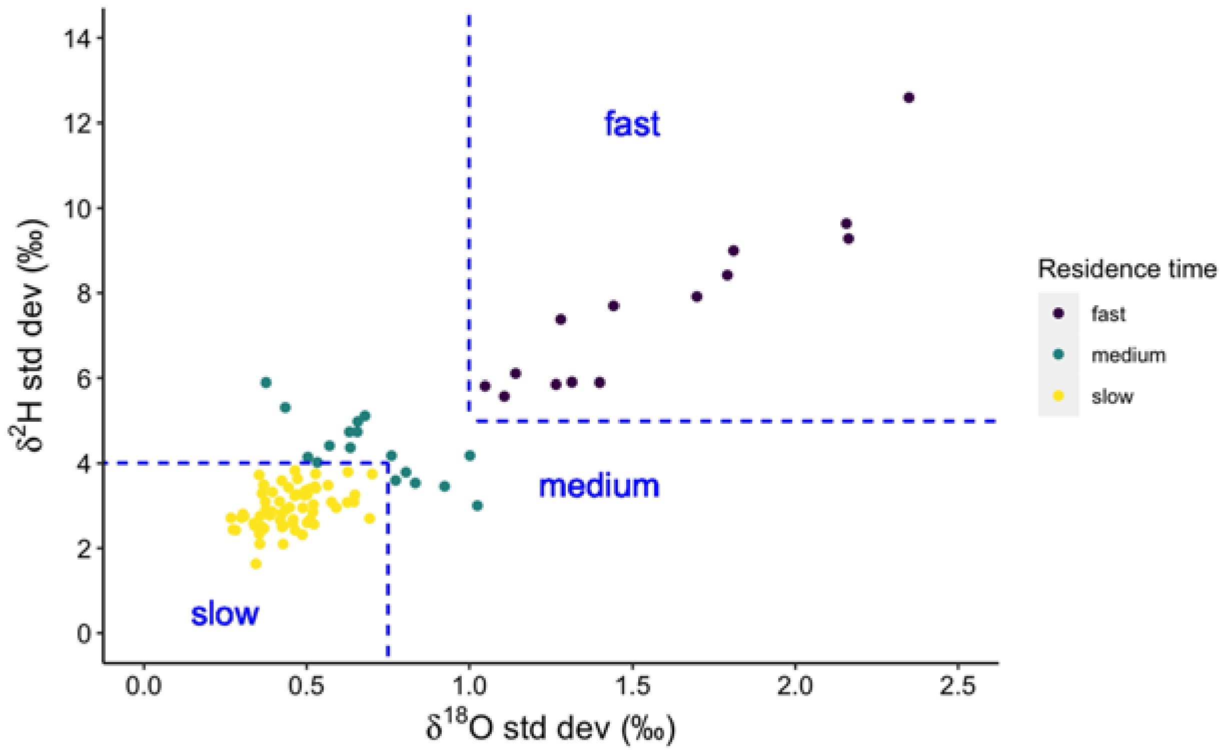

Figure 2.5. Each watershed's residence time was assigned to one of three classes based on its δ^2H and δ^{18}O standard deviations of repeat sampling over many years. Watersheds with larger standard deviations are classified as "faster" than watersheds with smaller standard deviations.

2.3.5 Tile drained area determination

Tile drained areas were estimated at 10-meter resolution within all watersheds using a method developed by Ale and Bowling (2010) that includes land use, soil drainage, and topography data. In this method, tile drained area includes any area that met the following three criteria: cropland land use; very poorly drained, poorly drained, or somewhat poorly drained soils; and slope <4%. Cropland was determined from the National Land Cover Database (NLCD) (Homer et al., 2012). Soil drainage classes were obtained from the Gridded National Soil Survey Geographic (gNATSGO) database (NRCS, 2019). Slope data was derived from the National Elevation Dataset (Gesch et al., 2018). All three datasets were imported into ArcMap 10.7, converted to raster format, and resampled at a 10-meter resolution. For each watershed, the fraction of tile drained area was calculated by dividing the tile drained grids by the total grids in the watershed.

2.3.6 Drainage score calculation

For the purpose of numeric correlation calculations with other measurements, 10-m resolution gNATSGO (NRCS, 2019) soil drainage classes were assigned a numerical drainage score and an area-weighted average was calculated to quantify the overall drainage condition in each watershed using Equation 2.3.

Equation 2.3

$$D = \frac{1(A_{VPD}) + 2(A_{PD}) + 3(A_{SPD}) + 4(A_{MWD}) + 5(A_{WD}) + 6(A_{SED}) + 7(A_{ED})}{A_T}$$

Where D is the watershed's numerical drainage score, A_{VPD} is the watershed area with very poorly drained soils, A_{PD} is the area with poorly drained soils, A_{SPD} is the area with somewhat poorly drained soils, A_{MWD} is the area with moderately well drained soils, A_{WD} is the area with well drained soils, A_{SED} is the area with somewhat excessively drained soils, A_{ED} is the area with excessively drained soils, and A_T is the total watershed area. Drainage scores can range from a minimum of 1 (the entire watershed is very poorly drained) to a maximum of 7 (the entire watershed is excessively drained), so watersheds with higher drainage scores have better overall drainage than watersheds with lower drainage scores.

2.3.7 Climate and meteorological conditions

The catchment's climate was determined from 1981 – 2010 monthly precipitation and temperature data collected at Purdue University Airport (IATA: LAF) near West Lafayette, Indiana (40.412°N, 86.937°W) (Arguez et al., 2010) (Table 2.1). The warmest month is July, and the coldest month is January. The wettest month is May, and the driest month is February. Precipitation is generally greatest from April to August with less precipitation during the fall and winter months.

Meteorological conditions prior to each sampling event were summarized using daily precipitation and temperature data from Purdue University Airport (Menne et al., 2012). Total precipitation, average daily high temperature, and average daily low temperature were calculated over 7-day time intervals leading up to each sampling event.

Table 2.1. Monthly normal precipitation and temperature data (1981-2010) for Purdue University Airport (IATA: LAF) near West Lafayette, Indiana.

Month	Normal Precipitation (mm)	Normal High Temperature (°C)	Normal Low Temperature (°C)
January	47.24	1.1	-7.2
February	44.70	3.7	-5.3
March	67.82	10.2	-0.4
April	89.82	17.2	4.9
May	106.43	22.8	10.4
June	104.14	28.1	15.8
July	100.84	29.4	17.9
August	87.88	28.8	17.1
September	67.56	25.4	12.5
October	73.41	18.4	6.4
November	75.44	10.7	1.3
December	63.75	3.1	-4.9
Annual	Total: 929.13	Mean: 16.6	Mean: 5.7

2.3.8 Moisture proxy

Streamflow from a gaging station was used as a proxy for moisture conditions within the study area. The USGS stream gage on Wildcat Creek near Lafayette, Indiana (USGS 03335000) records discharge in 15-minute intervals, and was used to determine general moisture conditions during each sampling event (U.S. Geological Survey, 2016). For each event, a 48-hour average discharge from 0:00 EST on the day prior to the sampling event to 23:45 EST on the day of the sampling event was calculated; higher average discharge indicates wetter conditions, and lower average discharge indicates drier conditions.

The stream gage on Wildcat Creek is located immediately to the east of the study area, but there is a stream gage within the study area on the Wabash River at Lafayette, Indiana (USGS 03335500). We elected to use the Wildcat Creek stream gage as the regional moisture proxy because the Wildcat Creek gage drains an area that is adjacent to our study area, has a similar size (2,056 km^2), and has similar physical characteristics. The Wabash River gage drains a much larger area (18,821 km^2), and therefore high discharge could be caused by precipitation and soil moisture conditions far upstream, outside of the study area.

2.3.9 Hydrologic connectivity proxy

We used the coefficient of determination between the percent of the watershed that is tile drained and nitrate concentrations (r^2) as a proxy for hydrologic connectivity for each sampling event (n = up to 205). Our hypothesis is that nitrate concentrations are strongly controlled by the percent of tile drained area. Tile drain discharge is initiated when both a soil moisture threshold is met and the water table is raised above the depth of the tile drains (Cain et al., in review). If both of these conditions are not met, then tile drain discharge is negligible. Areas drained by tiles must be hydrologically connected to the stream network when the tile drains are actively discharging, but these same areas have greatly reduced hydrologic connectivity when the tile drains are not discharging. We infer that there is greater hydrologic connectivity across the landscape when the r^2 is larger, but there is reduced landscape connectivity when r^2 is smaller.

2.3.10 Data analysis

The statistical software R (R Core Team, 2019) was used for data analysis. Sites had to meet the following criteria for inclusion in data analysis: 1) sampled at least 4 times, 2) had > 50% agricultural land use, and 3) had a watershed area > 5 km^2. A total of 96 sites met these criteria. Only agricultural sites were included to reduce bias from urban sites that had much smaller tile drained area percentages and much more impervious area. We used the 5 km^2 watershed area threshold because smaller sites were often associated with headwater streams and ditches that frequently held stagnant water with highly enriched δ^2H and δ^{18}O caused by evaporation. The means and standard deviations for water temperature, pH, DOC, nitrate, ammonia, orthophosphate, δ^2H, δ^{18}O, and d_{excess} were calculated for each site. Seasonal (spring and fall) means and standard deviations were also calculated for these variables at each site using only the data from the respective season's sampling events. Nutrient loads were not calculated because only two samples were collected per year and sites lacked discharge data for each event.

Seasonal differences in water chemistry and meteorological variables were evaluated using Welch's two-sample t-tests. Variables with non-normal distributions were log transformed to approximate normal distributions. Relationships between water chemistry, meteorological, and land use variables were analyzed with linear regression models. Water chemistry and land use differences between residence time classes were evaluated with analysis of variance (ANOVA) models.

2.4 Results

2.4.1 Meteorological conditions

The temperatures and antecedent moisture conditions varied considerably across the various sampling events.

Table 2.2 contains precipitation totals and mean daily high and low temperatures for the 7 days leading up to each sampling event. Precipitation in the week prior ranged from a minimum of 0.0 mm (multiple events) to a maximum of 34.5 mm (fall 2014). Spring events were slightly wetter with the average 7-day precipitation totals before spring and fall events of 13.6 mm and 10.9 mm, respectively, but the difference was not significant ($t = 0.61; df = 18; p = 0.55$).

The average daily high temperature over the week prior was 22.2°C with a minimum of 10.7°C (spring 2016) and a maximum of 30.9°C (fall 2013). The average daily low temperature over the 7-day period was 9.7°C, and the minimum and maximum were -1.0°C (spring 2016) and 17.5°C (fall 2013), respectively. Mean daily high and low temperatures were significantly warmer leading up to fall events over the 7-day time periods (high: $t = 5.18; df = 18; p < 0.001$, low: $t = 5.27; df = 18; p < 0.001$).

Several sampling events had unusually wet or dry conditions as indicated by discharge from the nearby Wildcat Creek. The spring 2012 event was exceptionally dry and occurred during the initial stages of the 2012 Midwest drought (Mallya et al., 2013). The spring 2014 event was exceptionally wet, and it had the highest 7-day precipitation total among spring sampling events (Table 2.2). The fall 2014 and fall 2018 events were wetter than other fall events, and both events had high 7-day precipitation totals and low daily temperatures. The low temperatures likely reduced evapotranspiration (ET), so more precipitation contributed to streamflow.

Table 2.2. Precipitation totals and mean daily high and low temperatures for 2, 7, and 30 days prior to each sampling event. Wildcat Creek discharge for each event is also reported. Mean daily temperatures and precipitation totals were derived from measurements at Purdue University Airport (IATA: LAF). Mean daily high and low temperatures are reported ±1 standard deviation.

Sampling Event	Date (MM/DD/YY)	Precip., prior 7 days (mm)	Mean Daily High Temp., prior 7 days (°C)	Mean Daily Low Temp., prior 7 days (°C)	Wildcat Creek Discharge, prior 48 hours ($ft^3 s^{-1}$)	Wildcat Creek Discharge Cumulative Percentile (%)
Fall 2009	09/18/09	0.3	28.0 ± 1.7	12.1 ± 2.2	97	1.91
Spring 2010	04/09/10	19.4	20.5 ± 5.7	8.8 ± 6.7	1347	78.99
Fall 2010	09/17/10	5.2	27.5 ± 3.1	12.7 ± 2.3	132	8.49
Spring 2011	04/15/11	12.5	21.7 ± 4.6	8.0 ± 5.4	945	69.81
Fall 2011	09/16/11	7.8	24.4 ± 5.3	11.9 ± 3.8	123	5.94
Spring 2012	04/13/12	0.0	16.8 ± 3.4	1.9 ± 4.3	257	30.04
Fall 2012	09/28/12	7.7	19.1 ± 2.9	7.2 ± 5.1	170	17.31
Spring 2013	05/10/13	16.8	21.9 ± 2.7	10.5 ± 2.0	829	66.00
Fall 2013	09/13/13	20.3	30.9 ± 5.4	17.5 ± 4.1	124	6.34
Spring 2014	04/11/14	25.1	14.8 ± 4.4	2.3 ± 3.7	2497	89.98
Fall 2014	09/12/14	34.5	21.9 ± 4.5	11.6 ± 2.8	494	49.18
Spring 2015	04/17/15	4.1	18.9 ± 2.8	6.4 ± 3.3	800	64.92
Fall 2015	09/11/15	11.2	29.0 ± 4.9	16.8 ± 2.6	154	14.05
Spring 2016	04/08/16	19.8	10.7 ± 4.0	-1.0 ± 3.3	1278	77.81
Fall 2016	09/16/16	11.2	26.0 ± 2.0	14.0 ± 2.8	NA	NA
Fall 2017	09/29/17	0.0	28.5 ± 4.5	14.1 ± 4.2	147	12.27
Spring 2018	04/13/18	2.8	11.8 ± 9.2	1.8 ± 8.7	910	68.80
Fall 2018	09/14/18	21.3	23.9 ± 4.7	12.9 ± 1.9	1033	72.30
Spring 2019	04/10/19	22.2	17.9 ± 4.5	7.0 ± 2.9	1239	77.09
Fall 2019	09/13/19	0.3	29.0 ± 4.1	17.2 ± 3.3	148	12.46

2.4.2 Water chemistry

Key water quality parameters for each sampling event are summarized in Table 2.3. The average nitrate concentration was 3.68 mg L^{-1} with a minimum of 1.00 mg L^{-1} (fall 2011) and a maximum of 8.89 mg L^{-1} (spring 2019). Ammonia concentrations averaged 0.09 mg L^{-1}, and the minimum and maximum concentrations were 0.00 mg L^{-1} (fall 2012) and 0.20 mg L^{-1} (spring 2019), respectively. Orthophosphate concentrations varied from 0.02 mg L^{-1} (multiple events) to 0.30 mg L^{-1} (fall 2019) with an average of 0.09 mg L^{-1}. The mean DOC concentration for the limited event analysis was 2.92 mg L^{-1}, and the minimum and maximum were 2.46 mg L^{-1} (spring 2011) and 3.29 mg L^{-1} (fall 2009), respectively. The average transparency was 76.3 cm with a minimum of 16.6 cm (fall 2019) and a maximum of 108.7 (spring 2012). Water temperatures ranged from 9.6°C (spring 2011) to 21.6°C (fall 2018), and the average was 15.3°C. The average lab-measured pH was 7.4 with a range from 6.5 (fall 2009) to 8.1 (spring 2010).

Table 2.3. Mean values (±1 standard deviation) for key water quality parameters from each sampling event. "NA" indicates that the parameter was not measured for that event.

Sampling Event	Nitrate-N (mg L^{-1})	Ammonia (mg L^{-1})	Ortho phosphate (mg L^{-1})	DOC (mg L^{-1})	Transparency (cm)	Water Temperature (°C)	pH
Fall 2009	1.17 ± 1.74	0.19 ± 0.93	0.10 ± 0.34	3.29 ± 1.90	NA	18.5 ± 2.6	6.5 ± 0.5
Spring 2010	5.83 ± 2.01	0.10 ± 0.03	0.04 ± 0.10	2.86 ± 2.78	NA	12.5 ± 1.6	8.1 ± 0.4
Fall 2010	1.12 ± 1.22	0.11 ± 0.05	0.08 ± 0.08	3.08 ± 1.97	78.7 ± 32.7	18.0 ± 4.1	7.9 ± 0.4
Spring 2011	5.84 ± 2.37	0.10 ± 0.00	0.02 ± 0.01	2.46 ± 2.51	105.7 ± 24.2	9.6 ± 2.6	7.1 ± 0.2
Fall 2011	1.00 ± 1.66	0.10 ± 0.02	0.06 ± 0.28	NA	89.3 ± 34.5	12.5 ± 3.5	7.4 ± 0.4
Spring 2012	3.22 ± 2.24	0.17 ± 0.38	0.05 ± 0.12	NA	108.7 ± 17.5	12.7 ± 2.3	7.2 ± 0.2
Fall 2012	1.22 ± 2.38	0.00 ± 0.12	0.11 ± 0.30	NA	93.4 ± 32.2	15.4 ± 2.7	7.3 ± 0.3
Spring 2013	6.28 ± 2.40	0.05 ± 0.04	NA	NA	NA	13.8 ± 2.3	7.7 ± 0.5
Fall 2013	NA	NA	NA	NA	34.6 ± 39.9	17.6 ± 2.8	NA
Spring 2014	6.94 ± 2.52	0.03 ± 0.11	0.04 ± 0.04	NA	58.8 ± 36.8	13.8 ± 2.3	7.0 ± 0.6
Fall 2014	3.18 ± 2.66	0.02 ± 0.12	0.06 ± 0.06	NA	74.7 ± 40.0	15.6 ± 1.5	7.4 ± 0.4
Spring 2015	4.70 ± 1.72	0.01 ± 0.02	0.02 ± 0.04	NA	92.5 ± 31.3	15.1 ± 3.7	7.9 ± 0.3
Fall 2015	1.47 ± 1.76	0.08 ± 0.27	0.09 ± 0.14	NA	80.8 ± 34.7	16.8 ± 2.5	7.6 ± 0.3
Spring 2016	6.80 ± 1.92	0.01 ± 0.04	0.02 ± 0.02	NA	78.9 ± 33.1	NA	7.6 ± 0.3
Fall 2016	3.14 ± 1.50	0.03 ± 0.09	0.06 ± 0.06	NA	91.8 ± 26.5	17.9 ± 5.4	7.5 ± 0.5
Fall 2017	1.04 ± 0.69	0.13 ± 0.08	0.17 ± 0.13	NA	NA	15.1 ± 5.1	7.3 ± 0.5
Spring 2018	4.90 ± 3.33	0.10 ± 0.05	0.07 ± 0.08	NA	NA	13.2 ± 10.1	7.2 ± 0.8
Fall 2018	1.74 ± 1.66	0.10 ± 0.07	0.21 ± 0.31	NA	NA	21.6 ± 3.1	7.0 ± 0.8
Spring 2019	8.89 ± 2.98	0.20 ± 0.13	0.22 ± 0.17	NA	62.9 ± 37.5	NA	NA
Fall 2019	1.41 ± 4.03	0.13 ± 0.16	0.30 ± 0.82	NA	16.6 ± 14.7	NA	NA
Fall Mean	**1.65 ± 2.21**	**0.09 ± 0.33**	**0.12 ± 0.33**	**3.18 ± 1.93**	**71.4 ± 41.7**	**16.9 ± 4.3**	**7.3 ± 0.6**
Spring Mean	**5.90 ± 2.88**	**0.09 ± 0.16**	**0.06 ± 0.11**	**2.68 ± 2.66**	**86.7 ± 65.2**	**13.0 ± 4.8**	**7.5 ± 0.6**
Overall Mean	**3.61 ± 3.30**	**0.09 ± 0.26**	**0.09 ± 0.26**	**2.94 ± 2.33**	**78.4 ± 54.3**	**15.4 ± 4.9**	**7.4 ± 0.6**

Event-mean nitrate concentrations varied by season, antecedent moisture conditions, and landscape hydrologic connectivity. Spring nitrate concentrations were significantly greater than fall nitrate concentrations in agricultural watersheds larger than 5 km^2 ($t = 41.94$; $df = 1669$; $p < 0.001$); the average nitrate concentration was 5.90 ± 2.88 mg L^{-1} in spring and 1.65 ± 2.21 mg L^{-1} in fall (Figure 2.6). Event-mean nitrate concentrations were significantly greater during wetter conditions (Figure 2.7A) ($r^2 = 0.641$; $F_{1,16} = 28.6$; $p < 0.001$). Antecedent moisture did not completely explain the seasonal variability in nitrate concentrations. Spring sampling events had greater nitrate concentrations than fall events with similar discharges. Most of the fall events (gold points) form a tight cluster with discharge around 150 ft^3 s^{-1} and nitrate concentrations around 1.5 mg L^{-1} (Figure 2.7A). We interpret this cluster as representing baseflow conditions and used this data to estimate the average groundwater nitrate concentration in the study area. The coefficient of determination (r^2) between site-level nitrate concentrations and percent tile drained area also varied substantially among sampling events (Figure 2.7B). We interpret larger correlation coefficients as a proxy for greater landscape hydrologic connectivity. Events with low nitrate concentrations had the lowest r^2 values. Events with intermediate nitrate concentrations had the highest r^2 values, but r^2 values decreased at the highest nitrate concentrations.

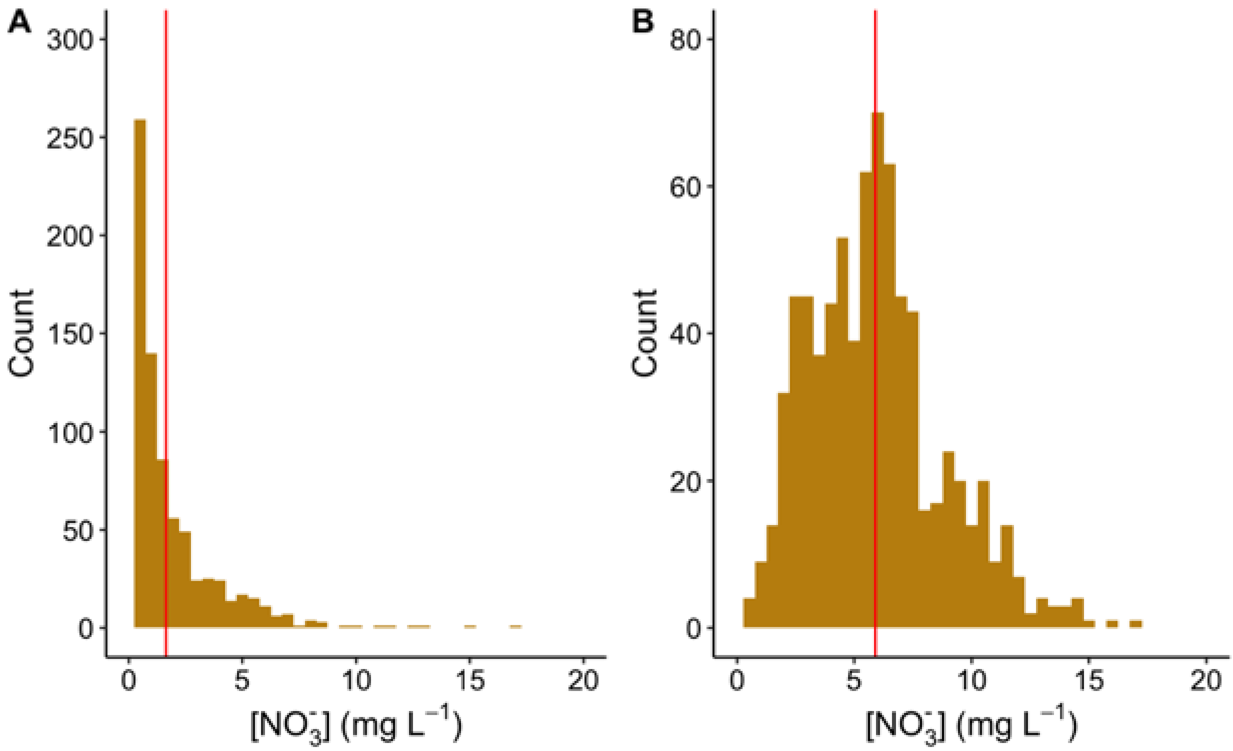

Figure 2.6. Histograms of nitrate concentrations (mg L^{-1}) from fall (**A**) and spring (**B**) sampling events. The vertical red lines indicate the mean concentration for each season (1.65 mg L^{-1} for fall and 5.90 mg L^{-1} for spring). Only measurements from watersheds larger than 5 km^2 with > 50% agricultural land use are included.

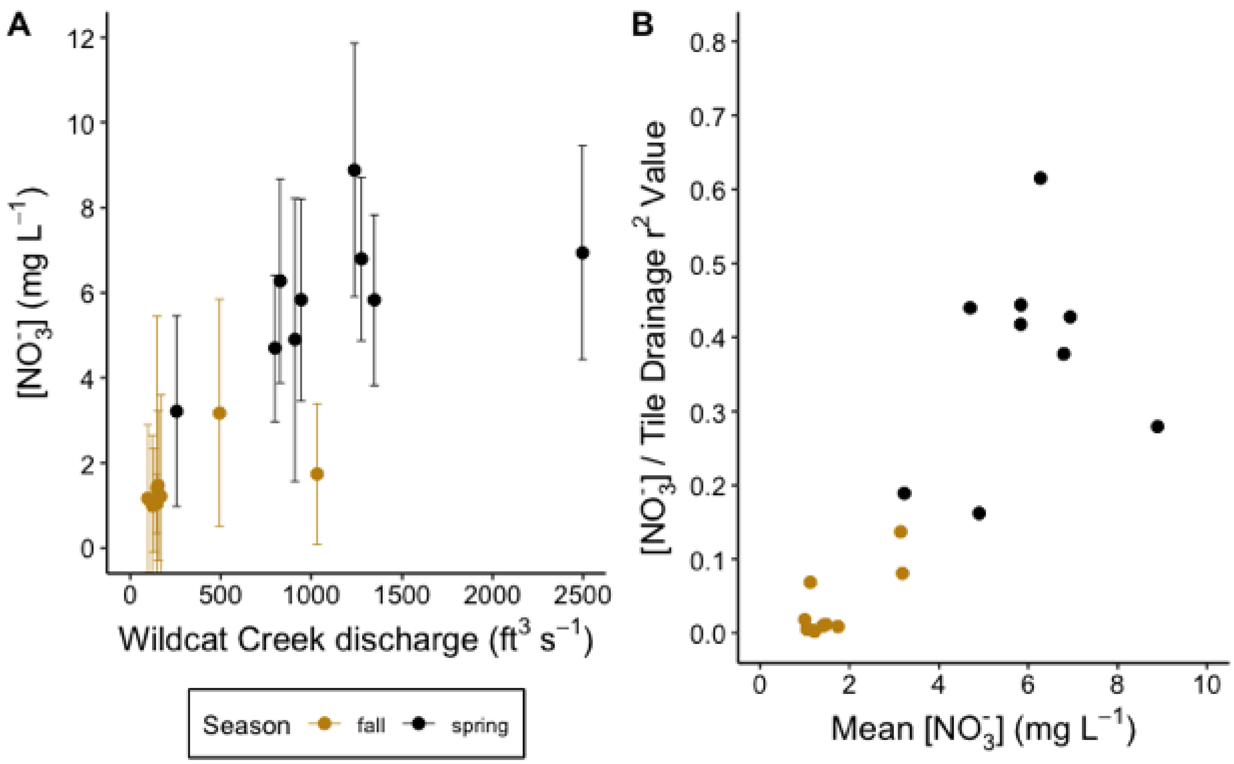

Figure 2.7. (**A**) Mean nitrate concentrations and Wildcat Creek discharge (moisture proxy) for each sampling event. (**B**) The coefficient of determination (r^2) between nitrate concentrations and percent tile drained area for each sampling event reflects landscape hydrologic connectivity. Event r^2 was lowest during events with low mean nitrate concentrations and low creek discharge, and it was greatest during events with intermediate nitrate concentrations and higher creek discharge. Events with the highest nitrate concentrations had lower r^2 values than events at intermediate concentrations. Gold and black points indicate fall and spring sampling events, respectively.

The presence of agricultural tile drains was a strong predictor of stream nitrate concentrations. Mean nitrate concentrations during spring sampling events were significantly greater in agricultural watersheds with a greater percentage of tile drained area ($r^2 = 0.503$; $F_{1,94} = 95.29$; $p < 0.001$) (Figure 2.8A). Mean spring nitrate concentrations were also greater in watersheds with greater percent agricultural land use ($r^2 = 0.295; F_{1,94} = 39.36; p < 0.001$), although this correlation was weaker than with tile drained area (Figure 2.8B). Agricultural watersheds with greater mean spring nitrate concentrations had significantly lower drainage scores ($r^2 = 0.527; F_{1,94} = 104.7; p < 0.001$) indicating poorer overall drainage conditions and likely presence of tile drainage (Figure 2.8C). Since the tile drained area was identified based on soil drainage scores, it had a strong negative relationship with drainage score ($r^2 = 0.834; F_{1,94} = 472.4; p < 0.001$) (Figure 2.8D).

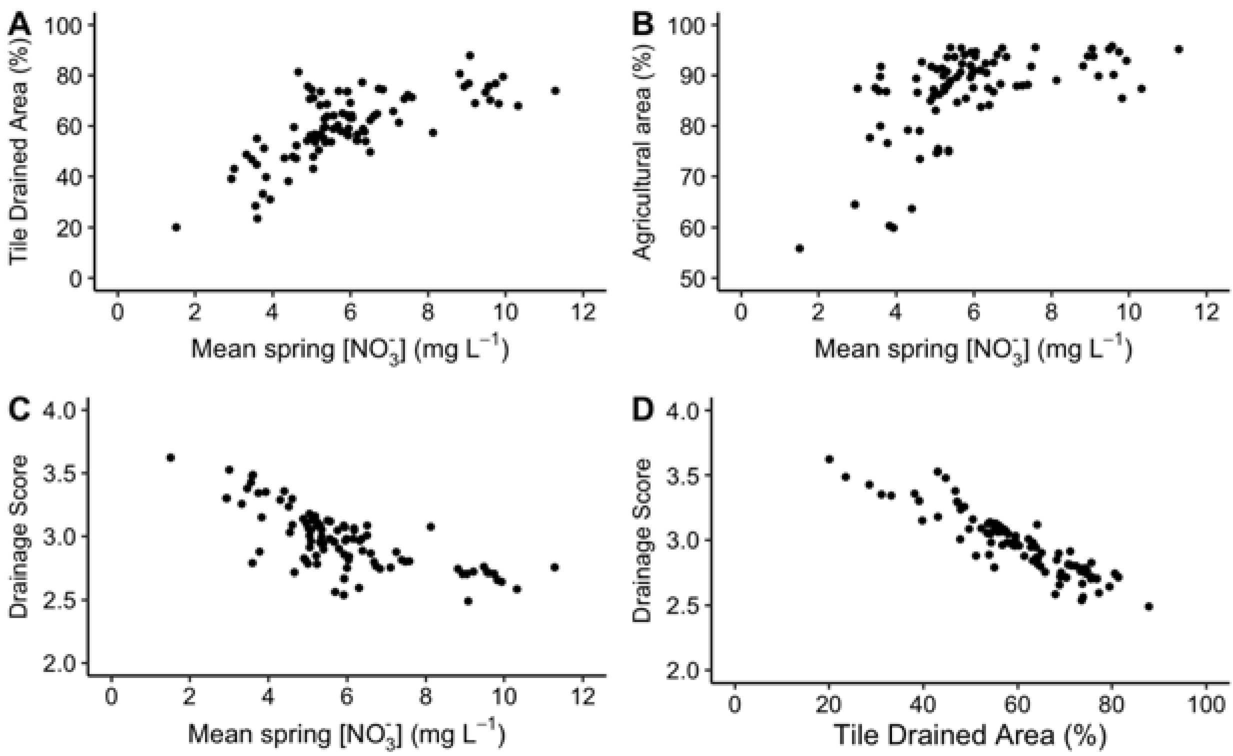

Figure 2.8. Agricultural watersheds > 5 km^2 with greater mean nitrate concentrations during spring tend to have (**A**) more tile drained area ($r(96) = 0.710$, $p < 0.001$), (**B**) more agricultural area ($r(96) = 0.543$, $p < 0.001$), and (**C**) lower drainage scores (which indicate poorer overall drainage) than watersheds with lower nitrate concentrations ($r(96) = -0.726$, $p < 0.001$). Tile drained area has a strong negative correlation with drainage score ($r(96) = -0.913$, $p < 0.001$) (**D**) because tile drains are assumed to be installed in poorly drained areas.

Watershed area influenced the variability of the 10-year mean spring nitrate concentrations across sites. The mean nitrate variations were largest among the small watersheds and decreased among larger watersheds (Figure 2.9). Among the smallest watersheds (< 100 km^2), mean spring nitrate concentrations ranged from 1.51 mg L^{-1} to 11.29 mg L^{-1} and had a robust relationship with tile drained area ($r^2 = 0.49$). As the smaller watersheds merge into larger watersheds downstream, the mean spring nitrate concentrations converged towards a mean value of 5.23 $\pm$ 0.81 mg L^{-1} for watersheds larger than 100 km^2.

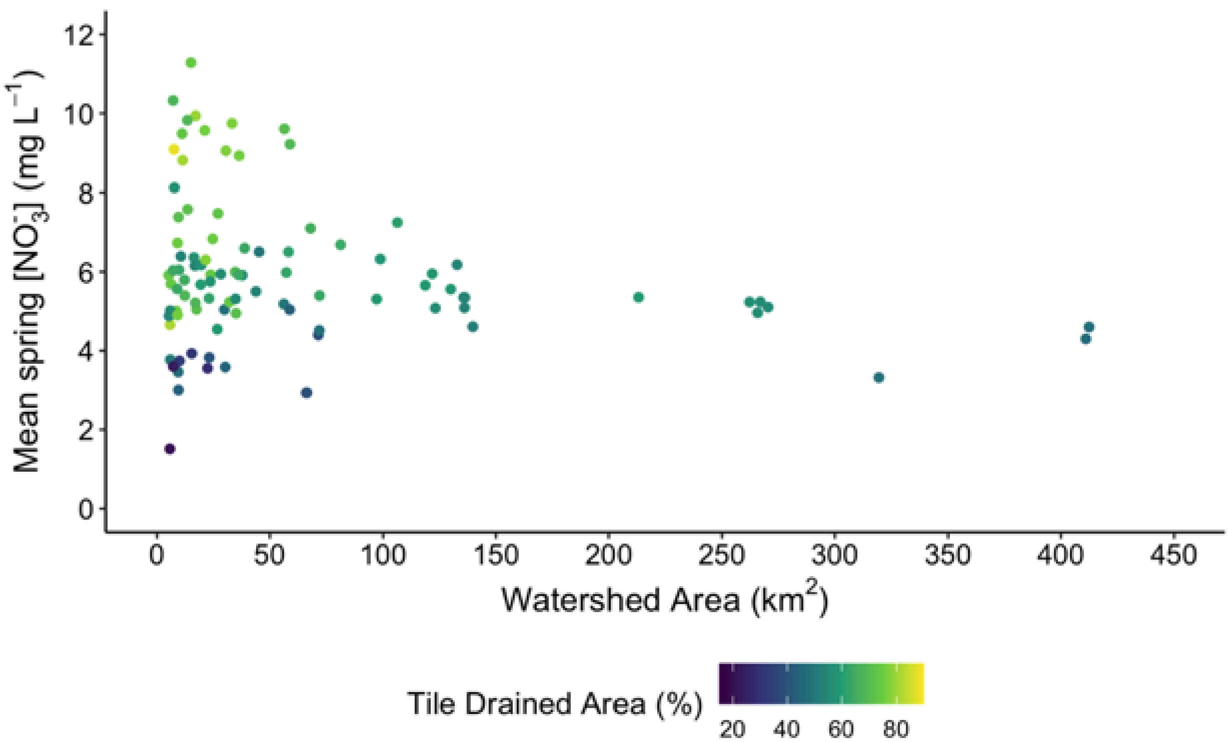

Figure 2.9. Mean spring nitrate varied widely in smaller watersheds (< 100 km^2), but concentrations in larger watersheds (> 100 km^2) converged towards an average of 5.23 $\pm$ 0.81 mg L^{-1}. The smaller watersheds had a fairly robust relationship ($r^2 = 0.49$) between concentration and tile drained area.

Classifying the watersheds into 4 classifications with similar size and tile drainage characteristics revealed an interesting pattern between antecedent moisture conditions and nitrate concentrations (Figure 2.10). Nitrate concentrations were generally greater during wetter sampling events but pronounced peaks of higher concentrations appeared in all 4 groups during intermediate moisture conditions.

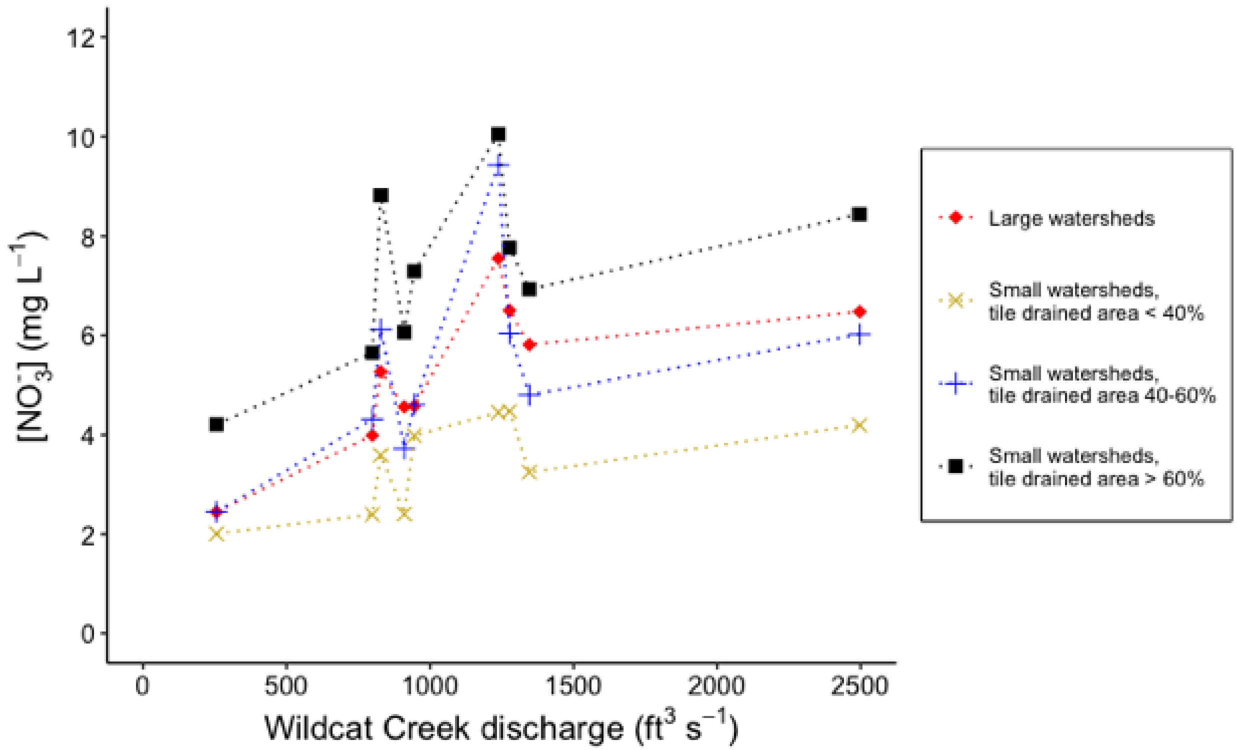

Figure 2.10. Spring nitrate concentrations averaged for watershed size and tile drained area classifications. All 4 classifications had broadly similar patterns between nitrate concentration and antecedent moisture. Spring nitrate concentrations generally increased under wetter conditions, but a peak of higher concentrations appeared during sampling events with intermediate antecedent moisture conditions.

2.4.3 Relationship between stable isotopes and nitrate concentrations

Mean spring nitrate concentrations were significantly greater in watersheds classified as "fast" than in watersheds classified as "medium" or "slow" based on their δ^2H and $\delta^{18}O$ standard deviations ($F_{2,93} = 12.4; p < 0.001$). Spring nitrate concentrations in watersheds classified as "medium" were not significantly different from "slow" watersheds (Figure 2.11A). "Fast" watersheds also had significantly greater tile drained areas than "slow" watersheds ($F_{2,93} = 3.518; p = 0.03$). Tile drained areas in "medium" watersheds do not significantly differ from "fast" or "slow" watersheds (Figure 2.11B). Drainage scores are significantly lower in "fast" watersheds than in "medium" and "slow" watersheds ($F_{2,93} = 6.645; p = 0.002$). "Medium" watersheds do not have significantly different drainage scores from "slow" watersheds (Figure 2.11C). It seems counter-intuitive that "fast" watersheds have lower drainage scores (i.e. more poorly drained) than "medium" and "slow" watersheds, but watersheds with lower drainage scores also have more tile drained area (Figure 2.8D). The increased prevalence of tile drains in watersheds with low drainage scores and the resulting drainage improvement could explain these results.

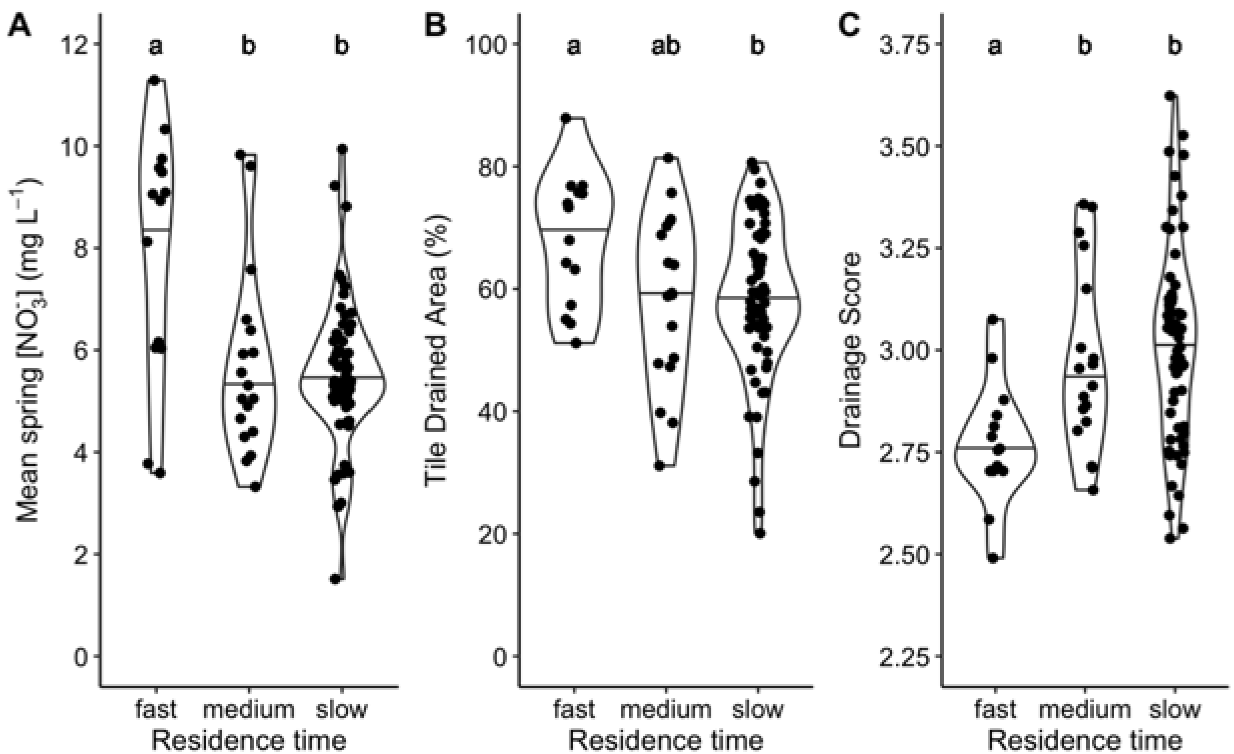

Figure 2.11. (**A**) "Fast" watersheds have significantly greater spring nitrate concentrations than "medium" or "slow" watersheds ($F_{2,93} = 12.4; p < 0.001$; Tukey HSD post-hoc test). (**B**) "Fast" watersheds have significantly more percent tile drained area than "slow" watersheds but are not significantly different from "medium" watersheds ($F_{2,93} = 3.518; p = 0.03$; Tukey HSD post-hoc test). (**C**) "Fast" watersheds also have significantly lower drainage scores than "medium" or "slow" watersheds ($F_{2,93} = 6.65; p = 0.002$; Tukey HSD post-hoc test). Median values are indicated by the horizontal lines within the violin plots, and significant differences are indicated by different lower-case letters.

2.5 Discussion

2.5.1 Seasonality

The agricultural watersheds in this study displayed clear seasonal differences in nitrate concentrations with greater concentrations observed during spring than in fall (Figure 2.6). Seasonal differences have previously been documented in the literature, but the specifics depend on land management timing and seasonal precipitation differences. Poor and McDonnell (2007) observed greater concentrations in the fall and winter because the application of N-rich manure and vegetable waste in their study system occurs in late summer and most precipitation occurs during fall and winter. Other studies from agricultural catchments in the midwestern United States find seasonal differences that are similar to what we observed in this study. A study in Michigan observed much higher nitrate concentrations in spring and summer than in fall and winter (Castillo et al., 2000). Two studies in east-central Illinois and another in Iowa also observed similar spring maximums (Cambardella et al., 1999; Gentry et al., 2009; Mitchell et al., 2000). A study of a central Indiana watershed observed the highest nitrate concentrations from December through July (Fenelon & Moore, 1998), and another study of an agricultural watershed in Ohio found the greatest concentrations from April to June (Tian et al., 2016). Higher spring nitrate concentrations coupled with higher discharge during spring result in higher loads during this season. A long-term study in central Ohio found consistently higher nitrate loads during higher discharges (King et al., 2016).

2.5.2 Tile drain influence

Percent tile drained area was a better predictor of stream nitrate concentrations than percent agricultural land use (Figure 2.8A, B). The role of tile drains in nitrate transport is especially clear in the smaller watersheds (< 100 km^2) where nitrate concentrations increased with greater tile drainage (Figure 2.9 and Figure 2.10). The relationship between nitrate concentrations and watershed area in this study is similar to hydrologic behaviors observed in previous studies (Frisbee et al., 2011; Uchida et al., 2005). It seems counter intuitive that poorly drained watersheds had faster travel times and greater nitrate concentrations (Figure 2.8C and Figure 2.11C), but poorly drained watersheds also had increased percent agricultural tile drained area (Figure 2.8D). The stable isotope travel time classifications provided further evidence that tile drainage shortens hydrologic landscape travel times (Figure 2.11B). These observations support the findings in Schilling et al. (2012, 2015) where increasing tile drainage intensity in groundwater travel time models reduced mean travel times by over 50%.

2.5.3 Antecedent moisture conditions

We observed greater nitrate concentrations during “wet” sampling events (Figure 2.7). Several other studies in agricultural watersheds also report greater nitrate concentrations when discharge is greater, although the magnitude of this relationship varies (Tiemeyer et al., 2006; Tomer et al., 2003). While nitrate concentrations generally increased under wetter conditions, the greatest nitrate concentrations we observed occurred during intermediate moisture condition events (Figure 2.10). Hansen and Singh (2018) used high-frequency data and observed that peak nitrate lags behind peak discharge in event hydrographs, so the greatest nitrate concentrations often occur during intermediate discharge. They argue that the offset between nitrate and discharge means that storm frequency is a more important driver of total nitrate export than storm magnitude.

Poor and McDonnell (2007) refer to positive relationships between discharge and nitrate concentration in event hydrographs as a “concentration” effect, and an inverse relationship between these two variables is a “dilution” effect. Dilution effects are often observed in nitrate source-limited systems, but concentration effects are usually observed in systems with a saturated nitrate source (Davis et al., 2014; Murphy et al., 2014; Poor & McDonnell, 2007). Our results suggest that the Great Bend of the Wabash River catchment experiences a concentration effect, implying that it has a saturated nitrate source. Previous work with a variety of geogenic solutes has revealed relatively constant concentrations over orders of magnitude changes in discharge, which is a hallmark of chemostatic behavior and results in linear load-discharge relationships (Godsey et al., 2009). Multiple studies on the concentration-discharge relationship for nitrate have observed non-chemostatic behavior at daily and monthly time scales (Basu et al., 2010; Guan et al., 2011), but long-term monitoring data from large watersheds within the MRB reveal consistently linear load-discharge relationships at the annual time scale (Basu et al., 2010). Several sources suggest this chemostatic behavior at longer time scales indicates that nitrate loss to streams is a transport-limited process instead of supply-limited, and annual accumulation of excess fertilizer over the last 75 years results in a legacy N source in the landscape (Basu et al., 2010; Haag & Kaupenjohann, 2001; Ilampooranan et al., 2019). Patterns in nitrate concentration data from the MRB could support this hypothesis: nitrate concentrations increased from 1950-1975 when fertilizer use greatly increased, but concentrations stabilized after 1975 (Aulenbach et al., 2007). Basu et al., (2010) suggest that the increase from 1950-1975 reflects the accumulation of legacy N, and the stabilized concentrations after 1975 indicate a shift from a supply-limited landscape to a transport-limited one. Legacy N limits the effectiveness of agricultural best management practices (BMPs) because most BMPs treat surface runoff but legacy N in soils and groundwater are not being treated (Ilampooranan et al., 2019; Schilling et al., 2015). Even if BMPs are extensively implemented throughout the MRB, it will take several decades to meet N reduction goals because of legacy N (Van Meter et al., 2018).

Hydrologic connectivity and N availability are important controls on tile drain flow and N export, and antecedent moisture conditions are an important factor in hydrologic connectivity (McMillan et al., 2018). More watershed area becomes hydrologically connected to the stream network under increasingly wet antecedent conditions, so there is a potential for greater N loss, especially if the newly connected areas were disconnected for enough time to allow N accumulation in the soil (Hornberger et al., 1994). Under dry antecedent conditions, more area becomes increasingly disconnected from both the stream network and deeper groundwater, which reduces N loss pathways but increases stored N (Davis et al., 2014). The greatest nitrate concentrations occur during spring events with intermediate moisture conditions (Figure 2.7A), and the connectivity proxy also appears greatest at intermediate nitrate concentrations (Figure 2.7B). The greatest connectivity is observed at intermediate nitrate concentrations because those sampling events also have the wettest antecedent conditions.

2.5.4 Groundwater nitrate concentrations

The inferred average groundwater nitrate concentration was about 1.5 mg L^{-1} based on the cluster of baseflow events in Figure 2.7. This estimate is most representative of shallow, phreatic aquifers, but it is also consistent with concentrations reported for deeper municipal water wells in the study area with reported nitrate concentrations between 0.42 to 1.83 mg L^{-1} from 2014-2019 (City of Lafayette, 2019). Although near-surface aquifer sensitivity is classified as moderate or high across most of the catchment based on groundwater recharge rates (Letsinger, 2015), our findings suggest that groundwater nitrate contamination is not widespread across the study area. However, we cannot rule out the possibility that some parts of the study area may have elevated groundwater nitrate concentrations.

2.6 Conclusions

Land use, water chemistry, and stable water isotope data were used to evaluate relationships between connectivity, tile drainage, nitrate concentrations, antecedent moisture conditions, and travel times across a 1,238 km^2 catchment in west-central Indiana. Our results indicate that nitrate concentrations are highly variable across the landscape, but tile drainage intensity is a good predictor of nitrate concentrations. Differences in stable isotope variability support the hypothesis that shorter travel times in highly drained watersheds lead to greater nitrate concentrations. Antecedent moisture conditions and hydrologic connectivity are an important control on stream N concentrations at the watershed scale, and nitrate concentrations are greatest during intermediate moisture conditions. Groundwater nitrate contamination appears to be ~1.5 mg L^{-1} based on nitrate concentrations during fall baseflow events.

2.7 References

Ahiablame, L. M., Chaubey, I., Smith, D. R., & Engel, B. A. (2011). Effect of tile effluent on nutrient concentration and retention efficiency in agricultural drainage ditches. *Agricultural Water Management*, *98*(8), 1271–1279. https://doi.org/10.1016/j.agwat.2011.03.002

Ale, S., & Bowling, L. C. (2010). Estimating potentially subsurface drained areas in Indiana and their influence on streamflow pattern. Presented at the National Water Conference, Hilton Head, South Carolina.

Anderson, D. M., Glibert, P. M., & Burkholder, J. M. (2002). Harmful algal blooms and eutrophication: Nutrient sources, composition, and consequences. *Estuaries*, *25*(4), 704–726. https://doi.org/10.1007/BF02804901

Arenas Amado, A., Schilling, K. E., Jones, C. S., Thomas, N., & Weber, L. J. (2017). Estimation of tile drainage contribution to streamflow and nutrient loads at the watershed scale based on continuously monitored data. *Environmental Monitoring and Assessment*, *189*(9), 426. https://doi.org/10.1007/s10661-017-6139-4

Arguez, A., Durre, I., Applequist, S., Squires, M., Vose, R., Yin, X., & Bilotta, R. (2010). U.S. Climate Normals Product Suite (1981-2010) [Data set]. NOAA National Climatic Data Center. https://doi.org/10.7289/V5PN93JP

Aulenbach, B. T., Buxton, H. T., Battaglin, W. A., & Coupe, R. H. (2007). *Streamflow and nutrient fluxes of the Mississippi-Atchafalaya River Basin and subbasins for the period of record through 2005* (USGS Numbered Series No. 2007–1080). *Streamflow and nutrient fluxes of the Mississippi-Atchafalaya River Basin and subbasins for the period of record through 2005* (Vol. 2007–1080). Reston, VA: U.S. Geological Survey. https://doi.org/10.3133/ofr20071080

Basu, N. B., Destouni, G., Jawitz, J. W., Thompson, S. E., Loukinova, N. V., Darracq, A., et al. (2010). Nutrient loads exported from managed catchments reveal emergent biogeochemical stationarity. *Geophysical Research Letters*, *37*(23). https://doi.org/10.1029/2010GL045168

Boles, C. M. W., Frankenberger, J. R., & Moriasi, D. N. (2015). Tile Drainage Simulation in Swat2012: Parameterization and Evaluation in an Indiana Watershed. *Transactions of the ASABE*, *58*(5), 1201–1213.

Cain, M. R., Woo, D. K., Kumar, P., Keefer, L., & Ward, A. S. (in review). Antecedent conditions control thresholds of tile-runoff generation and nitrogen export in intensively managed landscapes. *Water Resources Research*.

Cambardella, C. A., Moorman, T. B., Jaynes, D. B., Hatfield, J. L., Parkin, T. B., Simpkins, W. W., & Karlen, D. L. (1999). Water quality in Walnut Creek Watershed: Nitrate-nitrogen in soils, subsurface drainage water, and shallow groundwater. *Journal of Environmental Quality*, *28*(1), 25–34. https://doi.org/10.2134/jeq1999.00472425002800010003x

Carpenter, S. R., Caraco, N. F., Correll, D. L., Howarth, R. W., Sharpley, A. N., & Smith, V. H. (1998). Nonpoint Pollution of Surface Waters with Phosphorus and Nitrogen. *Ecological Applications, 8*(3), 559–568. https://doi.org/10.1890/1051-0761(1998)008[0559:NPOSWW]2.0.CO;2

Castillo, M. M., Allan, J. D., & Brunzell, S. (2000). Nutrient Concentrations and Discharges in a Midwestern Agricultural Catchment. *Journal of Environmental Quality*, *29*(4), 1142–1151. https://doi.org/10.2134/jeq2000.00472425002900040015x

City of Lafayette. (2019). City of Lafayette Water Works: Consumer Confidence Reports. Retrieved May 31, 2021, from https://www.lafayette.in.gov/1077/Reports

Coplen, T. B., & Wassenaar, L. I. (2015). LIMS for Lasers 2015 for achieving long-term accuracy and precision of δ2H, δ17O, and δ18O of waters using laser absorption spectrometry. *Rapid Communications in Mass Spectrometry*, *29*(22), 2122–2130. https://doi.org/10.1002/rcm.7372

David, M. B., Drinkwater, L. E., & McIsaac, G. F. (2010). Sources of nitrate yields in the Mississippi River Basin. *Journal of Environmental Quality*, *39*(5), 1657–1667. https://doi.org/10.2134/jeq2010.0115

Davis, C. A., Ward, A. S., Burgin, A. J., Loecke, T. D., Riveros-Iregui, D. A., Schnoebelen, D. J., et al. (2014). Antecedent Moisture Controls on Stream Nitrate Flux in an Agricultural Watershed. *Journal of Environmental Quality*, *43*(4), 1494–1503. https://doi.org/10.2134/jeq2013.11.0438

Diaz, R. J., & Rosenberg, R. (2008). Spreading Dead Zones and Consequences for Marine Ecosystems. *Science*, *321*(5891), 926–929. https://doi.org/10.1126/science.1156401

Feick, S., Siebert, S., & Döll, P. (2005). A Digital Global Map of Artificially Drained Agricultural Areas. Frankfurt University, Frankfurt am Main, Germany. Retrieved from https://agris.fao.org/agris-search/search.do?recordID=AV20120164581

Fenelon, J. M., & Moore, R. C. (1998). Transport of Agrichemicals to Ground and Surface Water in a Small Central Indiana Watershed. *Journal of Environmental Quality*, *27*(4), 884–894. https://doi.org/10.2134/jeq1998.00472425002700040024x

Feng, Z., Schilling, K. E., & Chan, K.-S. (2013). Dynamic regression modeling of daily nitrate-nitrogen concentrations in a large agricultural watershed. *Environmental Monitoring and Assessment*, *185*(6), 4605–4617. https://doi.org/10.1007/s10661-012-2891-7

Follett, R. F., & Delgado, J. A. (2002). Nitrogen fate and transport in agricultural systems. *Journal of Soil and Water Conservation; Ankeny*, *57*(6), 402–407.

Frisbee, M. D., Phillips, F. M., Campbell, A. R., Liu, F., & Sanchez, S. A. (2011). Streamflow generation in a large, alpine watershed in the southern Rocky Mountains of Colorado: Is streamflow generation simply the aggregation of hillslope runoff responses? *Water Resources Research*, *47*(6). https://doi.org/10.1029/2010WR009391

Gentry, L. E., David, M. B., Below, F. E., Royer, T. V., & McIsaac, G. F. (2009). Nitrogen mass balance of a tile-drained agricultural watershed in east-central Illinois. *Journal of Environmental Quality*, *38*(5), 1841–1847. https://doi.org/10.2134/jeq2008.0406

Gesch, D. B., Evans, G. A., Oimoen, M. J., & Arundel, S. (2018). The National Elevation Dataset (pp. 83–110). American Society for Photogrammetry and Remote Sensing.

Godsey, S. E., Kirchner, J. W., & Clow, D. W. (2009). Concentration–discharge relationships reflect chemostatic characteristics of US catchments. *Hydrological Processes*, *23*(13), 1844–1864. https://doi.org/10.1002/hyp.7315

Goolsby, D. A., & Battaglin, W. A. (2000). *Nitrogen in the Mississippi Basin--Estimating sources and predicting flux to the Gulf of Mexico* (USGS Numbered Series No. 135– 00). *Nitrogen in the Mississippi Basin--Estimating sources and predicting flux to the Gulf of Mexico* (Vol. 135–00). U.S. Geological Survey. https://doi.org/10.3133/fs13500

Gramlich, A., Stoll, S., Stamm, C., Walter, T., & Prasuhn, V. (2018). Effects of artificial land drainage on hydrology, nutrient and pesticide fluxes from agricultural fields – A review. *Agriculture, Ecosystems & Environment*, *266*, 84–99. https://doi.org/10.1016/j.agee.2018.04.005

Green, C. H., Tomer, M. D., Di Luzio, M., & Arnold, J. G. (2006). Hydrologic evaluation of The Soil and Water Assessment Tool for a large tile-drained watershed in Iowa. *Transactions of the ASABE*, *49*(2), 413–422.

Guan, K., Thompson, S. E., Harman, C. J., Basu, N. B., Rao, P. S. C., Sivapalan, M., et al. (2011). Spatiotemporal scaling of hydrological and agrochemical export dynamics in a tile-drained Midwestern watershed. *Water Resources Research*. https://doi.org/10.1029/2010WR009997@10.1002/(ISSN)1944-7973.FILTERS1

Haag, D., & Kaupenjohann, M. (2001). Landscape fate of nitrate fluxes and emissions in Central Europe: A critical review of concepts, data, and models for transport and retention. *Agriculture, Ecosystems & Environment*, *86*(1), 1–21. https://doi.org/10.1016/S0167-8809(00)00266-8

Hansen, A., & Singh, A. (2018). High-Frequency Sensor Data Reveal Across-Scale Nitrate Dynamics in Response to Hydrology and Biogeochemistry in Intensively Managed Agricultural Basins. *Journal of Geophysical Research: Biogeosciences*, *123*(7), 2168–2182. https://doi.org/10.1029/2017JG004310

Homer, C. G., Fry, J. A., & Barnes, C. A. (2012). *The National Land Cover Database* (USGS Numbered Series No. 2012–3020) (p. 4). Reston, Virginia, United States: U.S. Geological Survey. Retrieved from https://doi.org/10.3133/fs20123020

Hornberger, G. M., Bencala, K. E., & McKnight, D. M. (1994). Hydrological controls on dissolved organic carbon during snowmelt in the Snake River near Montezuma, Colorado. *Biogeochemistry*, *25*(3), 147–165. https://doi.org/10.1007/BF00024390

Ilampooranan, I., Meter, K. J. V., & Basu, N. B. (2019). A Race Against Time: Modeling Time Lags in Watershed Response. *Water Resources Research*, *55*(5), 3941–3959. https://doi.org/10.1029/2018WR023815

Jasechko, S., Kirchner, J. W., Welker, J. M., & McDonnell, J. J. (2016). Substantial proportion of global streamflow less than three months old. *Nature Geoscience*, *9*(2), 126–129. https://doi.org/10.1038/ngeo2636

Jiang, Y., Frankenberger, J. R., Sui, Y., & Bowling, L. C. (2014). Estimation of nonpoint source nitrate concentrations in Indiana rivers based on agricultural drainage in the watershed. *Journal of the American Water Resources Association*, *50*(6), 1501–1514. https://doi.org/10.1111/jawr.12216

Kalita, P. K., Cooke, R. a. C., Anderson, S. M., Hirschi, M. C., & Mitchell, J. K. (2007). Subsurface drainage and water quality: The Illinois experience. *Transactions of the Asabe*, *50*(5), 1651–1656.

Kennedy, C. D., Bataille, C., Liu, Z., Ale, S., VanDeVelde, J., Roswell, C. R., et al. (2012). Dynamics of nitrate and chloride during storm events in agricultural catchments with different subsurface drainage intensity (Indiana, USA). *Journal of Hydrology*, *466–467*, 1–10. https://doi.org/10.1016/j.jhydrol.2012.05.002

King, K. W., Williams, M. R., & Fausey, N. R. (2016). Effect of crop type and season on nutrient leaching to tile drainage under a corn–soybean rotation. *Journal of Soil and Water Conservation*, *71*(1), 56–68. https://doi.org/10.2489/jswc.71.1.56

Kladivko, E. J., Scoyoc, G. E. V., Monke, E. J., Oates, K. M., & Pask, W. (1991). Pesticide and Nutrient Movement into Subsurface Tile Drains on a Silt Loam Soil in Indiana. *Journal of Environmental Quality*, *20*(1), 264–270. https://doi.org/10.2134/jeq1991.00472425002000010043x

Kladivko, E. J., Grochulska, J., Turco, R. F., Scoyoc, G. E. V., & Eigel, J. D. (1999). Pesticide and nitrate transport into subsurface tile drains of different spacings. *Journal of Environmental Quality*, *28*(3), 997–1004. https://doi.org/10.2134/jeq1999.00472425002800030033x

Kladivko, E. J., Frankenberger, J. R., Jaynes, D. B., Meek, D. W., Jenkinson, B. J., & Fausey, N. R. (2004). Nitrate leaching to subsurface drains as affected by drain spacing and changes in crop production system. *Journal of Environmental Quality*, *33*(5), 1803–1813. https://doi.org/10.2134/jeq2004.1803

Letsinger, S. L. (2015). *Relationship of groundwater recharge rates to aquifer sensitivity to contamination in shallow aquifers in Indiana, using multiple regression analysis*. Bloomington, Indiana: Center for Geospatial Data Analysis, Indiana Geological Survey. Retrieved from https://maps.indiana.edu/metadata/Hydrology/Aquifer_Recharge_Near_Surface.html

Li, H., Sivapalan, M., Tian, F., & Liu, D. (2010). Water and nutrient balances in a large tile-drained agricultural catchment: a distributed modeling study. *Hydrology and Earth System Sciences*, *14*(11), 2259–2275. https://doi.org/10.5194/hess-14-2259-2010

Liu, W., Youssef, M. A., Birgand, F. P., Chescheir, G. M., Tian, S., & Maxwell, B. M. (2020). Processes and mechanisms controlling nitrate dynamics in an artificially drained field: Insights from high-frequency water quality measurements. *Agricultural Water Management*, *232*, 106032. https://doi.org/10.1016/j.agwat.2020.106032

Mallya, G., Zhao, L., Song, X. C., Niyogi, D., & Govindaraju, R. S. (2013). 2012 Midwest Drought in the United States. *Journal of Hydrologic Engineering*, *18*(7), 737–745. https://doi.org/10.1061/(ASCE)HE.1943-5584.0000786

McGuire, K. J., & McDonnell, J. J. (2006). A review and evaluation of catchment transit time modeling. *Journal of Hydrology*, *330*(3), 543–563. https://doi.org/10.1016/j.jhydrol.2006.04.020

McMillan, S. K., Wilson, H. F., Tague, C. L., Hanes, D. M., Inamdar, S., Karwan, D. L., et al. (2018). Before the storm: antecedent conditions as regulators of hydrologic and biogeochemical response to extreme climate events. *Biogeochemistry*, *141*(3), 487–501. https://doi.org/10.1007/s10533-018-0482-6

Menne, M. J., Durre, I., Korzeniewski, B., McNeill, S., Thomas, K., Yin, X., et al. (2012). Global Historical Climatology Network - Daily (GHCN-Daily), Version 3 [Data set]. NOAA National Centers for Environmental Information. https://doi.org/10.7289/V5D21VHZ

Merriman, K. R., Daggupati, P., Srinivasan, R., Toussant, C., Russell, A. M., & Hayhurst, B. (2018). Assessing the Impact of Site-Specific BMPs Using a Spatially Explicit, Field-Scale SWAT Model with Edge-of-Field and Tile Hydrology and Water-Quality Data in the Eagle Creek Watershed, Ohio. *Water*, *10*(10), 1299. https://doi.org/10.3390/w10101299

Mitchell, J. K., McIsaac, G. F., Walker, S. E., & Hirschi, M. C. (2000). Nitrate in river and subsurface drainage flows from an east central Illinois watershed. *Transactions of the Asae*, *43*(2), 337–342.

Murphy, J. C., Hirsch, R. M., & Sprague, L. A. (2014). Antecedent flow conditions and nitrate concentrations in the Mississippi River basin. *Hydrology and Earth System Sciences*, *18*(3), 967–979. https://doi.org/10.5194/hess-18-967-2014

Nangia, V., Gowda, P. H., Mulla, D. J., & Sands, G. R. (2008). Water Quality Modeling of Fertilizer Management Impacts on Nitrate Losses in Tile Drains at the Field Scale. *Journal of Environmental Quality*, *37*(2), 296–307. https://doi.org/10.2134/jeq2007.0224

NRCS. (2019). *Gridded National Soil Survey Geographic (gNATSGO) Database for Indiana*. https://nrcs.app.box.com/v/soils: United States Department of Agriculture, Natural Resources Conservation Service. Retrieved from https://nrcs.app.box.com/v/soils

Poor, C. J., & McDonnell, J. J. (2007). The effects of land use on stream nitrate dynamics. *Journal of Hydrology*, *332*(1), 54–68. https://doi.org/10.1016/j.jhydrol.2006.06.022

R Core Team. (2019). R: A language and environment for statistical computing (Version 3.6.1). Vienna, Austria: R Foundation for Statistical Computing. Retrieved from https://www.R-project.org/

Robertson, D. M., & Saad, D. A. (2019). *Spatially Referenced Models of Streamflow and Nitrogen, Phosphorus, and Suspended-Sediment Loads in Streams of the Midwestern United States* (Scientific Investigations Report No. 2019–5114) (p. 74). U.S. Geological Survey. Retrieved from https://doi.org/10.3133/sir20195114

Royer, T. V., Tank, J. L., & David, M. B. (2004). Transport and Fate of Nitrate in Headwater Agricultural Streams in Illinois. *Journal of Environmental Quality*, *33*(4), 1296–304.

Saadat, S., Bowling, L., Frankenberger, J., & Kladivko, E. (2018). Nitrate and phosphorus transport through subsurface drains under free and controlled drainage. *Water Research*, *142*, 196–207. https://doi.org/10.1016/j.watres.2018.05.040

Schilling, K. E., Jindal, P., Basu, N. B., & Helmers, M. J. (2012). Impact of artificial subsurface drainage on groundwater travel times and baseflow discharge in an agricultural watershed, Iowa (USA). *Hydrological Processes*, *26*(20), 3092–3100. https://doi.org/10.1002/hyp.8337

Schilling, K. E., Wolter, C. F., Isenhart, T. M., & Schultz, R. C. (2015). Tile drainage density reduces groundwater travel times and compromises riparian buffer effectiveness. *Journal of Environmental Quality*, *44*(6), 1754–1763. https://doi.org/10.2134/jeq2015.02.0105

Schilling, K. E., Streeter, M. T., Vogelgesang, J., Jones, C. S., & Seeman, A. (2020). Subsurface nutrient export from a cropped field to an agricultural stream: Implications for targeting edge-of-field practices. *Agricultural Water Management*, *241*, 106339. https://doi.org/10.1016/j.agwat.2020.106339

Skaggs, R. W., Youssef, M. A., Chescheir, G. M., & Gilliam, J. W. (2005). Effect of Drainage Intensity on Nitrogen Losses from Drained Lands. *Transactions of the ASAE*, *48*(6), 2169–2177. https://doi.org/10.13031/2013.20103

Sprenger, M., Stumpp, C., Weiler, M., Aeschbach, W., Allen, S. T., Benettin, P., et al. (2019). The demographics of water: A review of water ages in the critical zone. *Reviews of Geophysics*, *57*(3), 800–834. https://doi.org/10.1029/2018RG000633

Sui, Y., & Frankenberger, J. R. (2008). Nitrate Loss from Subsurface Drains in an Agricultural Watershed Using Swat2005. *Transactions of the ASABE*, *51*(4), 1263–1272.

Tian, S., Youssef, M. A., Richards, R. P., Liu, J., Baker, D. B., & Liu, Y. (2016). Different seasonality of nitrate export from an agricultural watershed and an urbanized watershed in Midwestern USA. *Journal of Hydrology*, *541*, 1375–1384. https://doi.org/10.1016/j.jhydrol.2016.08.042

Tiemeyer, B., Kahle, P., & Lennartz, B. (2006). Nutrient losses from artificially drained catchments in North-Eastern Germany at different scales. *Agricultural Water Management*, *85*(1), 47–57. https://doi.org/10.1016/j.agwat.2006.03.016

Tomer, M. D., Meek, D. W., Jaynes, D. B., & Hatfield, J. L. (2003). Evaluation of Nitrate Nitrogen Fluxes from a Tile-Drained Watershed in Central Iowa. *Journal of Environmental Quality*, *32*(2), 642–653. https://doi.org/10.2134/jeq2003.6420

Uchida, T., Asano, Y., Onda, Y., & Miyata, S. (2005). Are headwaters just the sum of hillslopes? *Hydrological Processes*, *19*(16), 3251–3261. https://doi.org/10.1002/hyp.6004

U.S. EPA. (1993a). *Method 350.1, Revision 2.0: Determination of ammonia nitrogen by semi-automated colorimetry* (Method No. 350.1) (p. 15). Cincinnati, Ohio: U.S. Environmental Protection Agency. Retrieved from https://www.epa.gov/esam/epa-method-3501-determination-ammonia-nitrogen-semi-automated-colorimetry

U.S. EPA. (1993b). *Method 353.2, Revision 2.0: Determination of nitrate-nitrite nitrogen by automated colorimetry* (Method No. 353.2) (p. 15). Cincinnati, Ohio: U.S. Environmental Protection Agency. Retrieved from https://www.epa.gov/sites/default/files/2015-08/documents/method_353-2_1993.pdf

U.S. EPA. (1993c). *Method 365.1, Revision 2.0: Determination of phosphorus by semi-automated colorimetry* (Method No. 365.1) (p. 18). Cincinnati, Ohio: U.S. Environmental Protection Agency. Retrieved from https://www.epa.gov/sites/default/files/2015-08/documents/method_365-1_1993.pdf

U.S. Geological Survey. (2016). *USGS Water Data for the Nation*. Retrieved from https://waterdata.usgs.gov/nwis/uv/?site_no=03335000&agency_cd=USGS

Van Meter, K. J., Cappellen, P. V., & Basu, N. B. (2018). Legacy nitrogen may prevent achievement of water quality goals in the Gulf of Mexico. *Science*. https://doi.org/10.1126/science.aar4462

Vitousek, P. M., Aber, J. D., Howarth, R. W., Likens, G. E., Matson, P. A., Schindler, D. W., et al. (1997). Human Alteration of the Global Nitrogen Cycle: Sources and Consequences. *Ecological Applications*, *7*(3), 737–750. https://doi.org/10.1890/1051-0761(1997)007[0737:HAOTGN]2.0.CO;2

Williams, M. R., Livingston, S. J., Penn, C. J., Smith, D. R., King, K. W., & Huang, C. (2018). Controls of event-based nutrient transport within nested headwater agricultural watersheds of the western Lake Erie basin. *Journal of Hydrology*, *559*, 749–761. https://doi.org/10.1016/j.jhydrol.2018.02.079

Wilson, G. L., Mulla, D. J., Galzki, J., Laacouri, A., Vetsch, J., & Sands, G. (2020). Effects of fertilizer timing and variable rate N on nitrate–N losses from a tile drained corn-soybean rotation simulated using DRAINMOD-NII. *Precision Agriculture*, *21*(2), 311–323. https://doi.org/10.1007/s11119-019-09668-4

Wurtsbaugh, W. A., Paerl, H. W., & Dodds, W. K. (2019). Nutrients, eutrophication and harmful algal blooms along the freshwater to marine continuum. *WIREs Water*, *6*(5), e1373. https://doi.org/10.1002/wat2.1373

Zhao, X., Christianson, L. E., Harmel, D., & Pittelkow, C. M. (2016). Assessment of drainage nitrogen losses on a yield-scaled basis. *Field Crops Research*, *199*, 156–166. https://doi.org/10.1016/j.fcr.2016.07.015

CHAPTER 3. MODELLING TRAVEL TIMES IN TILE-DRAINED LANDSCAPES USING GIS FLOW LINES

3.1 Abstract

Much of the agricultural land in the United States' Midwest requires drainage improvements that include networks of tile drains and ditches. Drainage improvements can alter travel time distributions (TTDs) and change N cycling and transport in agricultural landscapes. This chapter uses a previously developed geographic information systems (GIS) model to calculate TTDs for 205 nested catchments at three different drainage densities, and several relationships with other watershed properties are discussed. Travel times significantly decrease with increasing drainage intensity, and watersheds with longer travel times appear to have more evaporation influence based on relationships with $\delta^{18}O$ and $\delta^{2}H$. Travel times calculated using the model follow the drainage conditions indicated by the drainage score. However, they do not follow the drainage conditions indicated by the tile drained area because tile drained area follows an inverse relationship with the drainage score.

3.2 Introduction

Prior to the mid-1800s, much of the midwestern United States was unsuitable for agricultural purposes because the poorly-draining soils in the region limit crop growth (Kanwar et al., 1983). Beginning in the late-1800s and continuing to the present day, artificial drainage improvements have transformed the Midwest into one of the most productive agricultural regions on the planet (Skaggs et al., 1994). Some midwestern states require drainage improvements on over 50% of the available cropland, and these improvements usually contain extensive networks of subsurface tile drains, ditches, and channelized streams (Blann et al., 2009).

Tile drainage can substantially alter hydrologic properties at both field and watershed scales (Gramlich et al., 2018; Skaggs et al., 1994). Conflicting reports exist in the literature regarding the direction of these changes, but tile drainage generally shortens flow paths to stream channels in landscapes with little relief (Lennartz et al., 2011; Robinson, 1990; Turtola & Paajanen, 1995). Changes in flow path length affect travel times within a watershed, and shorter flow paths should reduce travel times because there is less distance that the water needs to move through to reach a stream (K. E. Schilling et al., 2015). The potential effect of tile drains on travel times can be profound; a hypothetical travel time calculation for a glacial till with hydraulic conductivity of 1×10^{-9} m s^{-1}, porosity of 0.4, and a hydraulic gradient of 0.01 reveals that it would take about 1.25 million years for a parcel of water to travel 1 km (Winter & LaBaugh, 2003). While this scenario would represent a soil with exceptionally poor drainage, it illustrates both the need for tile drainage in poorly-drained soils and the potential impacts they can have on travel times.

Changes to travel time distributions (TTDs) have important implications for N cycling and transport in tile-drained landscapes (Basu et al., 2012; Ilampooranan et al., 2019). This is especially true for nitrate because it is primarily transported through shallow groundwater and can undergo different transformation processes, including uptake by plants and denitrification in which nitrate is converted to N_2 and small amounts of N_2O and NO under anoxic conditions (Schepers et al., 2008; K. Schilling & Zhang, 2004). Best management practices (BMPs) such as controlled drainage, constructed wetlands, and grass waterways attempt to reduce N loss to waterways by increasing the travel time, so understanding how tile drainage impacts travel times is critical for these BMPs' success (K. E. Schilling & Wolter, 2007).

In this chapter, a previously published geographic information systems (GIS) travel time model was adapted for use on a large catchment with 205 nested watersheds in west-central Indiana. The model was evaluated using three different flow line densities to represent increasing drainage intensity. The objectives of this research were 1) model TTDs for nested watersheds within the Great Bend of the Wabash River catchment and 2) determine if the TTD could explain observed patterns with physical and biogeochemical properties of the watersheds.

3.3 Methods

3.3.1 Study area

Please refer to Chapter 2.3.1 for study area information as the study area for this chapter is identical to the study area in Chapter 2.

3.3.2 Watershed delineation

Watersheds were delineated using ArcMap 10.7 (ESRI, 2019) and USGS 1/3 arc-second digital elevation model (DEM) data (Gesch et al., 2018). Each stream sampling point functioned as the outlet for its corresponding watershed. The delineation process used the following tools from ESRI's Hydrology toolset: 1) Fill, to remove any minor imperfections in the DEM; 2) Flow Direction, to create a raster of flow directions from each cell to its downslope neighbors; 3) Flow Accumulation, to create a raster of accumulated flow into each cell; 4) Snap Pour Point, to align the sampling point (outlet) with a nearby cell with the highest flow accumulation; and 5) Watershed, to determine the contributing area above each sampling point.

3.3.3 Model description

The GIS model generally follows the method used by Schilling et al. (2015) with some minor modifications. The Python script for the model can be found in Appendix B. The model operates using the ArcMap 10.7 platform (ESRI, 2019), and each watershed's TTD is modelled as a raster dataset with a 10-m resolution. A travel time is calculated for each raster cell within the watershed using Equation 3.1.

Equation 3.1

$$t = \frac{n_e L}{(31{,}536{,}000\ s\ yr^{-1})(K)\left(\frac{dh}{dl}\right)}$$

Where n_e is effective porosity (dimensionless), L is the flow path length to reach a flow line (m), K is the hydraulic conductivity (m s^{-1}), $\frac{dh}{dl}$ is the hydraulic gradient (dimensionless), $31{,}536{,}000\ s\ yr^{-1}$ is a factor to convert t to years, and t is the time for a parcel of water to travel along the flow path from the grid cell to the flow line. Travel time was assumed to be very short once the water parcel reached a flow line, so it was not included in the TTD (McGuire & McDonnell, 2006). Mean and median travel times were calculated for each watershed from the corresponding TTD. Both mean and median travel times were included because TTDs are typically skewed (Kirchner et al., 2001), and the median is less affected by outliers with extremely long travel times.

3.3.4 Model inputs

Four model inputs were used in the model: 1) DEM, 2) effective porosity, 3) hydraulic conductivity, and 4) flow lines representing the stream/drainage network. All input data was in raster format with a 10-m resolution.

Digital elevation model (DEM)

The same DEM used for watershed delineation was used to determine flow path lengths. The water table was assumed to follow surface topography, and this assumption has been used and supported multiple times in the literature (Freeze & Cherry, 1979; Ilampooranan et al., 2019; K. E. Schilling et al., 2015; T. A. Williams & Williamson, 1989).

Effective porosity

Total porosity (n) is the volume of pores in a soil sample relative to the total sample volume. If a saturated soil sample is allowed to drain, some of the water will drain out of the sample (specific yield, S_y) and some water will be retained within the soil (specific retention, S_r). S_y and S_r can be related to n using Equation 3.2.

Equation 3.2

$$n = S_y + S_r$$

Effective porosity (n_e) represents the interconnected porosity that actually contributes to flow through the soil matrix. S_y is approximately equal to n_e ($n_e \approx S_y$) because it is the ratio of the volume of water that drains from the soil because of gravity relative to the total soil volume (Johnson, 1967). n_e was derived from specific yield (S_y) and geospatial data on the clay, sand, and silt content of soils from the USDA Gridded National Soil Survey Geographic (gNATSGO) database (NRCS, 2019). Johnson (1967) reports average S_y values for certain geologic materials, including clay, silt, and sand. These S_y values and the clay, silt, and sand contents reported in the gNATSGO database were used to calculate n_e with Equation 3.3.

Equation 3.3

$$n_e \approx S_y = S_{y,clay}(F_{clay}) + S_{y,silt}(F_{silt}) + S_{y,sand}(F_{sand})$$

Where $S_{y,clay}$, $S_{y,silt}$, and $S_{y,sand}$ have values of 0.02, 0.08, and 0.26, respectively (Johnson, 1967), and F_{clay}, F_{silt}, and F_{sand} represent the clay, silt, and sand content of the soil, respectively. n_e values ranged from 0.01 to 0.25, and the mean was 0.13 ± 0.03. These n_e values are consistent with those found in Daniels et al. (1991) by gravimetric analysis.

Hydraulic conductivity

Hydraulic conductivity (K) was identical to the saturated hydraulic conductivity (K_{sat}) data provided in the USDA gNATSGO database (NRCS, 2019). The raw data was converted from µm s^{-1} to m s^{-1} to keep units consistent. K values ranged from 4.1×10^{-7} m s^{-1} to 2.1×10^{-4} m s^{-1}, and the arithmetic mean K was $1.9 \times 10^{-5} \pm 2.4 \times 10^{-5}$ m s^{-1}.

Flow lines

Three sets of flow lines representing different drainage intensities were used to determine flow path lengths for the travel time calculations. The first iteration of the model had the lowest drainage intensity with flow lines representing stream channels (Figure 3.1). Travel time calculations using these flow lines represented drainage conditions with no drainage enhancements. In the second model iteration, any grid cell with a contributing area of at least 2.4 ha was considered part of a flow line (Figure 3.2). 2.4 ha is also the same contributing area threshold used to derive flow lines in the highest resolution National Hydrography Dataset (NHD) (U.S. Geological Survey et al., 2019). These flow lines approximate drainage conditions with surface drainage improvements and no tile drain influence. The final iteration had the greatest drainage intensity representing conditions with tile drain influence, and any grid cell with a contributing area ≥ 0.4 ha was considered part of a flow line (Figure 3.3). It is important to note that the additional flow lines in the third model iteration do not necessarily indicate the actual presence of tile drains in those locations, and this limitation should be considered when interpreting travel times derived using this method. Systematically mapping the locations of tile lines is very difficult once they have been installed, and existing methods generally rely on remote sensing data under specific environmental conditions (Naz et al., 2009; Naz & Bowling, 2008).

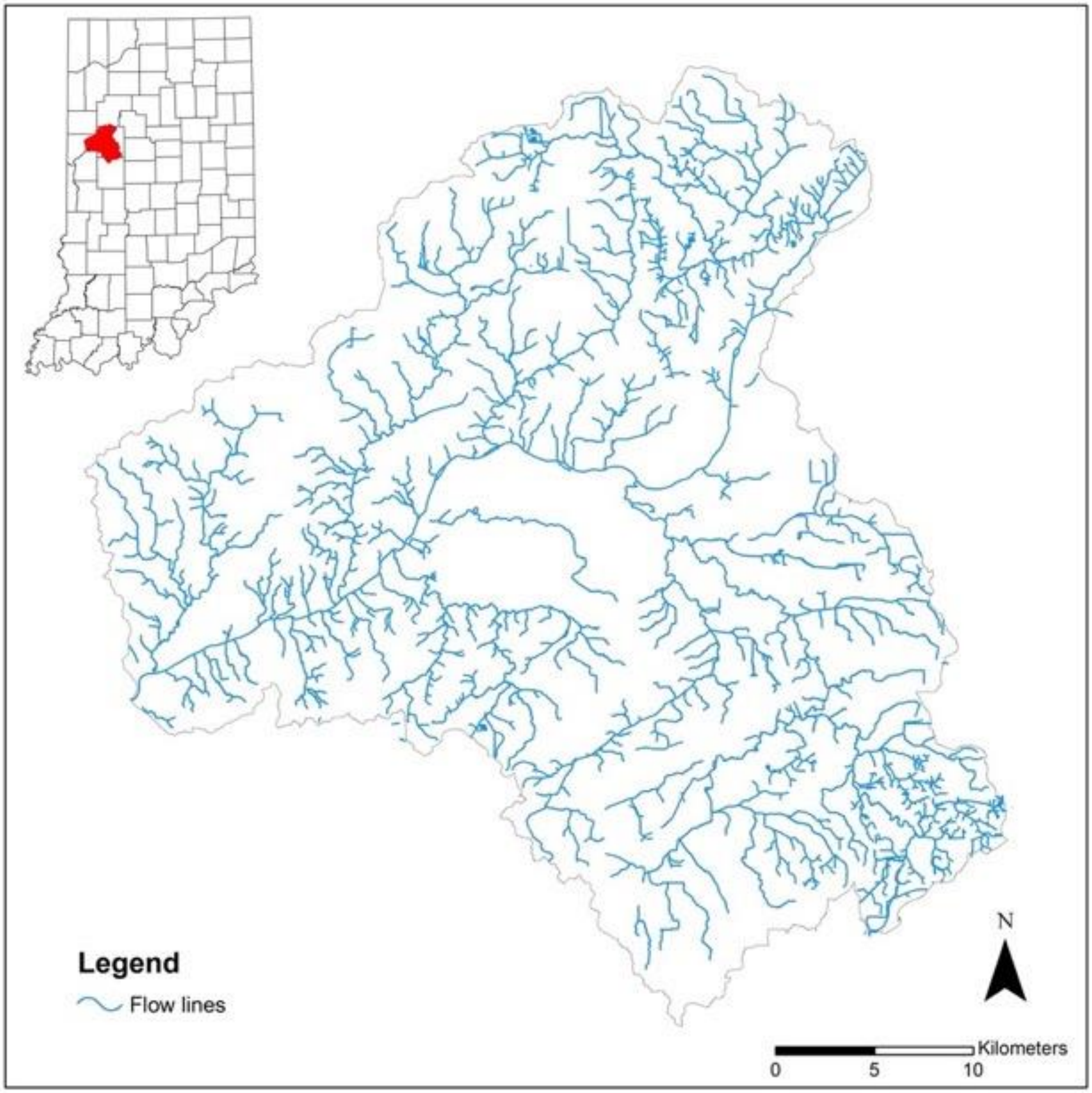

Figure 3.1. Flow lines approximating drainage conditions with only physical stream channels and no drainage improvements.

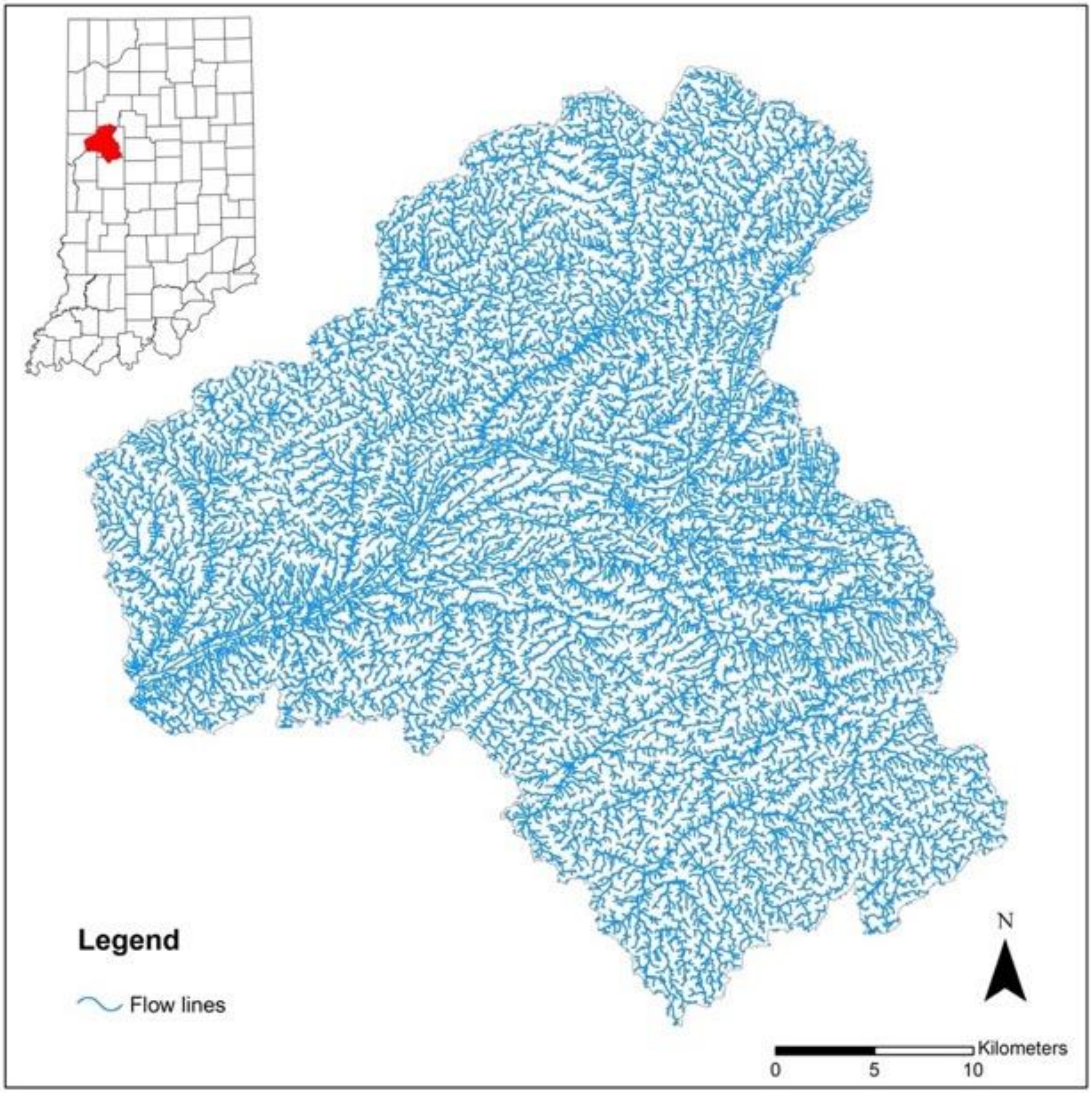

Figure 3.2. Flow lines with a contributing area ≥ 2.4 ha. These flow lines approximate drainage conditions with surface drainage improvements and no tile drain influence.

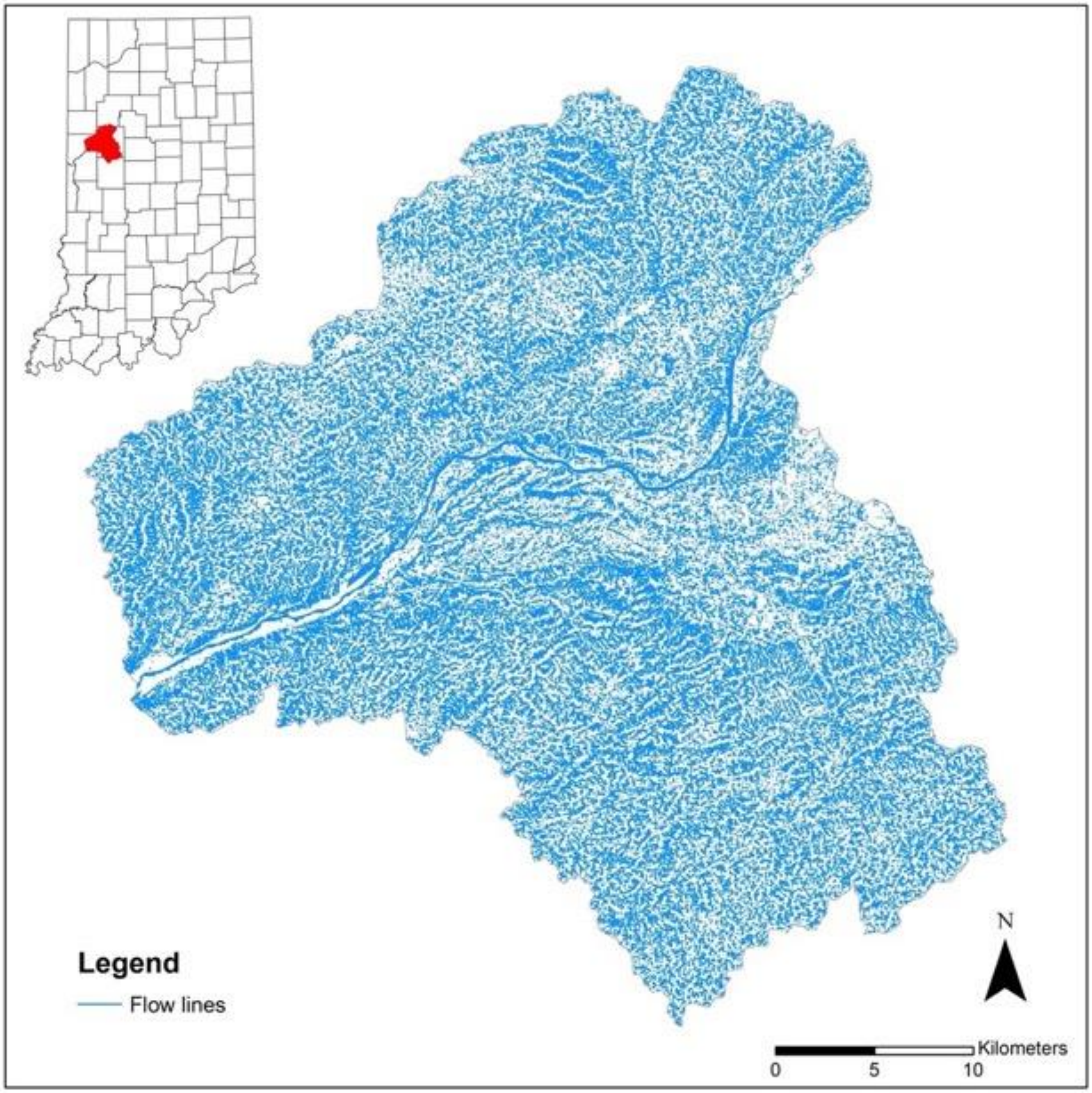

Figure 3.3. Flow lines with a contributing area ≥ 0.4ha. These flow lines approximate drainage conditions following tile drain installation.

3.3.5 Weighted average calculation

The 0.4 ha and 2.4 ha model iterations represent drainage with and without tile drain influence, respectively. However, most watersheds in the study area are not completely without tile drain influence nor are they completely drained by tiles. In reality, each watershed has areas with tile drainage and other areas that are without (Figure 2.4). Each watershed's mean ($\bar{t}$) and median (t_m) travel times were corrected to account for the watershed's percent tile drained area (A_{tile}) using Equation 3.4 and Equation 3.5, respectively.

Equation 3.4

$$\bar{t} = \bar{t}_{0.4}\left(\frac{A_{tile}}{100}\right) + \bar{t}_{2.4}\left(\frac{(1 - A_{tile})}{100}\right)$$

Equation 3.5

$$t_m = t_{m,0.4}\left(\frac{A_{tile}}{100}\right) + t_{m,2.4}\left(\frac{(1 - A_{tile})}{100}\right)$$

Where $\bar{t}_{0.4}$ and $t_{m,0.4}$ represent the mean and median from the 0.4 ha model iteration, respectively, and $\bar{t}_{2.4}$ and $t_{m,2.4}$ represent the mean and median from the 2.4 ha model iteration, respectively. Again, this approximates the actual watershed characteristics.

3.3.6 Data analysis

Data analysis and statistical tests were performed using R 3.6.1 (R Core Team, 2019). Mean and median travel times were 1og transformed to meet normality assumptions in ANOVA and t-tests.

3.4 Results and Discussion

3.4.1 Travel times using stream channel threshold

Mean travel times using the stream channel threshold ranged from 0.32 years to 148.2 years (Figure 3.4A), but median travel times only ranged from 0.03 to 52.8 years (Figure 3.4B). The average mean travel time was 34.5 ± 25.9 years, and the average median travel time was significantly shorter at 11.6 ± 9.1 years ($t(190) = 7.96$, $p < 0.001$). Similar mean travel times have been observed in other GIS modelling studies. Schilling et al. (2015) found a mean travel time of 82.5 ± 88.0 years in a 75 km^2 Iowa watershed using a 324 ha threshold for flow lines. A 52 km^2 watershed in Iowa had a mean travel time of 19.61 ± 18.84 years (Basu et al., 2012), and another study of a 502 km^2 watershed in central Iowa had a mean travel time of 13 years (Ilampooranan et al., 2019). In these two studies, flow lines were generated using a 40.5 ha threshold.

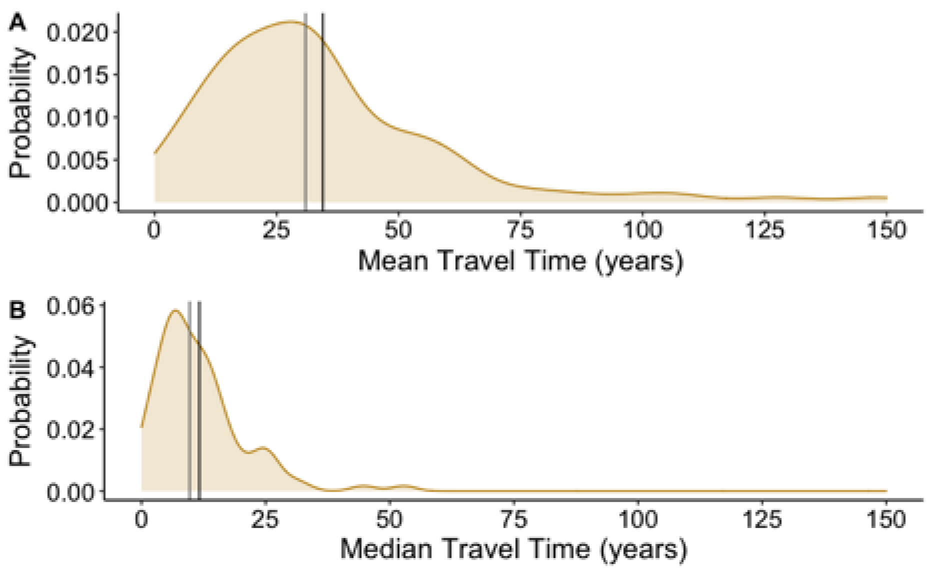

Figure 3.4. Distribution of (**A**) mean and (**B**) median travel times determined using the stream channel threshold. The black and gray lines indicate the mean and median of the distributions, respectively.

3.4.2 Travel times using 2.4 ha threshold

Mean travel times using the 2.4ha threshold ranged from 0.94 to 28.8 years (Figure 3.5A), and median travel times ranged from 0.26 to 5.57 years (Figure 3.5B). The average mean travel time (6.33 ± 3.65 years) was significantly longer than the average median travel time (2.39 ± 1.18 years) ($t(190) = 11.39$, $p < 0.001$). The study of a 75 km^2 Iowa watershed found a similar mean travel time of 5.57 ± 5.27 years when using the same 2.4 ha threshold (K. E. Schilling et al., 2015).

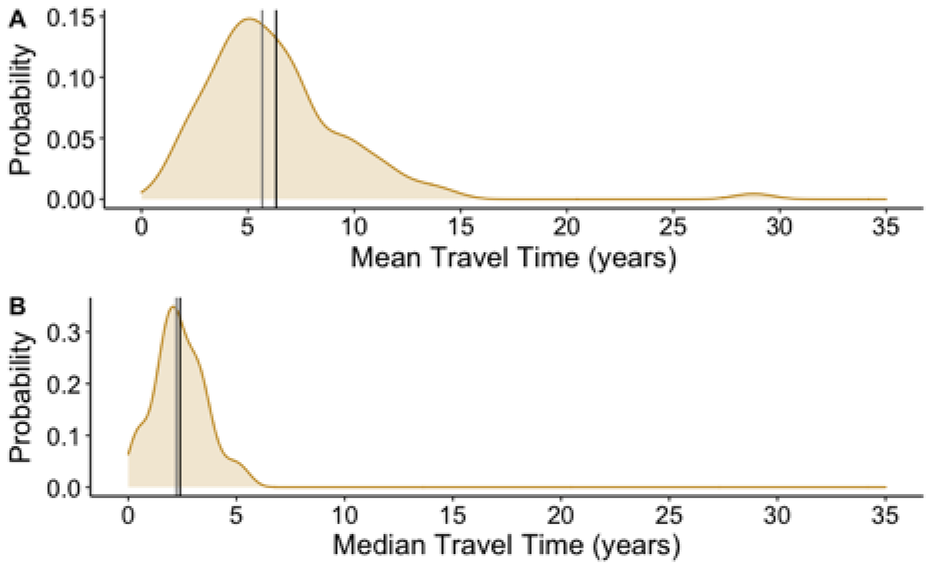

Figure 3.5. Distribution of (**A**) mean and (B) median travel times determined using the 2.4 ha threshold. The black and gray lines indicate the mean and median of the distributions, respectively. Note that the maximum x-axis value was reduced from 150 years (Figure 3.4) to 35 years.

3.4.3 Travel times using 0.4 ha threshold

Mean travel times using the 0.4ha threshold ranged from 0.82 to 20.1 years (Figure 3.6A), and median travel times ranged from 0.16 to 3.75 years (Figure 3.6B). The average mean travel time (4.39 ± 2.78 years) was significantly longer than the average median travel time (1.29 ± 0.66 years) ($t(190) = 13.67$, $p < 0.001$). Schilling et al. (2015) observed a similar mean travel time (2.64 ± 2.88 years) when using a 0.4 ha threshold.

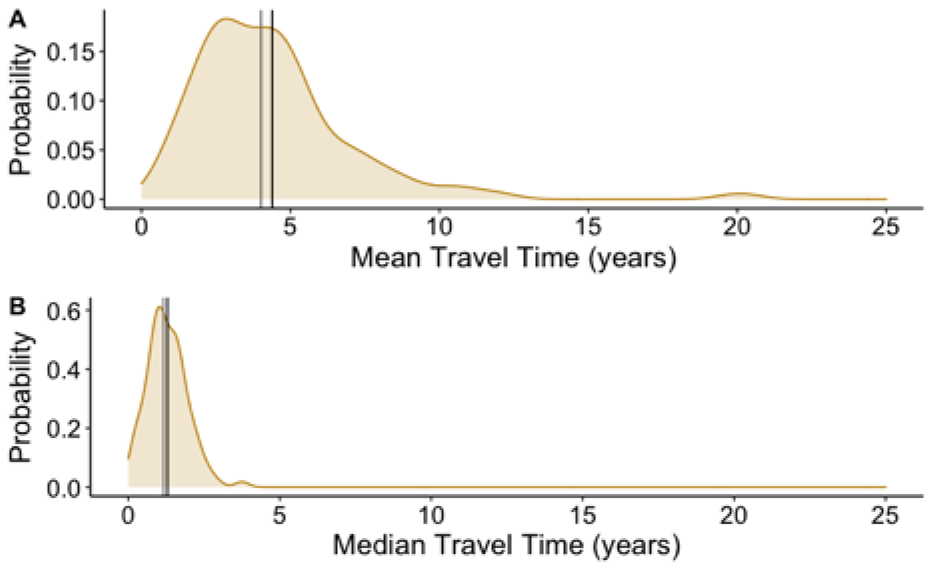

Figure 3.6. Distribution of (**A**) mean and (**B**) median travel times determined using the 0.4 ha threshold. The black and gray lines indicate the mean and median of the distributions, respectively. Note that the maximum x-axis value was reduced from 35 years (Figure 3.5) to 25 years.

3.4.4 Threshold comparisons

Changing the flow line density had a pronounced effect on travel times (Table 3.1). Decreasing the threshold area to 2.4 ha shortened the average mean travel time and average median travel time by 82% and 79%, respectively. Further decreasing the threshold area to 0.4 ha reduced the average mean by 87% and the average median by 89% compared to the stream channel threshold. All three thresholds had significantly different mean travel times as determined by a one-way ANOVA ($F(2,285) = 198.5$, $p < 0.001$, Tukey post-hoc test) (Figure 3.7). Mean median travel times were also significantly different between all three thresholds ($F(2,285) = 150.9$, $p < 0.001$, Tukey post-hoc test) (Figure 3.8).

Table 3.1. Descriptive statistics for travel times using the three different threshold areas.

Threshold area (ha)	Average mean (yrs)	Average median (yrs)	Maximum mean (yrs)	Minimum mean (yrs)	Maximum median (yrs)	Minimum median (yrs)
Stream channels	34.5 ± 25.9	11.6 ± 9.1	148.2	0.32	52.8	0.03
2.4	6.33 ± 3.65	2.39 ± 1.18	28.8	0.94	5.57	0.26
0.4	4.38 ± 2.78	1.29 ± 0.66	20.1	0.82	3.75	0.16

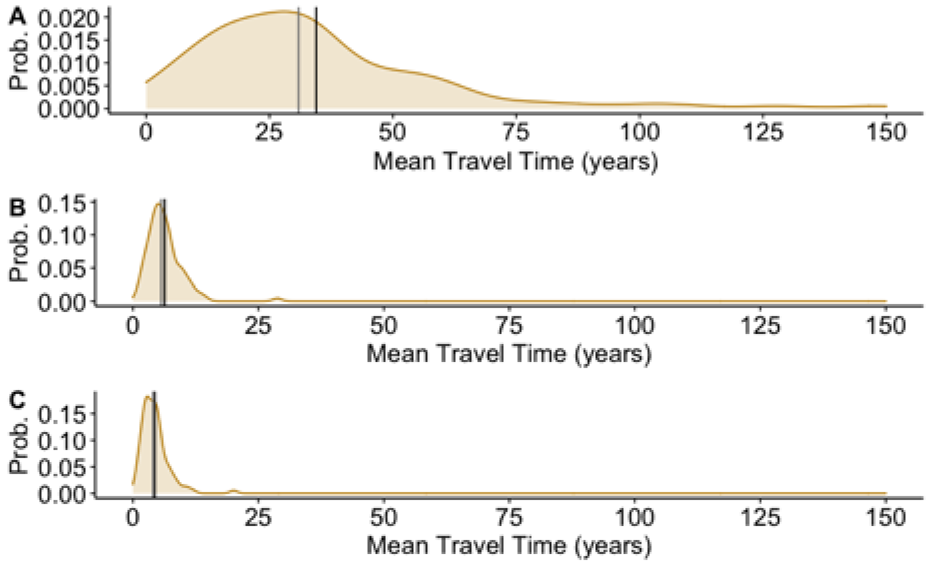

Figure 3.7. Distribution of mean travel times determined using (**A**) stream channel threshold, (**B**) 2.4 ha threshold, and (**C**) 0.4 ha threshold. The black and gray lines indicate the mean and median of the distributions, respectively.

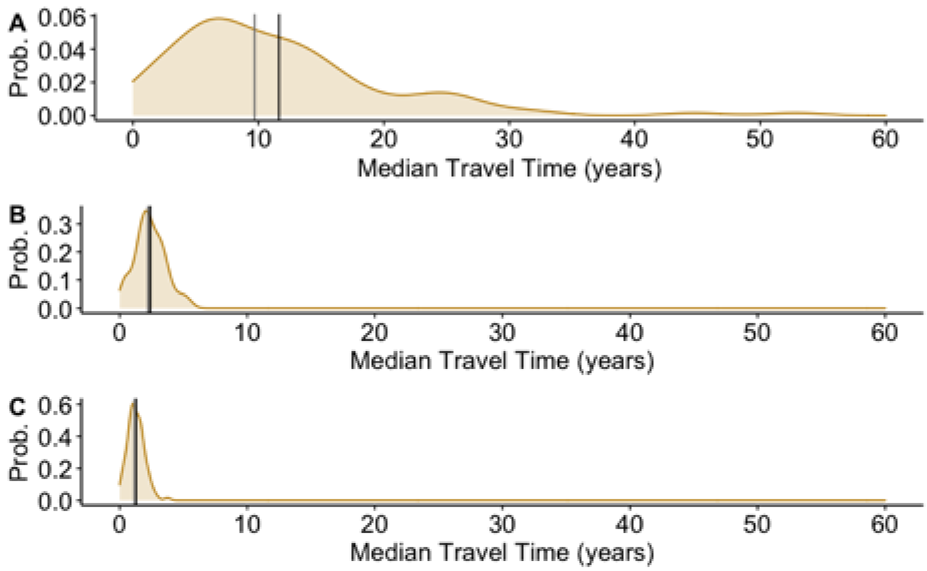

Figure 3.8. Distribution of median travel times determined using (**A**) stream channel threshold, (**B**) 2.4 ha threshold, and (**C**) 0.4 ha threshold. The black and gray lines indicate the mean and median of the distributions, respectively.

3.4.5 Weighted average travel times and patterns with watershed properties

Mean travel times calculated using the weighted average approach ranged from 0.88 to 22.8 years with an average of 5.18 ± 3.00 years (Figure 3.9A). Median travel times calculated using the weighted average approach ranged from 0.21 to 4.32 years with an average of 1.72 ± 0.79 years (Figure 3.9B).

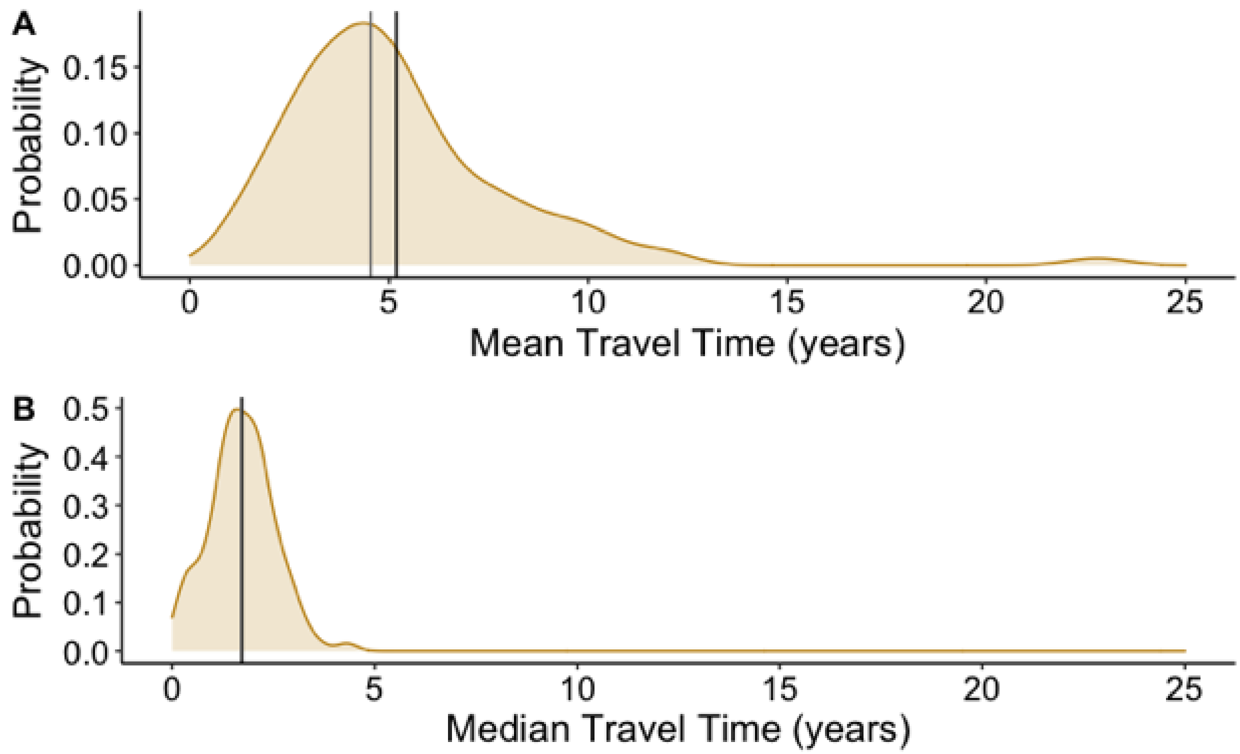

Figure 3.9. Distribution of (**A**) mean and (**B**) median travel times calculated with a weighted average between travel times using the 2.4 ha threshold and the 0.4 ha threshold.

Median travel times were positively correlated with mean δ^2H, $r(96) = 0.396$, $p < 0.001$, and mean $\delta^{18}O$, $r(96) = 0.392$, $p < 0.001$ (Figure 3.10). Watersheds with more enriched δ^2H and $\delta^{18}O$ had smaller deuterium excess values, $r(96) = -0.905$, $p < 0.001$. In general, smaller deuterium excess values indicate greater evaporative enrichment because evaporative loss causes $\delta^2H/\delta^{18}O$ enrichment in the remaining water, and this enrichment follows an evaporation line with a smaller slope than the meteoric water line (Gat, 1996). A parcel of water undergoing evaporative loss will move further along the evaporation line as more evaporative loss occurs, so greater $\delta^2H/\delta^{18}O$ enrichment indicates greater evaporative loss (Figure 3.11). It is possible that longer median travel times are associated with greater $\delta^2H/\delta^{18}O$ enrichment because the precipitation inputs are exposed to evaporation for a longer period of time before reaching a flow line, although further work would be necessary to test this hypothesis. The impact of travel times on evaporation would partly depend on how long precipitation remained near the surface because evaporation is usually limited to the top 30 cm of the soil (Sprenger et al., 2016). If precipitation rapidly infiltrates below this depth, then the evaporative enrichment signal would be much less than in precipitation that infiltrates slowly.

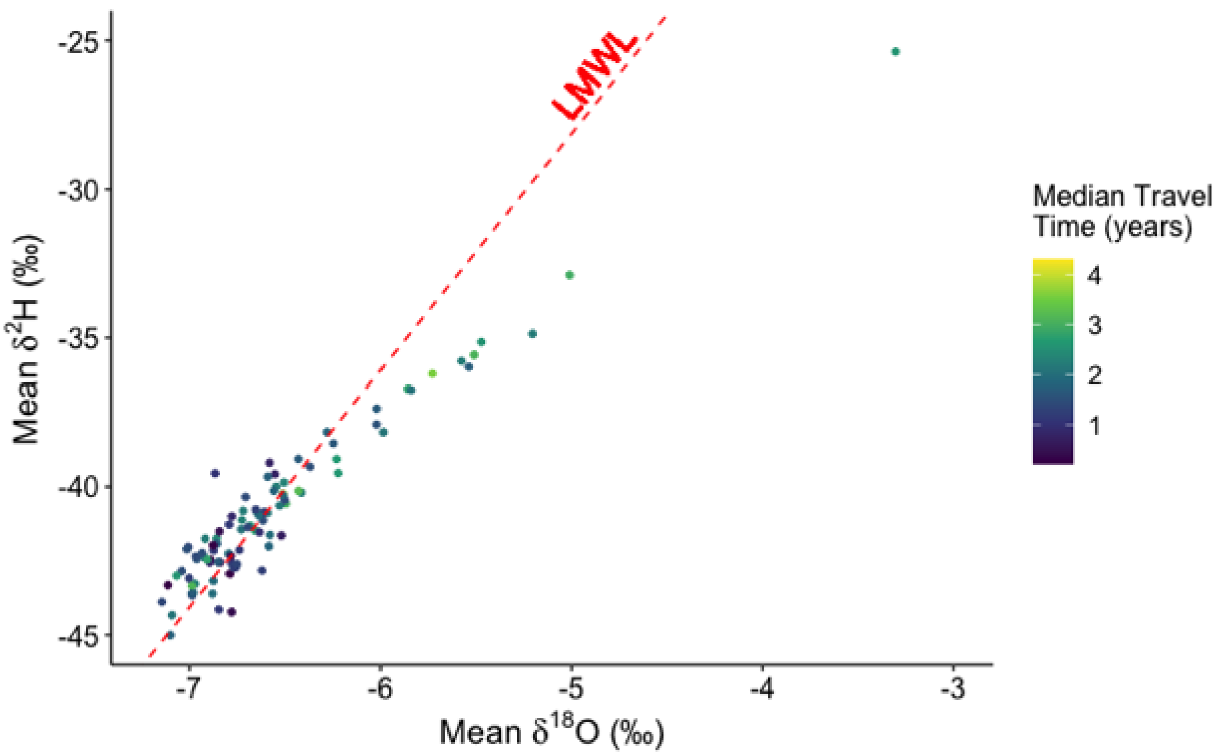

Figure 3.10. Median travel times were positively correlated with mean δ^2H ($r(1,93) = 0.395$; $p < 0.001$) and mean $\delta^{18}O$ ($r(1,93) = 0.392$; $p < 0.001$). The dashed red line represents the local meteoric water line (LMWL) with the following equation: $\delta^2H = 7.97 * \delta^{18}O + 11.73$.

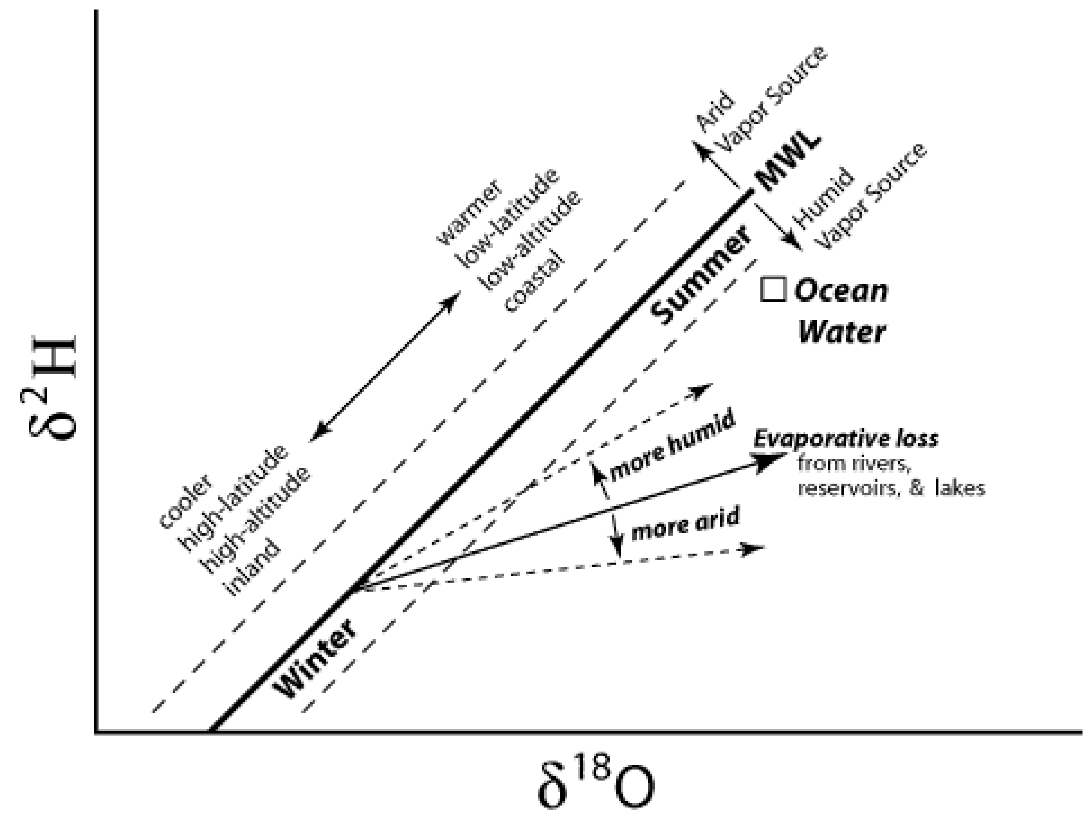

Figure 3.11. A generalized plot of δ^{18}O and δ^2H that shows the meteoric water line (MWL) and an evaporation line with a shallower slope than the MWL, from Ekwurzel (2005).

Median travel times had significant relationships with both drainage scores and tile drained area (Figure 3.12). Median travel times were negatively correlated with drainage scores, $r(96) = -0.576$, $p < 0.001$, and positively correlated with tile drained area, $r(96) = 0.486$, $p < 0.001$. These correlations suggest that travel times decrease in watersheds with higher drainage scores and increase in watersheds with a greater percentage of tile drained area. These findings seem to contradict each other because high drainage scores indicate better drainage and should have shorter travel times. Watersheds with greater tile drained area should also have shorter travel times because they enhance drainage (K. E. Schilling et al., 2015), but longer travel times are observed in watersheds with greater tile drained area.

These opposing observations are likely an unintended consequence of the method used to determine tile drained area. In this analysis, tile drained area was estimated from land use data, soil drainage classes, and slope data. A watershed with a greater percentage of cropland, more poorly-drained soils, and less relief has greater tile drained area when this method is used, all else being equal. A comparison of two hypothetical watersheds helps illustrate why these contradictory observations occur. In this example, 100% of the area is cropland and the slope is constant at 1% in both watersheds. If 75% of watershed A has very poorly, poorly, or somewhat poorly-drained soil and 25% of watershed B has very poorly, poorly, or somewhat poorly-drained soil, then 75% of watershed A and 25% of watershed B has tile drainage. Watershed A would have a lower drainage score but more tile drained area than watershed B. For simplicity's sake, we will assume that these differences balance each other so that both watersheds should have the same median travel time. However, watershed A would have a longer median travel time than watershed B using this TTD model because the model inputs are independent of tile drained area. In other words, the median travel times from this model accurately reflect the drainage conditions indicated by the drainage score, but they do not accurately reflect the drainage conditions indicated by the tile drained area because tile drained area follows an inverse relationship with the drainage score.

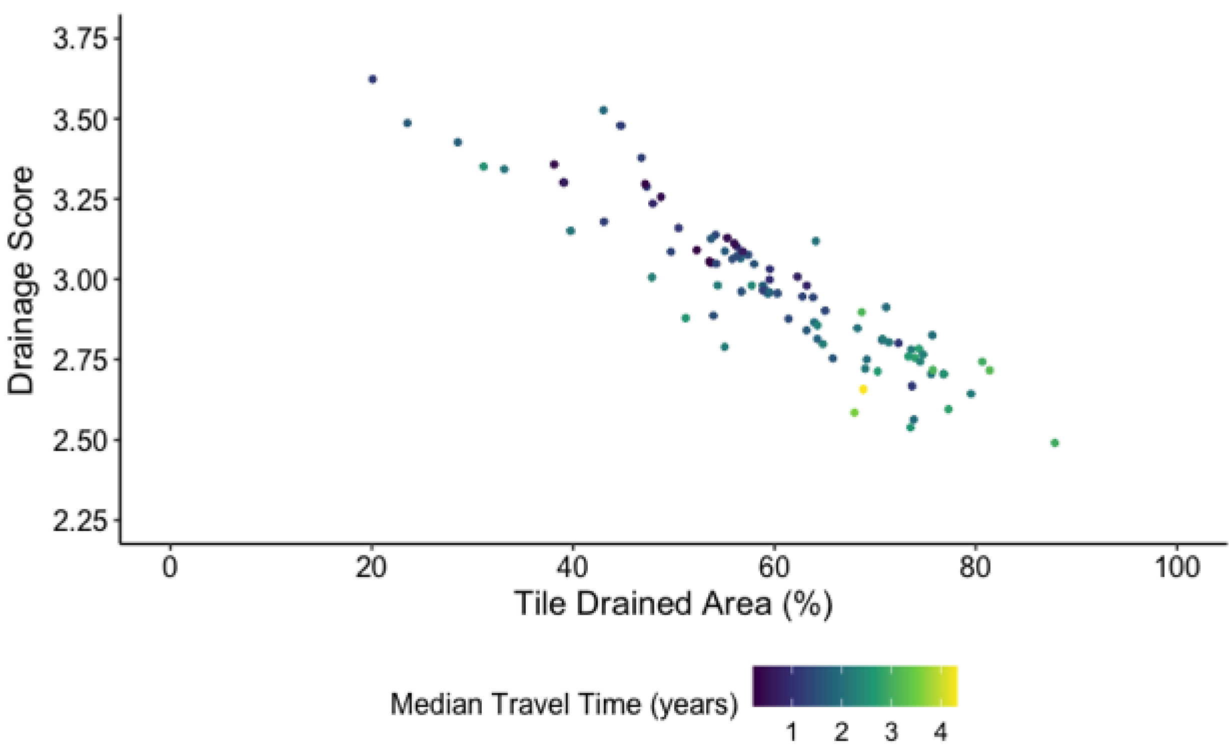

Figure 3.12. Median travel times decrease in watersheds with higher drainage scores and increase in watersheds with more tile drained area.

3.4.6 Water quality implications

Soils that remain saturated for extended periods of time may develop anoxic conditions that are necessary for denitrification to occur, but faster travel times reduce the length of time that agricultural soils are saturated (McIsaac & Hu, 2004). Reduced denitrification fluxes may benefit farmers by limiting N losses to the atmosphere, but this benefit is typically offset by increased N loss to waterways (Dinnes et al., 2002; Helmers et al., 2007; Meisinger & Randall, 1991).

3.5 Conclusions

A previously developed GIS TTD model was used to determine travel times for 205 nested watersheds in west-central Indiana. Relationships between travel times and several physical and biogeochemical properties were assessed. Travel times significantly decreased as the flow line initiation area was reduced to simulate increasing drainage intensities. Increased $\delta^{18}O$ and $\delta^{2}H$ enrichment in watersheds with longer travel times suggest that these watersheds experience greater evaporative influence. Travel times accurately reflect the drainage conditions indicated by drainage scores, but they reflect the opposite drainage conditions indicated by tile drained area. Across the landscape, the relationship between travel time and tile drained area follows the opposite of the expected pattern because model inputs are independent of tile drained area and tile drained area follows an inverse relationship with drainage scores.

3.6 References

Basu, N. B., Jindal, P., Schilling, K. E., Wolter, C. F., & Takle, E. S. (2012). Evaluation of analytical and numerical approaches for the estimation of groundwater travel time distribution. *Journal of Hydrology*, *475*, 65–73. https://doi.org/10.1016/j.jhydrol.2012.08.052

Blann, K. L., Anderson, J. L., Sands, G. R., & Vondracek, B. (2009). Effects of agricultural drainage on aquatic ecosystems: A review. *Critical Reviews in Environmental Science and Technology*, *39*(11), 909–1001. https://doi.org/10.1080/10643380801977966

Daniels, D. P., Fritz, S. J., & Leap, D. I. (1991). Estimating recharge rates through unsaturated glacial till by tritium tracing. *Groundwater*, *29*(1), 26–34. https://doi.org/10.1111/j.1745-6584.1991.tb00493.x

Dinnes, D. L., Karlen, D. L., Jaynes, D. B., Kaspar, T. C., Hatfield, J. L., Colvin, T. S., & Cambardella, C. A. (2002). Nitrogen management strategies to reduce nitrate leaching in tile-drained Midwestern soils. *Agronomy Journal*, *94*(1), 153–171. https://doi.org/10.2134/agronj2002.1530

Ekwurzel, B. (2005). Isotopes and Hydrology: Oxygen. Retrieved July 5, 2021, from http://web.sahra.arizona.edu/programs/isotopes/oxygen.html#8

ESRI. (2019). ArcMap (Version 10.7) [Windows]. Redlands, California, United States: Environmental Systems Research Institute. Retrieved from https://www.esri.com/en-us/home

Freeze, R. A., & Cherry, J. A. (1979). *Groundwater*. Prentice-Hall.

Gat, J. R. (1996). Oxygen and Hydrogen Isotopes in the Hydrologic Cycle. *Annual Review of Earth and Planetary Sciences*, *24*(1), 225–262. https://doi.org/10.1146/annurev.earth.24.1.225

Gesch, D. B., Evans, G. A., Oimoen, M. J., & Arundel, S. (2018). The National Elevation Dataset (pp. 83–110). American Society for Photogrammetry and Remote Sensing.

Gramlich, A., Stoll, S., Stamm, C., Walter, T., & Prasuhn, V. (2018). Effects of artificial land drainage on hydrology, nutrient and pesticide fluxes from agricultural fields – A review. *Agriculture, Ecosystems & Environment*, *266*, 84–99. https://doi.org/10.1016/j.agee.2018.04.005

Helmers, M. J., Isenhart, T. M., Kling, C. L., Moorman, T. B., Simpkins, W. W., & Tomer, M. (2007). Theme overview: Agriculture and water quality in the Cornbelt: Overview of issues and approaches. *Choices*, *22*(2), 79–85.

Ilampooranan, I., Meter, K. J. V., & Basu, N. B. (2019). A Race Against Time: Modeling Time Lags in Watershed Response. *Water Resources Research*, *55*(5), 3941–3959. https://doi.org/10.1029/2018WR023815

Johnson, A. I. (1967). *Specific yield: Compilation of specific yields for various materials* (Geological Survey Water Supply Paper No. 1662- D). Washington, D. C.: U.S. Geological Survey. Retrieved from https://pubs.usgs.gov/wsp/1662d/report.pdf

Kanwar, R. S., H. P. Johnson, D. Schult, T. E. Fenton, & R. D. Hickman. (1983). Drainage needs and returns in north-central Iowa. *Transactions of the ASAE*, *26*(2), 0457–0464. https://doi.org/10.13031/2013.33958

Kirchner, J. W., Feng, X., & Neal, C. (2001). Catchment-scale advection and dispersion as a mechanism for fractal scaling in stream tracer concentrations. *Journal of Hydrology*, *254*(1), 82–101. https://doi.org/10.1016/S0022-1694(01)00487-5

Lennartz, B., Janssen, M., & Tiemeyer, B. (2011). Effects of artificial drainage on water regime and solute transport at different spatial scales. In M. K. Shukla (Ed.), *Soil hydrology, land use and agriculture: measurement and modelling* (pp. 266–290). Wallingford: CABI. https://doi.org/10.1079/9781845937973.0266

McGuire, K. J., & McDonnell, J. J. (2006). A review and evaluation of catchment transit time modeling. *Journal of Hydrology*, *330*(3), 543–563. https://doi.org/10.1016/j.jhydrol.2006.04.020

McIsaac, G. F., & Hu, X. (2004). Net N input and riverine N export from Illinois agricultural watersheds with and without extensive tile drainage. *Biogeochemistry*, *70*(2), 253–273. https://doi.org/10.1023/B:BIOG.0000049342.08183.90

Meisinger, J. J., & Randall, G. W. (1991). Estimating Nitrogen Budgets for Soil-Crop Systems. In *Managing Nitrogen for Groundwater Quality and Farm Profitability* (pp. 85–124). John Wiley & Sons, Ltd. https://doi.org/10.2136/1991.managingnitrogen.c5

Naz, B. S., & Bowling, L. C. (2008). Automated Identification of Tile Lines from Remotely Sensed Data. *Transactions of the ASABE*, *51*(6), 1937–1950.

Naz, B. S., Ale, S., & Bowling, L. C. (2009). Detecting subsurface drainage systems and estimating drain spacing in intensively managed agricultural landscapes. *Agricultural Water Management*, *96*(4), 627–637. https://doi.org/10.1016/j.agwat.2008.10.002

NRCS. (2019). *Gridded National Soil Survey Geographic (gNATSGO) Database for Indiana*. https://nrcs.app.box.com/v/soils: United States Department of Agriculture, Natural Resources Conservation Service. Retrieved from https://nrcs.app.box.com/v/soils

R Core Team. (2019). R: A language and environment for statistical computing (Version 3.6.1). Vienna, Austria: R Foundation for Statistical Computing. Retrieved from https://www.R-project.org/

Robinson, M. (1990). *Impact of improved land drainage on river flows.* (No. 113) (p. 226). United Kingdom: Institute of Hydrology. Retrieved from https://www.cabdirect.org/cabdirect/abstract/19911957672

Schepers, J. S., Raun, W., & Agronomy, A. S. of. (2008). *Nitrogen in Agricultural Systems*. United States: American Society of Agronomy.

Schilling, K., & Zhang, Y.-K. (2004). Baseflow contribution to nitrate-nitrogen export from a large, agricultural watershed, USA. *Journal of Hydrology*, *295*(1), 305–316. https://doi.org/10.1016/j.jhydrol.2004.03.010

Schilling, K. E., & Wolter, C. F. (2007). A GIS-based groundwater travel time model to evaluate stream nitrate concentration reductions from land use change. *Environmental Geology*, *53*(2), 433–443. https://doi.org/10.1007/s00254-007-0659-0

Schilling, K. E., Wolter, C. F., Isenhart, T. M., & Schultz, R. C. (2015). Tile Drainage Density Reduces Groundwater Travel Times and Compromises Riparian Buffer Effectiveness. *Journal of Environmental Quality*, *44*(6), 1754–1763. https://doi.org/10.2134/jeq2015.02.0105

Skaggs, R. W., Brevé, M. A., & Gilliam, J. W. (1994). Hydrologic and water quality impacts of agricultural drainage∗. *Critical Reviews in Environmental Science and Technology*, *24*(1), 1–32. https://doi.org/10.1080/10643389409388459

Sprenger, M., Leistert, H., Gimbel, K., & Weiler, M. (2016). Illuminating hydrological processes at the soil-vegetation-atmosphere interface with water stable isotopes. *Reviews of Geophysics*, *54*(3), 674–704. https://doi.org/10.1002/2015RG000515

Turtola, E., & Paajanen, A. (1995). Influence of improved subsurface drainage on phosphorus losses and nitrogen leaching from a heavy clay soil. *Agricultural Water Management*, *28*(4), 295–310. https://doi.org/10.1016/0378-3774(95)01180-3

U.S. Geological Survey, U.S. Environmental Protection Agency, & Indiana Geological and Water Survey. (2019). *Streams, Rivers, Canals, Ditches, Artificial Paths, Connectors, Pipelines, and Intermittent Streams in Watersheds of Indiana* (Shapefile). Indianapolis, Indiana, USA: United States Geological Survey.

Williams, T. A., & Williamson, A. K. (1989). Estimating Water-Table Altitudes for Regional Ground-Water Flow Modeling, U.S. Gulf Coast. *Groundwater*, *27*(3), 333–340. https://doi.org/10.1111/j.1745-6584.1989.tb00457.x

Winter, T. C., & LaBaugh, J. W. (2003). Hydrologic considerations in defining isolated wetlands. *Wetlands*, *23*(3), 532. https://doi.org/10.1672/0277-5212(2003)023[0532:HCIDIW]2.0.CO;2

CHAPTER 4. INFERRING SEASONAL RECHARGE OF GROUNDWATER IN TIPPECANOE COUNTY, INDIANA FROM STABLE ISOTOPES

4.1 Abstract

Groundwater is a vital water resource, but many groundwater resources are threatened by unsustainable use. Groundwater recharge is the main process replenishing groundwater withdrawals, and recharge rates can vary seasonally. In this analysis, δ^2H and $\delta^{18}O$ data from precipitation and groundwater were used to evaluate seasonal recharge in Tippecanoe County, Indiana using a mass balance approach. The results suggest that ~55-65% of annual recharge occurs from April – September, and this is much larger than previous estimates at nearby locations. While a lack of long-term data limits this analysis, the results support previous conclusions that significant recharge occurs during the summer.

4.2 Introduction

Many groundwater resources are threatened by over-extraction and nutrient contamination (Charbeneau, 2006), and groundwater recharge is the primary process that replenishes the groundwater lost to stream networks or human use (Ward et al., 2016). Recharge can occur through numerous mechanisms including transmission losses from streams and deep percolation of precipitation through the soil, so an understanding of when and where recharge occurs is required to use groundwater resources sustainably (Fetter, 2018).

A water balance is a common approach used to estimate recharge (Ward et al., 2016). This is an indirect method of measuring recharge because the other inputs (precipitation) and outputs (ET and *Q*) in a hydrologic system are measured, and recharge is assumed to make up any difference between them. Precipitation and *Q* can be directly measured with high accuracy, but ET is usually estimated from other variables using a variety of techniques (Chow et al., 1988). These techniques may estimate potential evapotranspiration (PET) or actual evapotranspiration (AET), but PET and AET estimates can differ substantially from each other. The errors in ET estimates can be larger than the recharge estimates, so the reliability of the water balance approach may be questionable (Charbeneau, 2006).

Baseflow regression analyses can also be used to estimate groundwater recharge (Letsinger, 2015). These analyses calculate groundwater baseflow and surface runoff using hydrograph separation techniques (Gustard et al., 1992) and converted to recharge using runoff estimates from Wolock (2003). A previous study using this technique in Indiana to determine seasonal recharge ratios (recharge as a percentage of precipitation) and calculated a recharge ratio of 66% during winter, 44% during spring, 13% during summer, and 16% during autumn (S. Naylor et al., 2016). In Indiana, groundwater recharge estimates range from near 0 mm/yr to a maximum of 355 mm/yr and are generally greatest near major rivers when using this technique (Letsinger, 2015).

Another method to estimate seasonal recharge uses stable water isotope ratios (δ^2H and $\delta^{18}O$). Precipitation δ^2H and $\delta^{18}O$ display a distinct seasonal cycle with lighter values in the winter months and heavier values in the summer months (Tian et al., 2018; Tian & Wang, 2019). If seasonal δ^2H and $\delta^{18}O$ in precipitation and δ^2H and $\delta^{18}O$ in groundwater are known, then a mass balance approach can be used to determine the fraction of recharge from winter and summer (Daniels et al., 1991). Daniels et al. (1991) used this approach in Tippecanoe County, Indiana and found that summer recharge accounts for about a third of total recharge, and this is substantially more than other studies that assume summer recharge is negligible (Allison & Hughes, 1978; Reardon et al., 1980). However, this study used δ^2H and $\delta^{18}O$ measured in precipitation from Chicago, Illinois because that was the nearest location monitoring δ^2H and $\delta^{18}O$ in precipitation at the time. Chicago is about 150 km from Tippecanoe County, and precipitation δ^2H and $\delta^{18}O$ can vary over such a distance (Gat, 1996). The objectives of this study are 1) reevaluate seasonal recharge using δ^2H and $\delta^{18}O$ from precipitation and groundwater samples in Tippecanoe County and 2) determine the relative importance of groundwater withdrawals in 12 Indiana counties where a buried river valley is present.

4.3 Methods

4.3.1 Hydrogeologic setting

Much of north-central Indiana has low relief at the surface and is in the Tipton Till Plain, which is characterized by thick glacial till deposited during the last ice age about 20,000 years ago (Gray, 2000). Beneath these glacial deposits is a buried river valley called the Teays Bedrock Valley System that traverses through 12 counties from east to west (Figure 4.1). The unconsolidated materials filling the valley are usually about 90 m thick, but this can vary from 60 to 130 m (Naylor et al., 2016). These deposits often yield highly productive groundwater wells, especially in the western half of the valley (Bruns & Steen, 2003). The Teays Bedrock Valley System underlies about 40% of Tippecanoe County as well as parts of three aquifer systems in the county: the Iroquois/Tipton Till Aquifer System, the Iroquois/Tipton Complex Aquifer System, and the Wabash River and Tributaries Outwash Aquifer System (Grove, 2009). Wells using the Iroquois/Tipton Till Aquifer System are primarily used for irrigation, but wells in the Iroquois/Tipton Complex Aquifer System and the Wabash River and Tributaries Outwash Aquifer System generally have higher yields and are used for public water supply, industry, and irrigation (Grove & Dean, 2009).

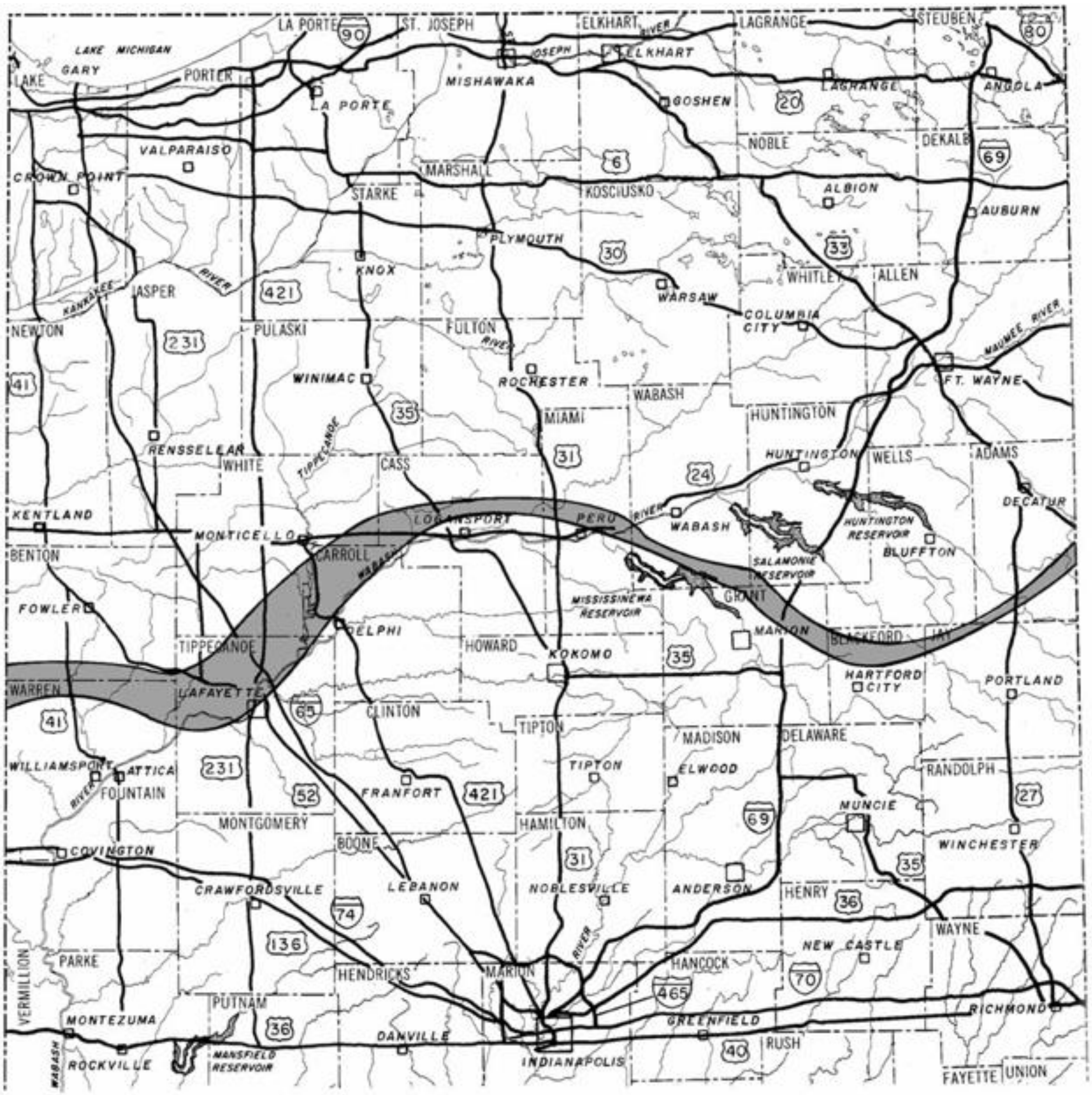

Figure 4.1. Location of the Teays Bedrock Valley in north-central Indiana, from Bruns and Steen (2003).

4.3.2 Water withdrawals

County-level groundwater and surface water withdrawals from Dieter et al. (2018) were used to evaluate the importance of groundwater for the 12 Indiana counties where the Teays Bedrock Valley is present. Each county's groundwater and surface water withdrawals were expressed as both a rate (Mgal d^{-1}) and as a percentage of total withdrawals. The percentages were compared to withdrawals across all of Indiana.

4.3.3 Monthly water balance calculations

Monthly normal precipitation data (1981 – 2010) for Purdue University Airport (IATA: LAF) near West Lafayette, Indiana (Arguez et al., 2010) was the input into the water balance equation. Estimated mean monthly AET data for the state of Indiana was obtained from Niyogi et al. (2020). Monthly AET was subtracted from monthly precipitation totals to determine the mean monthly water excess.

4.3.4 Sample collection

Precipitation sampling

Precipitation samples were collected at Purdue University (40.431°N, 86.915°W) from September 2015 to October 2019 using a Stratus RG202 precision rain gage. No paraffin or mineral oil was used, but samples were collected daily and filtered using 0.45 μm syringe filters.

Groundwater sampling

Groundwater was sampled indirectly by collecting tap water from the public water supply in West Lafayette, Indiana. West Lafayette's public water supply is obtained from the Wabash River and Tributaries Outwash Aquifer System and the Iroquois/Tipton Complex Aquifer System through 8 groundwater wells at depths between 25 and 70 m (Indiana American Water, 2020; Indiana DNR, Division of Water, 2009). Samples were collected once per month from May 2018 to September 2019, and they were stored in airtight vials at 4°C prior to analysis.

4.3.5 Stable isotope measurements

δ^2H and $\delta^{18}O$ were measured for each precipitation and groundwater sample using a laser absorption off-axis integrated cavity output spectrometer (Los Gatos Research (LGR) Triple Water Isotope Analyzer (TWIA)). Samples were injected ten times, discarding the first four to resolve memory effects and averaging the last six injections. Reproducible injection sizes minimized the water concentration dependence of the analyzer, but a small correction was made using the USGS LIMS for Lasers post-processing software (Coplen & Wassenaar, 2015). Isotope ratios are expressed in δ notation in permil (‰) using Equation 4.1.

Equation 4.1

$$\delta = \left[\frac{R_{sample}}{R_{standard}} - 1\right]1000$$

where R is the ratio of the heavy to light isotope ($^2H/^1H$ or $^{18}O/^{16}O$) in the sample or standard. All δ^2H and $\delta^{18}O$ values are reported relative to the Vienna Standard Mean Ocean Water (VSMOW) standard. Internal lab standards were used to define the VSMOW-SLAP scale. Analytical precision for repeated quality control samples was better than 0.2‰ for $\delta^{18}O$ and 1.0 ‰ for δ^2H.

4.3.6 Seasonal recharge calculations

Seasonal recharge calculations followed the mass-balance approach used by Jasechko et al. (2014). The 12 months were separated into two seasons: a cold season from October – March and a warm season from April to September. Seasonal amount-weighted $\delta^{18}O$ and δ^2H in precipitation were calculated for each season using Equation 4.2 (for the cold season) and Equation 4.3 (for the warm season).

Equation 4.2

$$\delta_{P,cold} = \frac{\delta_{P,10}P_{10} + \delta_{P,11}P_{11} + \delta_{P,12}P_{12} + \delta_{P,1}P_1 + \delta_{P,2}P_2 + \delta_{P,3}P_3}{P_{10} + P_{11} + P_{12} + P_1 + P_2 + P_3}$$

Equation 4.3

$$\delta_{P,warm} = \frac{\delta_{P,4}P_4 + \delta_{P,5}P_5 + \delta_{P,6}P_6 + \delta_{P,7}P_7 + \delta_{P,8}P_8 + \delta_{P,9}P_9}{P_4 + P_5 + P_6 + P_7 + P_8 + P_9}$$

Where $\delta_{P,i}$ represents the $\delta^{18}O$ or $\delta^{2}H$ in precipitation for the *i*th month of the calendar year, and P_i represents the amount of precipitation during the *i*th month of the calendar year. The fraction of annual recharge (R_{annual}) that occurs during the warm season (R_{warm}) was calculated using Equation 4.4.

Equation 4.4

$$\frac{R_{warm}}{R_{annual}} = \frac{\delta_{gw} - \delta_{P,cold}}{\delta_{P,warm} - \delta_{P,cold}}$$

Where δ_{gw} is the average annual $\delta^{18}O$ or $\delta^{2}H$ in groundwater.

4.4 Results and Discussion

4.4.1 Water withdrawals

The percentage of total water withdrawals from groundwater is significantly greater than the percentage from surface water in the 12 Indiana counties where the Teays Bedrock Valley is present ($t(22) = 4.78$, $p < 0.001$). The percentage of withdrawals from groundwater is also much higher in these 12 counties (67.0%) than the state of Indiana as a whole (9.7%). Among these 12 counties, only two (Carroll and Cass) had less than 50% groundwater withdrawals, and three (Tippecanoe, Wabash, and Warren) had > 90% groundwater withdrawals (Table 4.1). The high percentage of withdrawals from groundwater in counties above the Teays Bedrock Valley demonstrate the importance of the aquifer to local communities.

Table 4.1. Groundwater and surface water withdrawals for the 12 Indiana counties where the Teays Bedrock Valley is present. Data from Dieter et al. (2018).

County	Groundwater Withdrawals (Mgal d^{-1})	Surface Water Withdrawals (Mgal d^{-1})	Total Withdrawals (Mgal d^{-1})
Adams County	5.06 (64.7%)	2.76 (35.3%)	7.82
Benton County	1.07 (79.3%)	0.28 (20.7%)	1.35
Blackford County	1.85 (89.4%)	0.22 (10.6%)	2.07
Carroll County	3.73 (39.1%)	5.80 (60.9%)	9.53
Cass County	9.10 (34.8%)	17.05 (65.2%)	26.15
Grant County	6.39 (60.5%)	4.18 (39.5%)	10.57
Jay County	3.73 (69.2%)	1.66 (30.8%)	5.39
Miami County	4.54 (53.0%)	4.02 (47.0%)	8.56
Tippecanoe County	28.88 (98.3%)	0.49 (1.7%)	29.37
Wabash County	7.10 (92.9%)	0.54 (7.1%)	7.64
Warren County	1.85 (98.4%)	0.03 (1.6%)	1.88
White County	5.44 (75.1%)	1.80 (24.9%)	7.24
12-County Total	**78.74 (67.0%)**	**38.83 (33.0%)**	**117.57**
Indiana Total	**698.82 (9.7%)**	**6477.90 (90.3%)**	**7176.72**

4.4.2 Monthly water balance

Annual precipitation was 929.03 mm (Arguez et al., 2010), and the wettest months were April through August (Figure 4.2). Estimated AET exceeded precipitation from June through September. Water excess followed a seasonal cycle with a surplus from October to May and a deficit from June to September (Table C.1). An important limitation of the data used in this water balance is that the AET data was aggregated for the entire state of Indiana, and monthly AET in Tippecanoe County may differ from the state-wide monthly AET estimates.

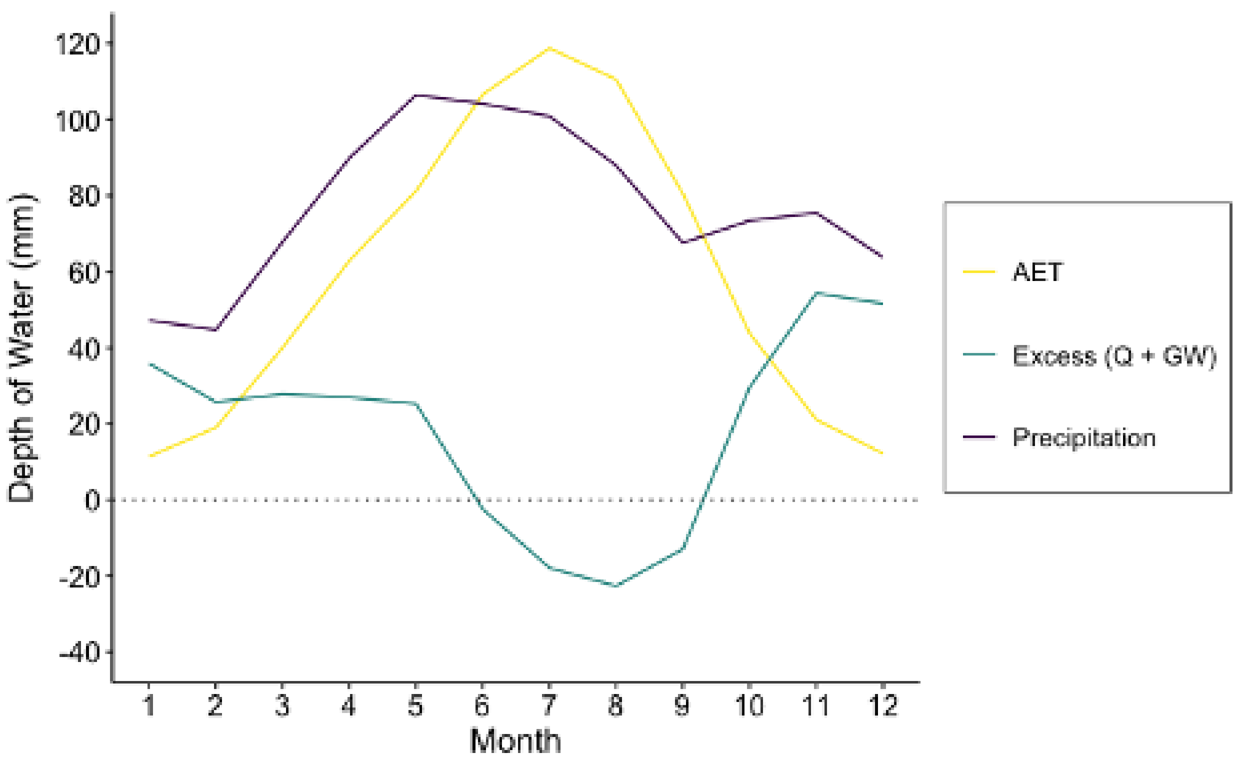

Figure 4.2. Monthly water balance for Tippecanoe County, Indiana.

4.4.3 Seasonal groundwater recharge using mass balance approach

Monthly amount-weighted $\delta^{18}O$ and $\delta^{2}H$ in precipitation displayed a clear seasonal cycle with lighter (more negative) values during the colder months and heavier (more positive) values during the warmer months (Figure 4.3). December had the lightest $\delta^{18}O$ (-18.29 ± 0.05 ‰), and August had the heaviest $\delta^{18}O$ (-4.38 ± 0.20 ‰). Monthly $\delta^{18}O$ and $\delta^{2}H$ in groundwater was much less variable than in precipitation. The difference between the lightest $\delta^{18}O$ (-6.75 ± 0.13 ‰) and the heaviest $\delta^{18}O$ (-6.15 ± 0.09 ‰) was only 0.6 ‰ in groundwater, but this difference was nearly 14 ‰ in precipitation.

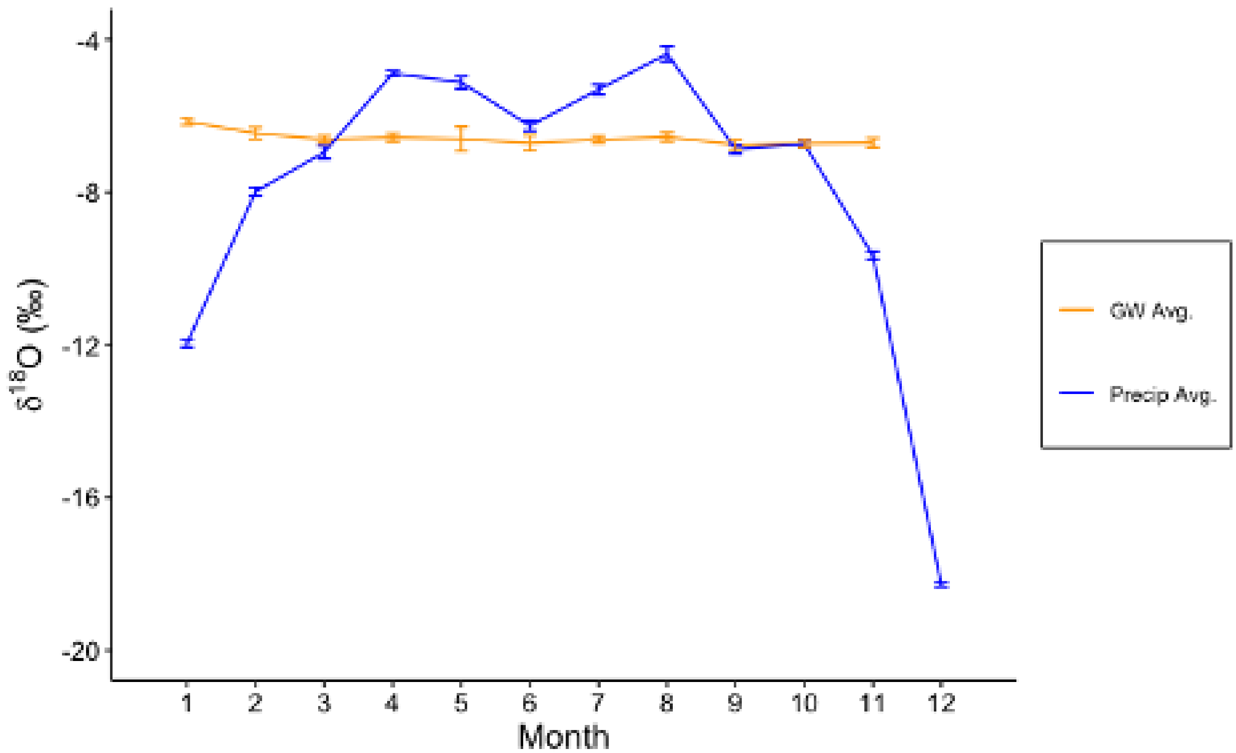

Figure 4.3. Average monthly $\delta^{18}O$ in precipitation and groundwater.

Average $\delta^{18}O$ and $\delta^{2}H$ were substantially different between the October – March and the April – September seasons (Figure 4.4). Average $\delta^{18}O$ during October – March (-8.65 ± 0.11 ‰) was about 3 ‰ lighter than during April – September (-5.40 ± 0.14 ‰), and average $\delta^{2}H$ differed by about 23 ‰ between the two seasons (Figure 4.4).

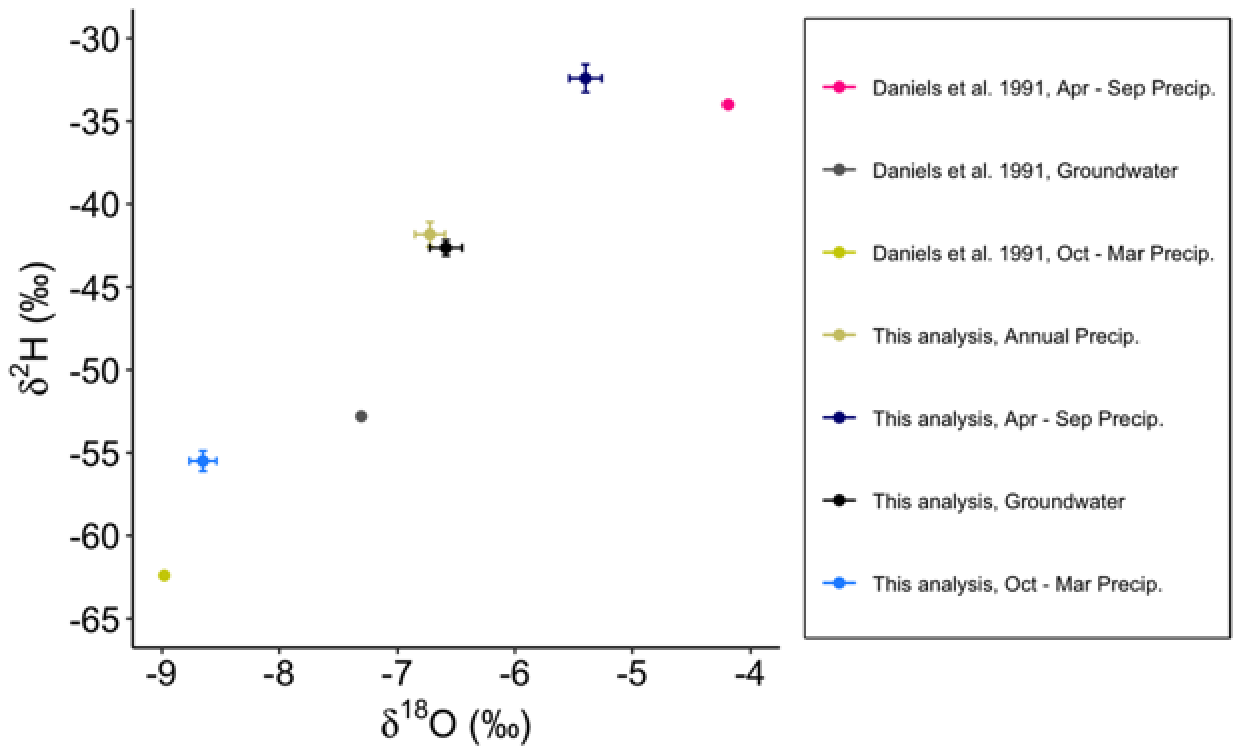

Figure 4.4. Average seasonal and annual $\delta^{18}O$ and $\delta^{2}H$ in precipitation and average annual $\delta^{18}O$ and $\delta^{2}H$ in groundwater.

Seasonal recharge calculations indicate that more recharge occurs during the summer than the winter. Summer recharge accounts for 63.4 ± 8.4% of annual recharge based on $\delta^{18}O$ data. The summer recharge estimate was somewhat less (55.7 ± 5.1%) based on $\delta^{2}H$ data. These estimates are much greater than previously reported estimates for Tippecanoe County (Daniels et al., 1991; Jasechko et al., 2014). Daniels et al. (1991) estimated that 34% of total recharge occurs from April – September. Jasechko et al. (2014) calculated that annual recharge in west-central Indiana is biased towards the winter, and that would suggest that less than 50% of annual recharge occurs during the summer. The large difference between previous recharge estimates and the estimate in this study could be a consequence of using a short period of precipitation data. This analysis used precipitation data from 2015 – 2019 (4 years), but Daniels et al. (1991) and Jasechko et al. (2014) used data from 1962 – 1978 (16 years) and 1960 – 1979 (19 years), respectively. While a lack of long-term data limits the reliability of this analysis, the results of the seasonal isotope estimates support previous conclusions that substantial recharge occurs during the summer in Tippecanoe County.

Isotope-based recharge estimates indicate substantial recharge during the warm season, but this finding is at odds with the large ET fluxes during the same period (Figure 4.2). This discrepancy may be caused by seasonal differences in precipitation intensity. Precipitation events during warmer months are typically more intense than during colder months in Tippecanoe County (Bonnin et al., 2004). Figure 4.5 displays the probability of a 2-year, 5-year, 10-year, 25-year, 50-year, or 100-year 24-hour precipitation total occurring for each month. These intense precipitation events are more likely during April – September than during October – March. In general, more intense precipitation events will have proportionally more runoff and less infiltration, and the additional runoff raises the water level in local streams in rivers (Ward et al., 2016). Most streams in the eastern United States are gaining streams during baseflow conditions, so groundwater usually discharges into the streams under these conditions (Fetter, 2018). However, these streams can temporarily become losing streams that recharge the groundwater when the water level is high (Tabidian et al., 1992). Recharge begins when the water level rises above the local water table and temporarily reverses the hydraulic gradient between the groundwater and the stream, and it continues until the flood passes and the hydraulic gradient returns to its original orientation. This mechanism could explain how summer recharge occurs near streams in Tippecanoe County, but further work would be necessary to verify this.

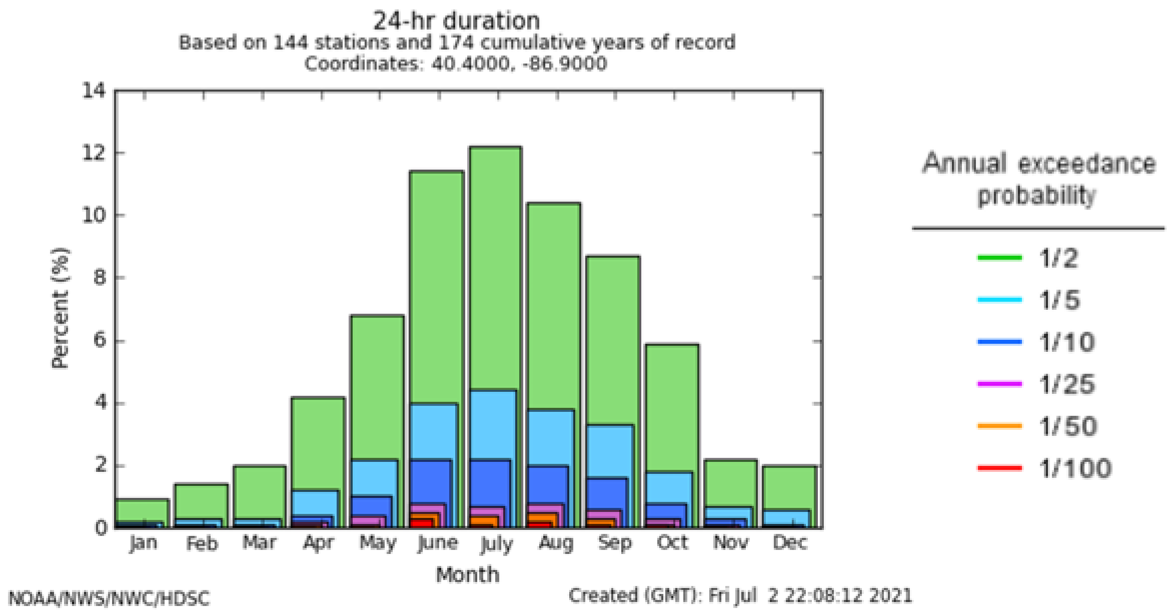

Figure 4.5. Probability of a 2-year (green), 5-year (light blue), 10-year (blue), 25-year (magenta), 50-year (orange), and 100-year (red) 24-hour precipitation total occurring for each month. From Bonnin et al. (2004).

4.5 Conclusions

The 12 Indiana counties where the Teays Bedrock Valley is present are more reliant on groundwater withdrawals than the state or national average, so understanding recharge processes is particularly important in these counties. Groundwater recharge appears to be negligible from June – September when a monthly water balance approach is used, but a previous recharge estimate using $\delta^{18}O$ and $\delta^{2}H$ data suggest that about one-third of annual recharge occurs from April – September. In this analysis, $\delta^{18}O$ and $\delta^{2}H$ data from precipitation and groundwater were used to estimate seasonal recharge. This data suggests that ~55-65% of annual recharge occurs from April – September, and this is similar to previous estimates for nearby locations. While the short precipitation data record limits the reliability of this analysis, the results support previous conclusions that substantial recharge occurs during the summer months. This summer recharge may occur near streams when the hydraulic gradient at the stream/water table interface is temporarily reversed following intense precipitation events, but further investigation is needed to verify this.

4.6 References

Allison, G. B., & Hughes, M. W. (1978). The use of environmental chloride and tritium to estimate total recharge to an unconfined aquifer. *Soil Research*, *16*(2), 181–195. https://doi.org/10.1071/sr9780181

Arguez, A., Durre, I., Applequist, S., Squires, M., Vose, R., Yin, X., & Bilotta, R. (2010). U.S. Climate Normals Product Suite (1981-2010) [Data set]. NOAA National Climatic Data Center. https://doi.org/10.7289/V5PN93JP

Bonnin, G. M., Martin, D., Lin, B., Parzybok, T., Yekta, M., & Riley, D. (2004). *Precipitation-frequency atlas of the United States* (3rd ed., Vol. 2). Silver Spring, Maryland: NOAA, National Weather Service. Retrieved from https://www.weather.gov/media/owp/hdsc_documents/Atlas14_Volume2.pdf

Bruns, T. M., & Steen, W. J. (2003). *Hydrogeology of the Lafayette (Teays) Bedrock Valley System, north-central Indiana* (Water Resource Assessment No. 2003–7) (p. 75). Indianapolis, Indiana, USA: Indiana Department of Natural Resources. Retrieved from https://www.in.gov/dnr/water/files/Teays.pdf

Charbeneau, R. J. (2006). *Groundwater hydraulics and pollutant transport*. Long Grove, IL: Waveland Press.

Chow, V. T., Maidment, D. R., & Mays, L. W. (1988). *Applied hydrology*. New York: McGraw-Hill.

Coplen, T. B., & Wassenaar, L. I. (2015). LIMS for Lasers 2015 for achieving long-term accuracy and precision of δ2H, δ17O, and δ18O of waters using laser absorption spectrometry. *Rapid Communications in Mass Spectrometry*, *29*(22), 2122–2130. https://doi.org/10.1002/rcm.7372

Daniels, D. P., Fritz, S. J., & Leap, D. I. (1991). Estimating recharge rates through unsaturated glacial till by tritium tracing. *Groundwater*, *29*(1), 26–34. https://doi.org/10.1111/j.1745-6584.1991.tb00493.x

Dieter, C. A., Maupin, M. A., Caldwell, R. R., Harris, M. A., Ivahnenko, T. I., Lovelace, J. K., et al. (2018). *Estimated use of water in the United States in 2015* (USGS Numbered Series No. 1441). *Estimated use of water in the United States in 2015* (Vol. 1441, p. 76). Reston, VA: U.S. Geological Survey. https://doi.org/10.3133/cir1441

Fetter, C. W. (2018). *Applied hydrogeology* (4th ed.). Long Grove, IL: Waveland Press.

Gat, J. R. (1996). Oxygen and Hydrogen Isotopes in the Hydrologic Cycle. *Annual Review of Earth and Planetary Sciences*, *24*(1), 225–262. https://doi.org/10.1146/annurev.earth.24.1.225

Gray, H. H. (2000). *Physiographic divisions of Indiana* (No. Special Report 61) (p. 15). Bloomington, Indiana: Indiana Geological and Water Survey. Retrieved from https://igws.indiana.edu/bookstore/details.cfm?Pub_Num=SR61

Grove, G. E. (2009). *Unconsolidated Aquifer Systems of Tippecanoe County, Indiana* (Division of Water, Resource Assessment Section) (p. 6). Indianapolis, Indiana: Indiana Department of Natural Resources. Retrieved from https://www.in.gov/dnr/water/files/58_Tippecanoe_County_UNC_AQSYS_text.pdf

Grove, G. E., & Dean, S. H. (2009). Unconsolidated aquifer systems of Tippecanoe County, Indiana. Indianapolis, Indiana: Indiana Department of Natural Resources. Retrieved from https://www.in.gov/dnr/water/files/58_Tippecanoe_County_UNC_AQSYS_map.pdf

Gustard, A., Bullock, A., & Dixon, J. M. (1992). *Low flow estimation in the United Kingdom* (No. 108) (p. 292). Wallingford, UK: Institute of Hydrology. Retrieved from http://nora.nerc.ac.uk/id/eprint/6050/1/IH_108.pdf

Healy, R. W., & Cook, P. G. (2002). Using groundwater levels to estimate recharge. *Hydrogeology Journal*, *10*(1), 91–109. http://dx.doi.org.ezproxy.lib.purdue.edu/10.1007/s10040-001-0178-0

Indiana American Water. (2020). *2020 annual water quality report* (p. 19). West Lafayette, Indiana: Indiana American Water. Retrieved from https://www.amwater.com/ccr/westlafayette.pdf?language_id=1

Indiana DNR, Division of Water. (2009). Registered significant ground-water withdrawal facilities in Tippecanoe County, Indiana. Indiana Department of Natural Resources. Retrieved from https://www.in.gov/dnr/water/files/58_Tippecanoe_County_Highcap_table.pdf

Indiana DNR, Division of Water. (2016, March 23). Significant water withdrawal facilities. Indianapolis, Indiana: Indiana Department of Natural Resources. Retrieved from https://www.in.gov/dnr/water/water-availability-use-rights/significant-water-withdrawal-facility-data/

Jasechko, S., Birks, S. J., Gleeson, T., Wada, Y., Fawcett, P. J., Sharp, Z. D., et al. (2014). The pronounced seasonality of global groundwater recharge. *Water Resources Research*, *50*(11), 8845–8867. https://doi.org/10.1002/2014WR015809

Letsinger, S. L. (2015). *Relationship of groundwater recharge rates to aquifer sensitivity to contamination in shallow aquifers in Indiana, using multiple regression analysis*. Bloomington, Indiana: Center for Geospatial Data Analysis, Indiana Geological Survey. Retrieved from https://maps.indiana.edu/metadata/Hydrology/Aquifer_Recharge_Near_Surface.html

Naylor, S., Letsinger, S. L., Ficklin, D. L., Ellett, K. M., & Olyphant, G. A. (2016). A hydropedological approach to quantifying groundwater recharge in various glacial settings of the mid-continental USA. *Hydrological Processes*, *30*(10), 1594–1608. https://doi.org/10.1002/hyp.10718

Naylor, Shawn, Schumacher, J., & Sperl, B. (2016). Map showing thickness of unconsolidated deposits in Indiana. Bloomington, Indiana: Indiana Geological and Water Survey. Retrieved from https://igws.indiana.edu/bookstore/details.cfm?ItemID=3726&Pub_Num=MM95A

Niyogi, D., Jamshidi, S., Smith, D., & Kellner, O. (2020). Evapotranspiration Climatology of Indiana Using In Situ and Remotely Sensed Products. *Journal of Applied Meteorology and Climatology*, *59*(12), 2093–2111. https://doi.org/10.1175/JAMC-D-20-0024.1

Reardon, E. J., Mozeto, A. A., & Fritz, P. (1980). Recharge in northern clime calcareous sandy soils: soil water chemical and carbon-14 evolution. *Geochimica et Cosmochimica Acta*, *44*(11), 1723–1735. https://doi.org/10.1016/0016-7037(80)90223-9

Tabidian, M. A., Pederson, A. D., & Tabidian, P. A. (1992). A paleovalley aquifer system and its interaction with the Big Blue River of Nebraska during a major flood. In R. C. Borden & W. L. Lyke (Eds.), *Proceedings of the National Symposium on the Future Availability of Ground Water Resources* (pp. 165–172). Bethesda, Maryland: American Water Resources Association. Retrieved from https://www.worldcat.org/title/proceedings-of-the-national-symposium-on-the-future-availability-of-ground-water-resources/oclc/26579403

Tian, C., & Wang, L. (2019). Stable isotope variations of daily precipitation from 2014–2018 in the central United States. *Scientific Data*, *6*. https://doi.org/10.1038/sdata.2019.18

Tian, C., Wang, L., Kaseke, K. F., & Bird, B. W. (2018). Stable isotope compositions (δ 2 H, δ 18 O and δ 17 O) of rainfall and snowfall in the central United States. *Scientific Reports*, *8*(1), 6712. https://doi.org/10.1038/s41598-018-25102-7

Ward, A. D., Trimble, S. W., Burckhard, S. R., & Lyon, J. G. (2016). *Environmental hydrology* (Third edition). Boca Raton, FL: CRC Press, Taylor & Francis Group.

Wolock, D. M. (2003). *Estimated mean annual natural ground-water recharge in the conterminous United States* (USGS Numbered Series No. 2003–311). *Estimated mean annual natural ground-water recharge in the conterminous United States* (Vol. 2003–311). Reston, VA: U.S. Geological Survey. https://doi.org/10.3133/ofr03311

CHAPTER 5. CONCLUSIONS

This thesis had 3 main objectives: 1) answer questions about N transport and hydrologic connectivity in a tile drained landscape in west-central Indiana using a decade of water quality and stable isotope data from 205 nested watersheds; 2) calculate TTDs for all 205 watersheds at three different drainage intensities using a previously developed GIS-based model; and 3) estimate seasonal groundwater recharge in Tippecanoe County using δ^2H and $\delta^{18}O$ data from precipitation and groundwater and a mass balance approach.

Tile drainage intensity is related to in-stream nitrate concentrations with higher concentrations observed at greater drainage intensities. Qualitative travel times derived from δ^2H and $\delta^{18}O$ variability support the idea that short travel times have greater nitrate concentrations than long travel times. Antecedent moisture conditions and hydrologic connectivity influence stream N concentrations because N in agricultural fields cannot reach the stream unless a hydrologic connection exists between them. Consistently low nitrate concentrations during fall baseflow conditions suggest that groundwater nitrate concentrations are ~1.5 mg L^{-1}, but this finding may not hold true for groundwater sources that are disconnected from surface streams.

The results of the GIS TTD model support the hypothesis that increasing drainage intensity reduces travel times. Greater $\delta^{18}O$ and δ^2H enrichment in watersheds with longer travel times suggest that these watersheds experience greater evaporative influence than those with shorter travel times. Across the landscape, travel times appear to have opposing relationships with drainage scores (which reflect USDA soil drainage classes) and the percentage of a watershed drained by tiles (tile drained area). Travel times follow the expected relationship with drainage scores, but follow the opposite of the expected pattern with tile drained area. The relationship between travel time and tile drained area follows the opposite of the expected pattern because model inputs are independent of tile drained area and tile drained area follows an inverse relationship with drainage scores.

Counties in north-central and west-central Indiana where the Teays Bedrock Valley is present rely on groundwater withdrawals more than the state or national average. In Tippecanoe County, groundwater recharge appears to be negligible during the summer based on a monthly water balance. However, ~55-65% of annual recharge occurs during the summer based on a mass balance approach using δ^2H and $\delta^{18}O$ data from precipitation and groundwater. This estimate is much larger than previous estimates for nearby locations. While a short period of data limits the reliability of this analysis, the results support the hypothesis that substantial recharge occurs during summer months. Summer recharge may be linked to intense precipitation events that are more common during the summer months. The hydraulic gradient at the stream/water table interface can temporarily reverse when intense precipitation events raise the water level in streams, and stream water seeps into the streambank to raise the water table during these reversals.

APPENDIX A. NITROGEN FERTILIZER USAGE, 2011-2015

Table A.1. Indiana statewide nitrogen fertilizer usage, 2011-2015 (in short tons). Data from the Office of Indiana State Chemist (2017).

Time Period	Anhydrous Ammonia (82-0-0)	Ammonium sulfate (21-0-0)	UAN (28-0-0)	Urea (46-0-0)	Total
Jan-Jun 2011	221,652	19,979	510,515	75,072	827,218
Jul-Dec 2011	65,409	NA	188,676	11,104	265,190
Jan-Jun 2012	290,400	NA	587,547	91,513	969,460
Jul-Dec 2012	40,036	NA	134,262	NA	174,298
Jan-Jun 2013	251,740	23,810	574,572	84,869	934,990
Jul-Dec 2013	40,580	NA	143,671	NA	184,250
Jan-Jun 2014	261,428	32,380	607,732	96,892	998,432
Jul-Dec 2014	19,401	8,607	122,632	8,162	158,801
Jan-Jun 2015	199,002	29,878	483,093	88,097	800,070
Jul-Dec 2015	38,704	10,696	166,178	20,511	236,088
Jan-Jun Total	**1,224,222**	**106,046**	**2,763,459**	**436,443**	**4,530,170 (81.6%)**
Jul-Dec Total	**204,129**	**19,303**	**755,418**	**39,777**	**1,018,627 (18.4%)**
Total	**1,428,351 (25.7%)**	**125,349 (2.26%)**	**3,518,877 (63.4%)**	**476,220 (8.58%)**	**5,548,797 (100%)**

.

Table A.2. Fountain County nitrogen fertilizer usage, 2011-2015 (in short tons). Data from the Office of Indiana State Chemist (2017)

Time Period	Anhydrous Ammonia (82-0-0)	Ammonium sulfate (21-0-0)	UAN (28-0-0)	Urea (46-0-0)	Total
Jan-Jun 2011	3,190.3	1.7	9,224.8	958.3	13,375.1
Jul-Dec 2011	1,313.9	NA	297.8	10.5	1,622.2
Jan-Jun 2012	4,498.7	NA	9,515.3	703.2	14,717.3
Jul-Dec 2012	3,335.0	NA	1,705.9	NA	5,040.8
Jan-Jun 2013	2,039.8	5.5	10,810.7	824.3	13,680.3
Jul-Dec 2013	1,227.5	NA	292.2	NA	1,519.6
Jan-Jun 2014	3,522.9	2.9	9,187.4	641.6	13,354.9
Jul-Dec 2014	838.5	0.0	1,119.6	8.4	1,966.5
Jan-Jun 2015	1,865.3	38.8	6,582.0	700.3	9,186.4
Jul-Dec 2015	1,032.3	5.5	299.1	76.4	1,413.3
Jan-Jun Total	**15,177.1**	**48.9**	**45,320.2**	**3,827.8**	**64,313.9 (84.8%)**
Jul-Dec Total	**7,747.1**	**5.5**	**3,714.6**	**95.2**	**11,562.4 (15.2%)**
Total	**22,864.2 (30.1%)**	**54.4 (0.07%)**	**49,034.8 (64.62%)**	**3,923.0 (5.17%)**	**75,876.4 (100%)**

Table A.3. Tippecanoe County nitrogen fertilizer usage, 2011-2015 (in short tons). Data from the Office of Indiana State Chemist (2017).

Time Period	Anhydrous Ammonia (82-0-0)	Ammonium sulfate (21-0-0)	UAN (28-0-0)	Urea (46-0-0)	Total
Jan-Jun 2011	2,639.6	430.9	11,213.0	219.6	14,503.1
Jul-Dec 2011	2,416.9	NA	1,959.0	43.1	4,419.0
Jan-Jun 2012	4,152.5	NA	11,549.7	643.0	16,345.1
Jul-Dec 2012	2,160.4	NA	2,652.0	NA	4,812.4
Jan-Jun 2013	5,787.8	61.5	16,327.6	423.4	22,600.3
Jul-Dec 2013	4,988.8	NA	3,035.2	NA	8,023.9
Jan-Jun 2014	6,143.3	292.0	17,750.3	242.3	24,427.9
Jul-Dec 2014	54.0	165.8	1,467.3	191.7	1,878.7
Jan-Jun 2015	1,513.8	246.3	10,473.4	539.8	12,773.3
Jul-Dec 2015	755.2	88.8	2,816.6	540.4	4,201.0
Jan-Jun Total	**20,237.0**	**1,030.7**	**67,314.0**	**2,068.0**	**90,649.7 (79.5%)**
Jul-Dec Total	**10,375.2**	**254.6**	**11,930.2**	**775.1**	**23,335.1 (20.5%)**
Total	**30,612.2 (26.9%)**	**1,285.3 (1.13%)**	**79,244.2 (69.5%)**	**2,843.1 (2.49%)**	**113,984.7 (100%)**

Table A.4. Warren County nitrogen fertilizer usage, 2011-2015 (in short tons).

Time Period	Anhydrous Ammonia (82-0-0)	Ammonium sulfate (21-0-0)	UAN (28-0-0)	Urea (46-0-0)	Total
Jan-Jun 2011	1,803.2	59.0	7,969.7	1,154.1	10,985.9
Jul-Dec 2011	4,300.2	NA	3,023.1	27.5	7,350.9
Jan-Jun 2012	2,966.9	NA	8,497.5	1,818.7	13,283.1
Jul-Dec 2012	3,800.6	NA	964.5	NA	4,765.2
Jan-Jun 2013	1,336.6	51.6	6,550.5	1,371.6	9,310.3
Jul-Dec 2013	872.4	NA	2,335.7	NA	3,208.1
Jan-Jun 2014	1,270.5	174.6	9,990.8	3,999.1	15,435.0
Jul-Dec 2014	643.8	16.1	801.6	32.8	1,494.4
Jan-Jun 2015	3,035.5	146.0	10,090.8	578.6	13,850.9
Jul-Dec 2015	0.0	142.5	266.5	45.9	455.0
Jan-Jun Total	**10,412.7**	**431.1**	**43,099.3**	**8,922.0**	**62,865.1 (78.5%)**
Jul-Dec Total	**9,617.1**	**158.6**	**7,391.5**	**106.2**	**17,273.4 (21.5%)**
Total	**20,029.8 (25.0%)**	**589.7 (0.74%)**	**50,490.8 (63.0%)**	**9,028.3 (11.3%)**	**80,138.6 (100%)**

APPENDIX B. TTD SCRIPT

```
# -*- coding: utf-8 -*-
# ---------------------------------------------------------------------------
# TTD_tool_for_complete_watersheds.py
# Created on: 2021-06-10 09:44:34.00000
#   (generated by ArcGIS/ModelBuilder)
# Description:
# ---------------------------------------------------------------------------

# Import arcpy module
import arcpy

# Load required toolboxes
arcpy.ImportToolbox("Model Functions")

# Local variables:
Watershed_Shapefile_Folder = "F:\\GIS\\ArcGIS_Data\\CompleteWatershedShapes"
Single_Shapefile = "F:\\GIS\\ArcGIS_Data\\CompleteWatershedShapes\\LR.shp"
Effective_Porosity__n__Raster =
"F:\\GIS\\ArcGIS_Data\\ImprovedModelInput.gdb\\effective_porosity"
Extracted_n =
"F:\\GIS\\ArcGIS_Data\\ImprovedModelOutput\\ExtractPorosity.gdb\\extract_effective_porosity
_channel_complete_%Name%"
Flow_Line_Raster =
"F:\\GIS\\ArcGIS_Data\\Hydrology\\Streams.gdb\\blitz_streams_channel_raster"
Extracted_Flow_Lines =
"F:\\GIS\\ArcGIS_Data\\ImprovedModelOutput\\ExtractStreams.gdb\\extract_stream_effpor_cha
nnel_complete_%Name%"
DEM = "F:\\GIS\\ArcGIS_Data\\ImprovedModelInput.gdb\\dem_10m_fill"
Extracted_DEM =
"F:\\GIS\\ArcGIS_Data\\ImprovedModelOutput\\ExtractDEM.gdb\\extract_dem_effpor_channel
_complete_%Name%"
Flow_Distance__L__Raster =
"F:\\GIS\\ArcGIS_Data\\ImprovedModelOutput\\FlowDistance.gdb\\flow_distance_effpor_chan
nel_complete_%Name%"
Numerator =
"F:\\GIS\\ArcGIS_Data\\ImprovedModelOutput\\Numerator.gdb\\numerator_effpor_channel_co
mplete_%Name%"
Hydraulic_Conductivity__K__Raster =
"F:\\GIS\\ArcGIS_Data\\ImprovedModelInput.gdb\\Ksat"
Extracted_K =
"F:\\GIS\\ArcGIS_Data\\ImprovedModelOutput\\ExtractKsat.gdb\\extract_Ksat_effpor_channel_
complete_%Name%"
```

```
Hydraulic_Gradient__i__Raster =
"F:\\GIS\\ArcGIS_Data\\ImprovedModelInput.gdb\\slope_USE"
Extracted_i =
"F:\\GIS\\ArcGIS_Data\\ImprovedModelOutput\\ExtractSlope.gdb\\extract_slope_effpor_channe
l_complete_%Name%"
Denominator =
"F:\\GIS\\ArcGIS_Data\\ImprovedModelOutput\\Denominator.gdb\\denominator_effpor_channe
l_complete_%Name%"
TTD_in_Seconds =
"F:\\GIS\\ArcGIS_Data\\ImprovedModelOutput\\TravTimeSeconds.gdb\\ttd_seconds_effpor_ch
annel_complete_%Name%"
Seconds_per_Year = "31536000"
TTD_in_Years =
"F:\\GIS\\ArcGIS_Data\\ImprovedModelOutput\\TravTimeYearsCompleteEffPorChannel.gdb\\tt
d_years_effpor_channel_complete_%Name%"
Ten_Thousand = "10000"
TTD_x_10000 =
"F:\\GIS\\ArcGIS_Data\\ImprovedModelOutput\\CompleteEffPorChannelTTD10000.gdb\\%Na
me%"
TTD_x_10000_as_Integer =
"F:\\GIS\\ArcGIS_Data\\ImprovedModelOutput\\CompleteEffPorChannelTTD10000Int.gdb\\%
Name%"
Median_of_TTD_x_10000 =
"F:\\GIS\\ArcGIS_Data\\ImprovedModelOutput\\CompleteEffPorChannelTTD10000Median.gdb
\\%Name%"
Median_of_TTD_x_10000_as_Float =
"F:\\GIS\\ArcGIS_Data\\ImprovedModelOutput\\CompleteEffPorChannelTTD10000Float.gdb\\
%Name%"
TTD_Median =
"F:\\GIS\\ArcGIS_Data\\ImprovedModelOutput\\CompleteEffPorChannelTTDMedian.gdb\\%N
ame%"
One_Year = "1"
Fraction_of_TTD_<_1_Year =
"F:\\GIS\\ArcGIS_Data\\ImprovedModelOutput\\CompleteEffPorChannelTTDLess1Year.gdb\\
%Name%"
Name = "LR"

# Process: Iterate Feature Classes
arcpy.IterateFeatureClasses_mb(Watershed_Shapefile_Folder, "", "", "NOT_RECURSIVE")

# Process: Extract n by Mask
arcpy.gp.ExtractByMask_sa(Effective_Porosity__n__Raster, Single_Shapefile, Extracted_n)

# Process: Extract Flow Lines by Mask
arcpy.gp.ExtractByMask_sa(Flow_Line_Raster, Single_Shapefile, Extracted_Flow_Lines)
```

```
# Process: Extract DEM by Mask
arcpy.gp.ExtractByMask_sa(DEM, Single_Shapefile, Extracted_DEM)

# Process: Flow Distance
arcpy.gp.FlowDistance_sa(Extracted_Flow_Lines, Extracted_DEM,
Flow_Distance__L__Raster, "", "HORIZONTAL", "D8", "MINIMUM")

# Process: L Times n
arcpy.gp.Times_sa(Extracted_n, Flow_Distance__L__Raster, Numerator)

# Process: Extract K by Mask
arcpy.gp.ExtractByMask_sa(Hydraulic_Conductivity__K__Raster, Single_Shapefile,
Extracted_K)

# Process: Extract i by Mask
arcpy.gp.ExtractByMask_sa(Hydraulic_Gradient__i__Raster, Single_Shapefile, Extracted_i)

# Process: K Times i
arcpy.gp.Times_sa(Extracted_K, Extracted_i, Denominator)

# Process: Numerator Divide Denominator
arcpy.gp.Divide_sa(Numerator, Denominator, TTD_in_Seconds)

# Process: Divide
arcpy.gp.Divide_sa(TTD_in_Seconds, Seconds_per_Year, TTD_in_Years)

# Process: TTD Times 10000
arcpy.gp.Times_sa(TTD_in_Years, Ten_Thousand, TTD_x_10000)

# Process: Int
arcpy.gp.Int_sa(TTD_x_10000, TTD_x_10000_as_Integer)

# Process: Zonal Statistics (Median)
arcpy.gp.ZonalStatistics_sa(Single_Shapefile, "Site_Num", TTD_x_10000_as_Integer,
Median_of_TTD_x_10000, "MEDIAN", "DATA")

# Process: Float
arcpy.gp.Float_sa(Median_of_TTD_x_10000, Median_of_TTD_x_10000_as_Float)

# Process: Divide by 10000
arcpy.gp.Divide_sa(Median_of_TTD_x_10000_as_Float, Ten_Thousand, TTD_Median)

# Process: Less Than Equal
arcpy.gp.LessThanEqual_sa(TTD_in_Years, One_Year, Fraction_of_TTD_<_1_Year)
```

APPENDIX C. WATER BALANCE DATA

Table C.1. Monthly water balance using precipitation, AET, and water excess.

Month	Precipitation (mm)	AET (mm)	Water Excess (mm)
January	47.24	11.38	35.86
February	44.70	19.00	25.70
March	67.82	40.02	27.80
April	89.82	62.87	26.95
May	106.43	81.21	25.22
June	104.14	106.59	-2.45
July	100.84	118.72	-17.88
August	87.88	110.51	-22.63
September	67.56	80.51	-12.95
October	73.41	43.82	29.59
November	75.44	21.07	54.37
December	63.75	12.14	51.61
Total	929.03	707.85	221.19